8-2010

Shape-based detection of cortex variability for more accurate discrimination between autistic and normal brains.

Matthew Joseph Nitzken 1987-
University of Louisville

Shape-Based Detection of Cortex Variability for More Accurate Discrimination Between Autistic and Normal Brains

By:
Matthew Joseph Nitzken
Bachelors of Science,
University of Louisville Speed School of Engineering, August 15th, 2009

A Thesis
Submitted to the Faculty of the
University of Louisville
J.B. Speed School of Engineering
As Partial Fulfillment of the Requirements
For the Professional Degree

MASTER OF ENGINEERING
Department of Biomedical Engineering

August, 2010

Shape-Based Detection of Cortex Variability for More Accurate Discrimination Between Autistic and Normal Brains

Submitted by: ___________________________________

Matthew Joseph Nitzken

A Thesis Approved On

____

Date

By the Following Reading and Examination Committee:

____

Ayman El-Baz, Ph.D
Thesis Director,

____

Manuel F. Casanova, M.D.

____

Guruprasad Giridharan, Ph.D.

____

Palaniappan Sethu, Ph.D.

ACKNOWLEDGEMENTS

I wanted to extend my thanks to a number of individuals who have helped me see the work presented in this thesis through to this stage. First and foremost I want to thank Dr. Ayman El-Baz for his countless hours of patience and assistance in helping me overcome obstacles during this process. Thanks to his generous access to knowledge, labs and vast resources I have been able to complete my work. It has been a great honor to work with him and I could not have asked for a better advisor. Without his enduring help and assistance this thesis would have been next to impossible to complete.

I would also like to extend my thanks to Moo Chung, Qianqian Fang and John Valdes for their helpful and much appreciated correspondence in the fields of mesh generation and spherical harmonic analysis. Without their forward looking insights in to this field this work and this field would not be where it is today.

I am grateful for everything that the University of Louisville Bioengineering Department has given me as well. As a member of the first class of bioengineering students I have gotten to see and experience the growth of the department and the passion and dedication of the professors. I greatly appreciate everything I have been taught and am tremendously grateful for the opportunities and support I have been given from the faculty, staff and department as a whole.

Finally I want to profusely thank my family for the countless hours spent helping me finalize this thesis, giving me inspiration and for the years of support they have given me during this degree program and throughout life itself. I cannot thank them enough for giving me the opportunities in education, allowing me to pursue my desired path through life, and then giving me the assistance and loving support to walk that road. Above all others, they are ultimately responsible for the work I present here, and all my future endeavors.

ABSTRACT

Introduction: Autism is a complex developmental disability that typically appears during the first three years of life, and is the result of a neurological disorder that affects the normal functioning of the brain, impacting development in the areas of social interaction and communication skills. According to the Centers for Disease Control and Prevention (CDC) in 2009, about 1 in 110 American children will fall somewhere in the autistic spectrum. Although the cause of autism is still largely not clear, researchers have suggested that genetic, developmental, and environmental factors may be the cause or the predisposing effects towards developing autism. While shape based statistical analysis methods for autism are still in their early stages, current results show positive outlooks on the ability to detect differences between autistic and normal patients.

Methods: The goal of this thesis is to construct a complete package that is capable of taking 2-dimensional images from a standard medical scanner, and be able to construct a three-dimensional representation of the object and examine it through combination of its weighted linear spherical harmonics. The desired outcome is that a distinction can be made between the analysis of autistic and normal brain data. The analysis package created is divided into three distinct components that are capable of performing the complete analysis on a subject. The components included in the package in order of runtime are: volumetric extraction and mesh generation from 2-dimensional medical scanner data, spherical deformation of the constructed mesh, and weighted spherical harmonic representation and analysis.

Results: The minimum error for each brain following spherical harmonic reconstruction was calculated along with the fastest iteration at which the brain converged below the error thresholds of 11% and 10%. It was expected that due to the complexity of an Autistic brain these would require more iterations to converge to the same error level as a normal brain. It was also likely that within the number of iterations tested the autistic brains would record a larger final error due to this slower convergence rate. This was confirmed by the data. A global result was examined as well for the autistic and normal data groups. The overall minimum error for normal brain data was significantly lower than the autistic brain data. The average error for autistic brain data was significantly higher in both convergence measurements, but was dramatically higher in the 10% category.

Conclusion: Using this method of analyzing data can demonstrate accurate differences in normal and autistic brains. The research that has been generated in this thesis can clearly demonstrate that the normal brain data converged both faster and with a lower rate of error level than the Autistic brain data. This result proves that the autistic brain is a more complex structure, and would be more difficult to reconstruct using this Shape-Based Detection of Cortex Variability process.

TABLE OF FIGURES

LIST OF TABLES

TABLE OF CONTENTS

I. Introduction

A. Defining Autism

Autism is a complex developmental disability that typically appears during the first three years of life, and is the result of a neurological disorder that affects the normal functioning of the brain, impacting development in the areas of social interaction and communication skills. Difficulties can be identified in both children and adults with autism. The symptoms are identifiable in verbal and non-verbal communication, social interactions, and leisure or play activities. The classic form of autism involves a triad of impairments, these are typically in social interaction, in communication and the use of language, and in limited imagination as reflected in restricted, repetitive and stereotyped patterns of behavior and activities [1].

B. Historical Perspective

It was in 1943, that Leo Kanner, a psychiatrist at Johns Hopkins University, created the diagnosis of autism. Leo Kanner was an Austrian psychiatrist and physician known for his work related to autism. Kanner's work formed the foundation of child and adolescent psychiatry in the U.S. and worldwide. His first textbook, *Child Psychiatry* in 1953, was the first English language textbook to focus on the psychiatric problems of children [2]. His seminal 1943 paper, "Autistic Disturbances of Affective Contact", together with the work of Hans Asperger, forms the basis of the modern study of autism. By definition, patient symptoms are manifested by 36 months of age and are characterized by delayed and disordered language, impaired social interaction, abnormal responses to sensory stimuli, events and objects, poor eye contact, an insistence on sameness, an unusual capacity for rote memory, repetitive and stereotypic behavior and a normal physical appearance [3].

Relatively few neuropathological studies have been performed on the brains of autistic subjects. Of those reported, abnormalities have been described in the cerebral cortex, the brainstem, the limbic system and the cerebellum. Although, those individuals who have the disorder present with a specific set of core characteristics, each individual patient is somewhat different from another. Thus, it should not be surprising that the brains of these subjects should show a wide range of abnormalities. However, it is important to delineate the anatomic features, which are common to all cases, regardless of age, sex and IQ, in order to begin to understand the central neurobiological profile of this disorder. The results of systematic studies indicate that the anatomic features that are consistently abnormal in all cases include a reduced numbers of Purkinje cells in the cerebellum, and small tightly packed neurons in the entorhinal cortex, and in the medially placed nuclei of the amygdala. It is known that the limbic system is important for learning and memory, and that the amygdala plays a role in emotion and behavior. Research in the cerebellum indicates that this structure is important as a modulator of a variety of brain functions and impacts on language processing, anticipatory and motor planning, mental imagery and timed sequencing. Defining the differences and similarities in brain anatomy in autism and correlating these observations with detailed clinical descriptions of the patient may allow us greater insight into the underlying neurobiology of this disorder [4]

The many patterns of abnormal behavior that cause diagnostic confusion include one originally described by the Austrian psychiatrist, Hans Asperger [5]. The name he chose for this pattern was “autistic psychopathy” using the latter word in the technical sense of an abnormality of personality. This has led to misunderstanding because of the popular tendency to equate psychopathy with sociopathic behavior. Asperger emphasized the stability of the clinical picture throughout childhood, adolescence, and at least into early adult life, apart from the increase in skills brought about by maturation. The major characteristics appear to be impervious to the effects of environment and education. He considered the social prognosis to be generally good, meaning that most developed far enough to be able to use their special skills to obtain employment. He also observed that some who had especially high levels of ability in the area of their special interests were able to follow careers in, for example, science and mathematics.

C. Increase of Incidence

The reported incidence of autism spectrum disorders has increased markedly over the past decade [6]. It is believed that autism affects the information processing found in the brain through the alteration of nerve collections and their synapses [7].

From Congress to popular media, speculation is increasing that more children have autism than ever before. The three classifications of autism include autism spectrum disorders (ASD), Asperger syndrome (AS) and pervasive developmental disorder (PDD) [8].

A study done in 2008 by Rapin et al, shows that autism is now recognized in one out of 150 children making it a prevalent disorder [9, 10]. Additional studies by DiGuiseppi show a high prevalence among screened American children with as high as 6.4% of screened children showing at least a mild form of an autistic spectrum disorder [11, 12]. According to the Centers for Disease Control and Prevention (CDC) in 2009, about 1 in 110 American children will fall somewhere in the autistic spectrum. Although the cause of autism is still largely not clear, researchers have suggested that genetic, developmental, and environmental factors may be the cause or the predisposing effects towards developing autism [13].

There are other mathematical relationships between incidence and prevalence. An important nuance about prevalence is that its accuracy is only as good as the degree to which each individual who actually has the condition is counted (the numerator or top number of the fraction), and the completeness with which the “general” or other population has been counted (the denominator or bottom number of the fraction.) Accuracy in these two figures can be hard to achieve. In fact, there are no scientifically based epidemiological prevalence estimates for ASD in the United States at this time. Federal agencies have, however, called upon researchers to submit proposals that will develop better prevalence rates. [8].

Until research in the United States results in more accurate figures, the National Institutes of Health (NIH) have suggested the following prevalence rates for ASD based upon research in other Westernized, developing nations:

- 10/10,000 people with “classic” autism
- 20/10,000 people with ASD, including PDD
- 50/10,000 people with ASD, including PDD and Asperger syndrome.

These estimates are inclusive; that is, the third estimate includes people in the first two groups. This means that in a given large population, on average 0.5%, one-half percent of the population could be diagnosed with an ASD. [8]

D. Early Detection

Early detection allows for treatments to be attempted, thus minimizing the impact of the autism on the individual. Given currently available diagnostic instruments, autism and other pervasive developmental disorders (PDD) are difficult to detect in very young children. This may be due to several factors: presentation of symptoms varies from case to case; social and language deficits and delays may not be identified until the child is given the opportunity for peer interaction in preschool, low incidence leads to a low index of suspicion, and motor milestones are usually unaffected. Furthermore, there is no standard and easily administered screening instrument for young children. For all of these reasons, pediatric evaluations rarely identify autism before the age of 3 (Gillberg, 1990). However, evidence indicates that there is a large gap between the age of the child at the parents' first concern, the age of the first evaluation, and the age of a definitive diagnosis [12]. Parents are typically first concerned between the ages of 15 and 22 months (earlier for children who have co-morbid mental retardation), but the child is often not seen by a specialist until 20–27 months [14]. In addition, there is often further delay between the first visit to a specialist and a definitive diagnosis (Siegel et al., 1988). However, evidence shows that this delay in diagnosis causes additional distress to parents, as well as wasting valuable intervention time, indicating that professionals in the field of autism need instruments to aid in the detection of autism in very young children. [14].

Some forms of autism merely result in the individual exhibiting low social interaction, but more severe forms can result in severe mental retardation. These individuals may be prone to self injuring and aggressive behavior. There is no current cure for any forms, of autism. However, educational, behavioral, or skill-oriented therapies were designed to remedy specific symptoms in each individual. Such therapies can result in a notable improvement for the individual, especially when begun at a young age. [14].

E. Neuropathology of Autism

In identification of autism, the analysis of the neuropathology is important. The role of single-stranded microdeletions and epigenetic influences on brain development has dramatically altered our understanding of the etiology of the autisms. Recent research has focused on the role of synapse structure and function as central to the development of autism and suggests possible targets of interventions. Brain under connectivity has been a focus in recent imaging studies, and has become a central theme in conceptualizing autism. Despite increased awareness of autism, there is no 'epidemic' and no one cause for autism. Data from the sibling studies are identifying early markers of autism and defining the broader autism phenotype. [9].

The three sections of the brain analyzed are the gray matter, the white matter and the corpus callosum. Examination of the individual sections shows significant changes to the neuropathology of autistic individuals, suggesting a higher complexity in the autistic brain than the normal brain. [15]

The grey matter is the brain cortex that contains the nerve cells responsible for routing sensory or motor stimuli to inter-neurons of the central nervous system. In autistic individuals Abel et al. identified a decreased gray matter volume relative to a control group in the right paracingulate sulcus, the left inferior frontal gyrus, and an increased gray matter volume in amygdala and periamygda- loid cortex, middle temporal gyrus, inferior temporal gyrus, and in regions of the cerebellum [16]. Additionally Boddaert et al. found significant decreases of grey matter concentration in the superior temporal sulcus when comparing autistic child patients to normal child patients[17]. The autistic children also demonstrated a decrease in white matter concentration located in the right temporal pole and in the cerebellum. Herbert et al. applied a voxel-based-morphometry (VBM) approach to male patients between the ages of 7 and 11 years and showed that those with autism had a significantly larger volume of cerebral white matter (CWM) while cerebral cortex and hippocampus-amygdala had smaller volumes [18]. The corpus callosum is largest single fiber bundle in the brain and is responsible for connecting the two hemispheres of the brain. It has been proposed that there are significant differences between the CC of autistic and normal patients [19, 20].

The concept that the cerebellum might play a role in the coordination of attention in a fashion analogous to the role it plays in motor control and that in autism, cerebellum mal-development is a consistent feature that renders the child unable to adjust his or her mental focus of attention to follow the rapidly changing verbal, gestural, postural, tactile, and facial cues that signal changes in a stream of social information [21]. Such cues signal the normal child to move his or her "spotlight of attention" from one source of information (e.g., auditory) to another (e.g., visual). This process involves disengaging attention from one source and then moving and reengaging it on another (i.e., inhibition of one source and enhancement of another). To selectively adjust the focus of attention, the nervous system must quickly and accurately alter the pattern of neural responsiveness to sensory signals—from an enhanced neural response to certain stimuli (e.g., vocalizations) to an enhanced response to other stimuli (e.g., gestures), and from inhibited neural response to some stimuli to inhibited response to others. [22, 23].

F. Autism Detection Methods

One method of early detection intervention, utilizes medical providers to screen children using the M-CHAT as they were referred for early intervention services. The

Modified Checklist for Autism in Toddlers (M-CHAT) is designed to screen for early identification of autism spectrum disorder (ASD) in toddlers over the age of 12 months. Ideally, it is given at the 18-24 month well baby check. Parents complete the items on the checklist independently or by interview. Meeting the criteria suggests the risk of ASD and indicates a positive diagnosis for autism. The purpose is to survey parents to determine how their child responds to varied stimuli from toddler locomotion to a child's reaction to other people. M-CHAT users also incorporate the M-CHAT Follow-up Interview into the screening process, given that recent findings demonstrate that the interview greatly reduces the false positive rate, which avoids unnecessary referrals [14]. Therefore, these children were considered to be at risk for a developmental disorder, but none had received any specific diagnoses and none had received more than several weeks of minimal intervention services.

In new experiments at Yale University, the researchers studied a group of 2-year-olds with autism, as well as typically developing children with developmental disabilities other than autism. The Yale program of research focuses on mechanisms of socialization and their disruption in the autism spectrum disorders. This work includes a close collaboration with Warren Jones in the development of novel techniques to quantify social processes using eye-tracking technologies with a view to visualize and measure the ontogeny of social engagement. New data analysis strategies have been used with children, adolescents, and adults with autism spectrum disorders revealing abnormalities of visual scanning behaviors when viewing naturalistic social approaches and situations. In this study autistic children showed a preference for audio-visual synchronicity in the use of "pat-a-cake" videos, while the other children were more interested in the figure's movements regardless of audio-visual synchronicity. That pattern could be a clue about brain development and early signs of autism. [24, 25, 26, 27]

Dr. Klin of Yale University explains that within a few days after birth, normal developing children prefer watching biological motion -- the movement of living beings, such as their parents -- and that preference is an important survival skill and a building block for relationships. [25]

But Klin's group found that autistic children were more interested in "nonsocial contingencies," which are synchronicities that don't have any social meaning -- like two balls colliding and making a sound, or a stone falling when someone drops it. [24]

Researchers hope that a simple brain scan performed in infants and toddlers can presage the development of autism, leading to early detection and early intervention. The test involved using functional MRI to measure brain responses to spoken words in sleeping children. For this study, Dr. Eyler and her colleagues monitored the brain activity of 30 children with an autism spectrum disorder (aged 14 months to 46 months) and 14 "typical" children of roughly the same age. [28]

Children slept in the MRI machine while researchers read them bedtime stories. This allowed the investigators to see which parts of the brain were being activated in typical children versus children with autism. "In the typically developing children, both sides of the brain involved in language processing were activated. In the youngest children, the activation was about equal in both the right and left hemisphere, while in the older children, activity became more pronounced on the left side, which is similar to adult patterns and to be expected," Dr. Lisa T. Eyler explained. But in the autistic children, there was slightly more right hemisphere response than left hemisphere, and there was no change in activity across the age range. [28]

This leads to the conclusion that, in many children with autism, there are alterations either in structure growth or connectivity of the brain, but we really don't understand the implications of that for core features of autism, one of which is the problem with communication," David G. Amaral said. "This provides more evidence for abnormal connectivity in the brain." [28].

Further analysis of neurological MRI scans has been pursued in automated computer analysis of specific components of the brain. Approaches by El-baz et al. examine the shape model comparison between the corpus callosum in individuals with and without autism. This analysis focuses on comparison of the 3-dimensional voxel positioning. In such an automated technique, specific areas of MRI scan images are extracted. These images are then placed in a stack to recreate a volume of the image. The difference between regions of this volume can be statistically measured. While statistical analysis methods are still in their early stages, current results show positive outlooks on the ability to detect differences between autistic and normal patients based on voxel based analysis. The positive findings from automated analysis research provide the basis for the research done in this thesis. [15]

II. Data Analysis

A. Introduction

The goal of this thesis is to construct a complete package that is capable of taking 2-dimensional images from a standard medical scanner, and be able to construct a three-dimensional representation of the object and examine it through combination of its weighted linear spherical harmonics. The desired outcome is that a distinction can be made between the analysis of autistic and normal brain data.

B. Data Acquisition

The data for this thesis was acquired from a 1.5 T Signa MRI scanner (General Electric, Milwaukee, Wisconsin) using a 3-D spoiled gradient recall acquisition in the steady state (time to echo, 5 ms; time to repeat, 24 ms; flip angle, 45◦; repetition, 1; field of view, 24 cm2). Contiguous axial slices (1.5 mm thick) were obtained for each subject with 124 slices acquired per brain. The images were collected in a 192×256 acquisition matrix, and were 0-filled in k space to yield an image of 256×256 pixels. The effective voxel resolution of the scans is 0.9375×0.9375×1.5 mm^3. The positioning and placement of the subjects inside the MRI scanner was standardized. A total of 17 normal patients and 13 autistic brain data sets were used in this thesis. The test subjects age range is from age 8 to age 38 for both groups.

C. Package Overview

The analysis package created is divided into three distinct components that are capable of performing the complete analysis on a subject. The components included in the package in order of runtime are:

- Volumetric Extraction and Mesh Generation
- Spherical Deformation of the Mesh
- Weighted Spherical Harmonic Analysis

D. Volumetric Extraction

To begin a folder was selected containing images of MRI data for a brain. The images were segmented prior to being loaded into the software. In each image, a black pixel represented the background or portions of the image where no data existed, and the white pixels represented areas where data existed. (See figure1)

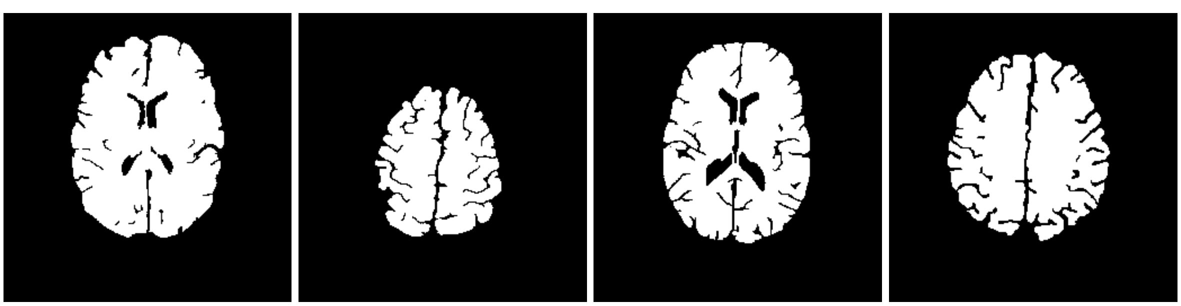

(a) (b) (c) (d)

Figure 1 - Normal (a-b) and Autistic (c-d) segmented brain images

The images were loaded into the software one at a time. It was first necessary to convert the images to binary format from their original grayscale format. It was assumed that any pixel with a value greater than zero would constitute a pixel containing data. Data values ranged from 0 to the maximum grayscale value (in many cases this value was 255 and represented a white pixel.)

Instead of iterating through the image and setting, each pixel to a value of 0 or 1 a simple mathematic manipulation was used. All values in the image were divided by the maximum value in the image. This made the upper bounds of the image 1 and the lower bounds 0. The entire image was then modified by using the ceiling command to raise all non-zero values to 1.

After each image was converted to a binary representation, the images were assembled in a 3-dimensional matrix stack. Each matrix was represented by an X, Y and Z dimension. The X dimensions represented the rows in an image. The Y dimension represented the columns in an image. The Z dimension represented the layers in the volume, with each layer containing a separate distinct image. Each X,Y,Z coordinate represented a single voxel in 3-dimensional space. An enhanced close-up view of the binary voxels in the brain volume matrix can be seen in Figure 2. Figures 3 and 4 show the 3-dimensional binary surface representation of an autistic and normal brain.

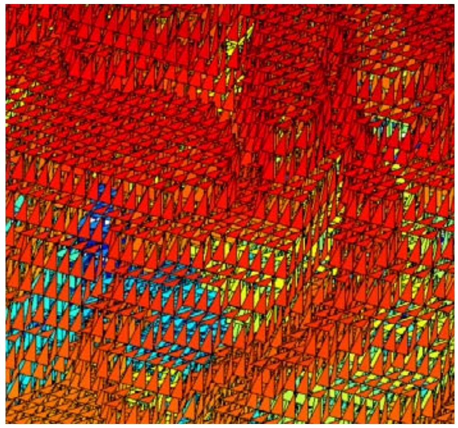

Figure 2 – Enhanced view of 3-dimensional binary voxels in a brain volume matrix

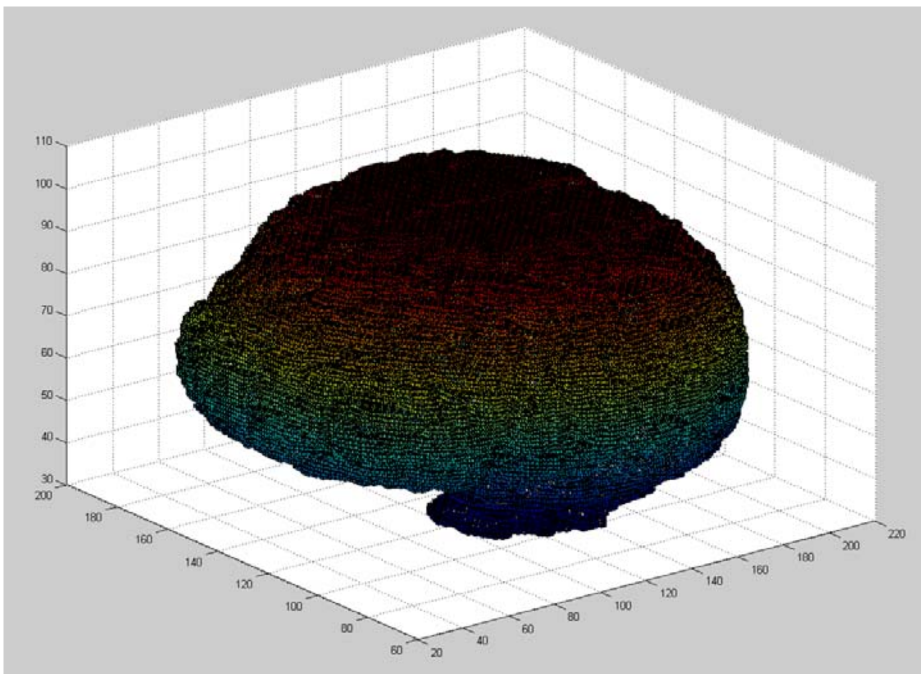

Figure 3 –3-dimensional binary representation of an autistic brain

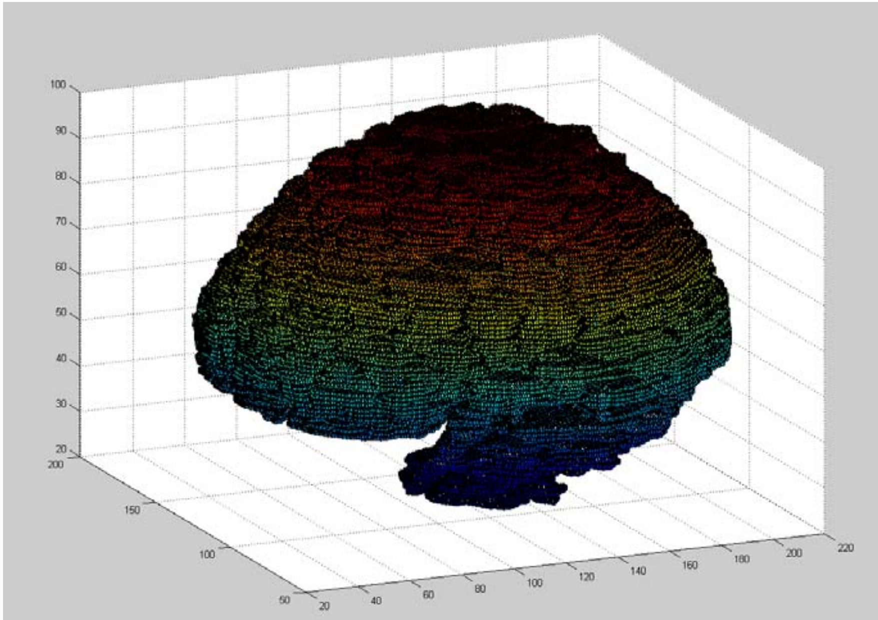

Figure 4 –3-dimensional binary representation of a normal brain

The MRI scan images were loaded into the memory with data holes intact. While initially the decision was made to remove all holes in the 2-dimensional images prior to being loaded into the program, this proved ineffective after the images were placed in a 3-dimensional volume. The initial hole removal procedure was done using Adobe Photoshop CS2. The exterior of the image, the area outside the outer edge of the brain, was initially selected as the mask. This mask was then inverted to select the outer bounds of the brain and all pixels inside the brain slice. The area inside the mask was then deleted. This process removed all holes found in the 2-dimensional image. Initially, this technique was believed to be successful, but it was later determined that 3-dimensional holes existed between image layers causing problems during mesh generation.

To solve this problem, the images were loaded with 2-dimensional holes still intact, as previously mentioned. The holes were removed using a custom algorithm. The algorithm began by loading the images into the 3-dimensional volume matrix as previously described. After creating the 3-dimensional volume matrix, an iterative pass was made across the X, Y and Z axis of the volume using the Matlab " fillholes()" command. To accomplish this, a 2-dimensional image slice was removed on each plane of the volume. This image slice was then passed through the "fillholes()" algorithm, and the modified image slice was reinserted into the volume. In this way, the holes were removed from the 2-dimensional representations in the X, Y and Z directions. Following this procedure, it was discovered that there still remained a large quantity of small holes throughout the image that could not be removed by converging the image using a 2-dimensional technique. These holes were formed from differing overlaps in the volume between layers, and the tendency of the 2-dimensional algorithms to produce small holes in the planes not being converged.

To remove these holes, each individual pixel was iterated in the 3-dimensional matrix. For each pixel, it was calculated if there was a pixel belonging to the image in the ±X, ±Y and ±Z directions between the origin pixel and the edge of the volume. In Figure 5 (a), the origin pixel is defined as the red pixel, the blue neighbor pixels are the ±X, ±Y and ±Z directional pixels, and the clear pixels represent unchecked points. Figure 5 (b), shows the same image with the unchecked pixels removed for easier visibility. From the image points, outgoing vectors were tested in each of the six directions. Figure 5 (c), illustrates the path of testing that each neighbor pixel would expand from towards the outer edge. If a pixel value of 1 was found in a given direction, a value of true was marked for the boolean corresponding with that direction.

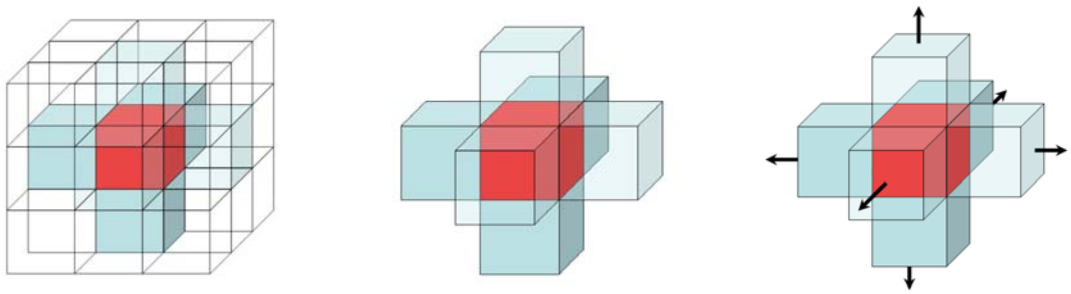

(a) (b) (c)

Figure 5 –(a) The original cube of pixels, (b) Showing the starting neighbor pixels in the 6 cardinal directions, (c) The outward directions of movement for the detection iterations

If a pixel was found radiating out in all six directions, it was determined that the pixel was a hole in the image. A pixel that did not contain pixels surrounding it on all six sides was ignored. This procedure was repeated until holes no longer remained in the image. This was often accomplished in a single iteration. To ensure that the volume was clean, an additional iteration was always repeated to verify that no holes remained in the volume.   This procedure did add a significant amount of time to the pre-meshing procedure, but the benefits of this step outweighed the time cost significantly because it prevented the occurrence of holes during mesh construction.

<u>E. Mesh Generation</u>

Once the 3-dimensional volume had been properly constructed, the mesh was generated. The mesh generation was performed using a modified version of the iso2mesh Matlab based mesh generation system, written by Qianqian Fang and David

Boas [29, 30]. This system is built on the CGAL Delaunay Triangulation mesh engine. This is a non-rigid mesh generation engine, and points are not constrained to contain a specific number of neighbor nodes. The upper limit to the number of nodes was initially restricted to 49,762 nodes. Due to the complexity of the spherical deformation algorithms, the maximum node count was reduced to 12,500 nodes, so that calculations could be completed in a time appropriate manner.

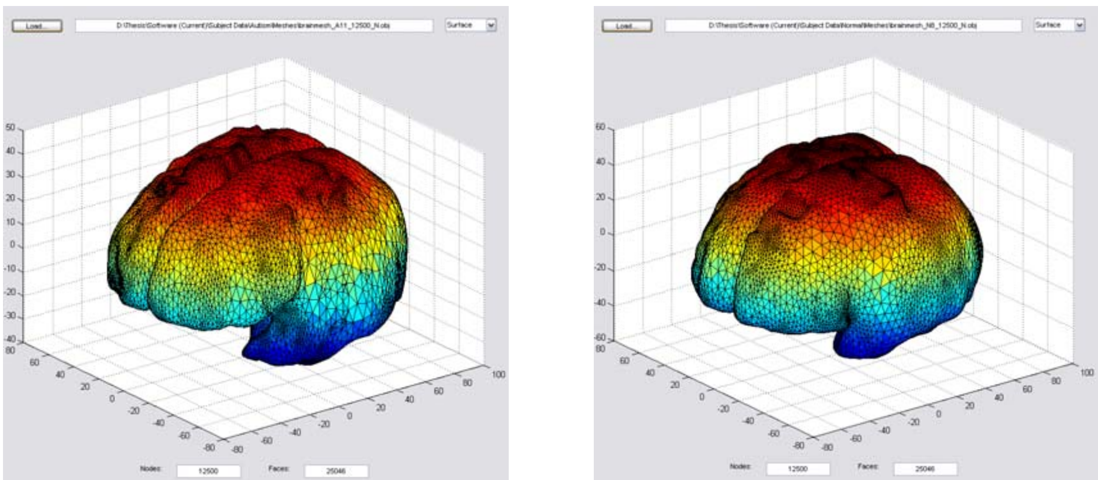

(a) (b)

Figure 6 – Mesh renders for (a) an autistic and (b) a normal brain.

The data received from the mesh generation, was a collection of nodes and triangulations. The nodes matrix was of dimensions 3xN, and the triangulations matrix was of dimensions 4xT, where N is the maximum allowable amount of nodes and T varies based on the positions used by the mesh engine and the triangulations created between points. The fourth column in the triangulation matrix, represented that the face connectivity at this point existed. This column was removed to create the traditional 3xT representation of mesh triangulations, because in a restricted mesh all values in this column were true.

Once the initial mesh was created, it was necessary to reposition it in 3-dimensional space and to resize the mesh to appropriate proportions. The centroid of the mesh was calculated in the X, Y and Z directions. Using the coordinates of the centroid, the mesh was repositioned so that it was centered on the origin in 3-dimensional Cartesian space (x = 0,y = 0,z = 0). The initial mesh results were not scaled properly due to the acquisition methods of the MRI scanner. To appropriately resize the mesh, original image slice acquisition scaling was used. The images were repositioned according to the X, Y and Z magnification parameters. The X and Y planes were multiplied by a magnification factor of 0.93, taken from the MRI scanner acquisition parameters. The Z plane was scaled by a factor of 1.5, the distance between slices taken during MRI acquisition.

The mesh generation returned a node and face cluster where vertices were positioned at sharp angles to one another. This made the mesh appear to be "spiky." To solve this problem, a Vertex-based anisotropic smoothing filter was applied to the data. The filter performed a low-pass filter Laplace smoothing algorithm across the exterior of the mesh. The low-pass filter Laplace smoothing algorithm was based on code written by Zhang and Hamza in the paper "Vertex-based anisotropic smoothing of 3D mesh data, IEEE CCECE" [31]. The smoothing algorithm was applied iteratively three times during the procedure, and was configured to smooth at a minimal value with each pass. The result was a mesh with smooth and accurate contours.

The file format chosen to save the mesh was the Wavefront OBJ format, developed by Wavefront Technologies. Initially, it was suggested to use the MNI OBJ format. This format was ultimately decided against due to a restriction in the maximum number of neighbor nodes it was capable of storing. Another factor was that it was largely incompatible with the standardized Wavefront OBJ format that is the format of choice for OBJ file representations in a majority of commercial applications. The Wavefront OBJ format is capable of being read by nearly all modern commercial and open-source application dealing with mesh analysis, and would allow for future integration of the system with third-party software. The exact format can be found in Appendix I. Custom algorithms were written to save and load meshes in this format.

F. Spherical Deformation

Following the generation of a stable, hole-free initial mesh, it was necessary to generate a corresponding unit sphere. The accuracy of the sphere creation is relative to the accuracy of the statistical analysis. There were several techniques attempted including Cartesian and spherical registration methods.

The initial attempt to create a unit sphere was to simply inflate the original mesh into a unit sphere. This technique was done by reducing all points in the mesh to a maximum distance of 1.0 from the origin. Once the mesh had been scaled, all points with a value less than 1.0 were upscaled to a value of 1.0. This inflation technique resulted in numerous problems, with the most problematic being vertex overlap and poor distribution of points. The natural shape of the brain sulci and the valley located between hemispheres in the brain created this overlap by inverting points and face connectivity, as they were forced to the outer edges of the inflated sphere.

In the creation of a unit sphere, it became imperative that all points remain in their correct orientation with their neighbor points during the deformation process. This means that during deformation the triangulation connections could not become crossed. A unit sphere that contained crossed triangulations produced an erroneous spherical representation. The spherical harmonics are based on angular values, and points with incorrectly crossed angles caused the system to produce "garbage" result data and a spherical representation could not be created.

The accuracy of the spherical representation was also based on the distribution of the vertex coordinates throughout the sphere. A sphere with clusters of vertices and other areas of sparse vertex placement produced significantly more error and had a greater difficulty converging. The ideal spherical representation would have all vertices spaced equidistant from one another across the surface of the sphere. While it is possible to perform an analysis using an improperly spaced unit sphere, the results were less than desirable. The original method left large clusters of vertices around areas of significant sulcus curvature in the brain.

F. Cartesian Coordinate Registration

In an effort to refine the spherical representation, several approaches were attempted. The first attempted method, was 3-dimensional Cartesian volume registration. A perfect unit sphere was used as the destination mesh and the brain mesh undergoing registration functioned as the origin mesh. Points were associated with the nearest coordinate based on Euclidean distance. Once a point was identified, the point was then removed from the possible pool of points to be selected from for registration. This method seemed like it would be effective, but it was quickly discovered that a representation of the brain is irregular. Points deep in between the two lobes of the brain caused significant problems. These points would often be associated with corresponding locations on the destination unit sphere on the opposite side of the sphere from where they should be. Due to occurrences of this phenomenon at numerous locations, the origin mesh became stretched inside out. While the ultimate result did align all points on a sphere, it created an unusable mesh. Nearly 95% of the triangulations became crossed during this process rendering the registration invalid.

G. Spherical Coordinate Registration

Following the failure of the Cartesian registration, a registration technique based on spherical angles was attempted. A perfect unit sphere was once again generated as the destination mesh, and the inclination angle and azimuth angle for each coordinate was extracted. The same angles were calculated for every point in the origin mesh. The registration was based on angular locations as the difference in radial distance became irrelevant. The following equation was used to calculate the error between angles.

$$\epsilon = \left|\theta_i - \theta_j\right| + \left|\varphi_i - \varphi_j\right|, \qquad (1)$$

$$1 \leq i \leq \#\, nodes, \qquad 1 \leq j \leq \#\, unregistered\ nodes$$

Equation 1

The angles that produced the lowest error (closest to zero) were then registered to one another. The registered coordinates were then removed to prevent reuse. This method produced a more acceptable result but ultimately failed as well. This was due to the positioning and number of neighbor triangulations in the unit sphere. A perfect unit sphere has only 6 neighbor nodes for every point, while each node in the brain mesh possessed between 3 and 14 neighbor nodes depending on its location. After the discovery in the number of neighbor nodes, it was decided that this technique would not be feasible without a highly complex unfolding algorithm to unravel the triangulations after registration. This required the development of a method other than registration to an already existing unit sphere.

G. Attraction-Repulsion Deformation

The final process, used in the creation of a unit sphere is a four phase deformation technique, created for the purpose of deforming the brain meshes. Before running the spherical deformation, the brain was heavily smoothed using a Laplacian based smoothing algorithm. The mesh was loaded into the freely available software, MeshLab v1.2.3b written by Paolo Cignoli. It was determined through trial and error that an average smoothing of 400 iterations per 12,500 nodes deformed the mesh so that no existing points in the mesh could be found residing on the same theta and azimuth angles, when examined in spherical coordinate space. (See Figure 7) The choice to use MeshLab instead of a Matlab based smoothing algorithm was made to improve speed. The comparable Matlab algorithm took approximately 30 seconds to run one complete Laplacian smoothing pass. The same algorithm run in MeshLab was capable of performing 2000 Laplacian smoothing passes in slightly under one minute.

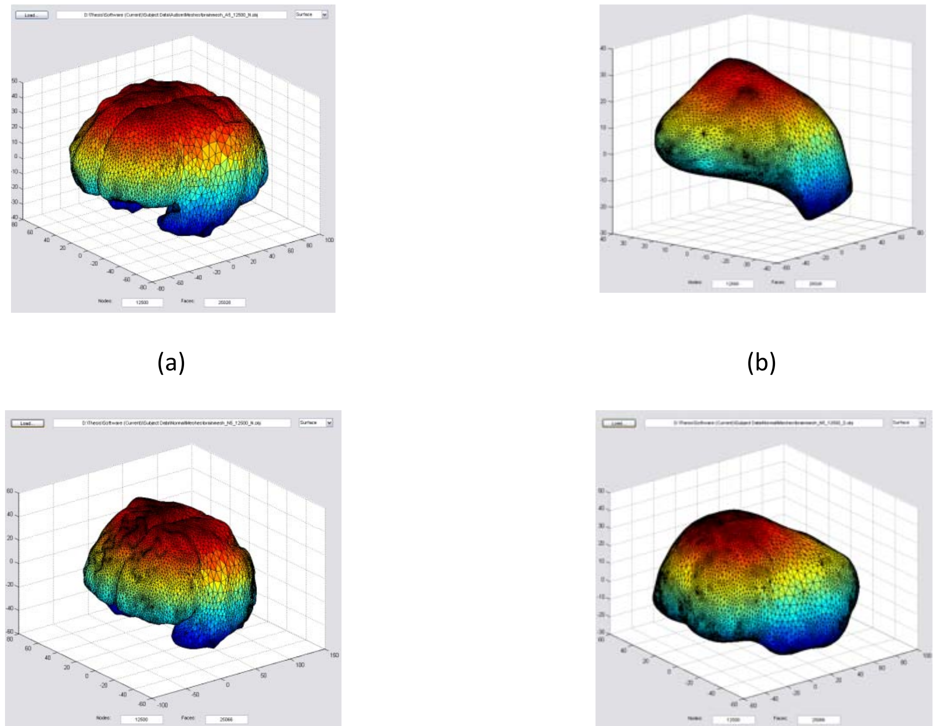

(a) (b) (c) (d)

Figure 7 – (a) An autistic brain render and (b) the render after 400 iterations of Laplacian smoothing. (c) A normal brain render and (d) the render after 400 iterations of Laplacian smoothing.

The technique is composed of the following four phases

- The Laplacian deformation step.
- The unit sphere distance deformation.
- The Attraction-Repulsion algorithm refinement step.
- A second unit sphere distance deformation.

In the Laplacian deformation phase, the brain is smoothed until all curves, peaks and valleys of the cortex are flattened across the brain. This ensures that no more than one point will be found for a given set (azimuth and theta angles) of spherical coordinates. This mesh is then resaved as a smooth mesh object which will be loaded for the second through fourth phases.

The unit sphere distance deformation involves inflating the smoothed mesh to the distance of a unit sphere. To increase the speed of the spherical inflation it is necessary to manipulate the mesh in the spherical coordinate domain. The Cartesian mesh is first converted to spherical coordinates using the "cart2sph" command in Matlab. This returns a Theta angle, Azimuth (Phi) angle and R distance for each point in the mesh. The R distance is removed and replaced with a matrix of the same size with all values equal to 1.0. The coordinates are then reconverted to Cartesian using the sph2cart command in Matlab. This provides a fast and effective conversion that is extremely efficient, because it requires no iterative processing and does not involve examining each node individually or performing any distance calculations. These inflated points are then passed on to the third phase.

In the third phase, the attraction-repulsion algorithm is used to refine the inflated sphere. The attraction-repulsion algorithm is based on a standard spring algorithm. The algorithm was inspired by a concept used in Graphic Art Design for inflating objects. The purpose of this algorithm is to reposition the nodes in the mesh. After the second phase of the spherical deformation, there are large clusters of nodes spaced near one another in areas of the mesh that contain a high density of nodes. Looking at the mesh, it is possible to see large clusters near the lower lobes of the brain and around complex areas. As previously mentioned, it is necessary to evenly space the nodes across the sphere. To accomplish this, the attraction-repulsion algorithm was created.

The attraction-repulsion algorithm is composed of two steps, the attraction step and the repulsion step. Each node is altered by being processed in the attraction step and then the repulsion step. In the attraction step the node is altered based on its neighbor nodes. The distance between a node and each of its neighbor nodes is calculated. The node is then pulled based on numerical weighting, so that it becomes centered between its neighbors. The attraction for iteration i is defined as:

$$A_{i+1} = A_i + \left(\overline{Q_N P_j}\right)(D^2)(0.01) + \left(\overline{P_j Q_N}\right)\left(\frac{0.00001}{D}\right),$$
$$1 \le j \le number\ of\ nodes, \qquad 1 \le N \le number\ of\ neighbors \qquad (2)$$

Equation 2 – Attraction algorithm

where A_{i+1} represents the new node coordinate and A_i is the original node coordinate. P represents the original coordinate of the unmodified node that is and Q is the coordinate of neighbor node N. The distance from P to Q is a 3-dimensional Euclidean distance.

After the node has been centered between its neighbors it is processed in the repulsion step. Here the node is slightly readjusted by every node in the mesh. Each node minimally repels one another so that the nodes do not cross or touch. The repulsion is defined as:

$$R_{i+1} = R_i + \left(\overline{Q_k P_j}\right)(T)\left(\left(\frac{1.5}{\left(\overline{Q_k P_j}\right)^2}\right)\left(\frac{1}{2N}\right)\right), \qquad (3)$$

$$1 \leq j \leq number\ of\ nodes, \qquad 1 \leq k \leq number\ of\ nodes$$

Equation 3 – Repulsion algorithm

where R_{i+1} represents the new node coordinate and R_i is the original node coordinate. N represents the total number of nodes in the mesh. T is a value between 0 and 1 and stands for the time step of the algorithm. A larger time step enables the algorithm to converge faster but increases the chance of error as nodes are capable of moving larger distances.

This algorithm also causes an inflation effect to occur during repeat iterations as each node is gently repelled from interior angles by nodes opposite it on the unit sphere. Because there are no nodes outside the unit sphere to repel the nodes back toward the center this inflation occurs. This step is repeated several times until a satisfactory node distribution is reached. (See Figures 8 and 9)

Once the attraction-repulsion algorithm has completed, the nodes are more evenly spaced on the sphere. Due to the previously described interior repulsion, the sphere is also much larger than a unit sphere of radius 1 at this point. To alleviate this phenomenon, the unit sphere distance deformation algorithm is run a second time. While this algorithm does not alter the angular placement of the nodes, it will reduce the R values back to 1 for all nodes. This is the same algorithm that is run during phase 2. Following this deformation the newly created unit sphere mesh is written back into a Wavefront OBJ file. (See Appendix I)

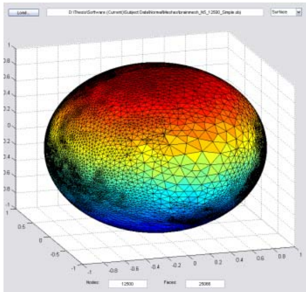

(a)

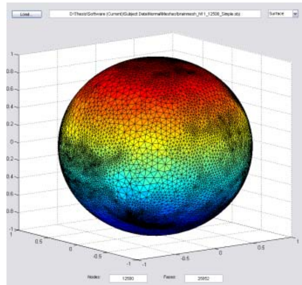

(b)

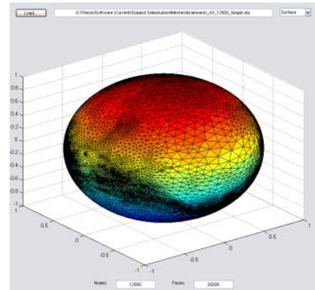

(c)

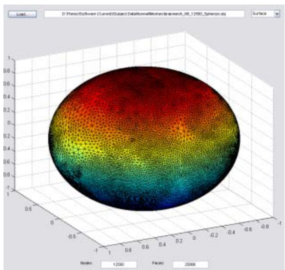

(d)

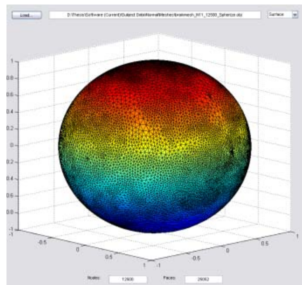

(e)

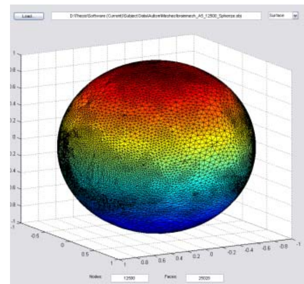

(f)

Figure 8 – Simple spherical inflation of normal brains (a,b) and an autistic brain (c) and the spheres after 3 iterations of the Attraction-Repulsion algorithm have been applied (d-f).

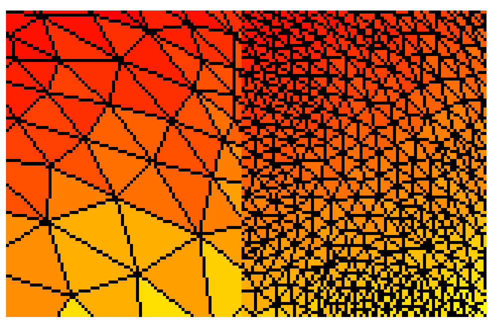

Figure 9 – Simple spherical inflation of normal brains (a,b) and an autistic brain (c) and the spheres after 3 iterations of the Attraction-Repulsion algorithm have been applied (d-f).

H. Weighted Spherical Harmonic Analysis

The weighted spherical harmonic representation (weighted-SPHARM) is a surface modeling framework that can be used in encoding cortical shape information. The technique was developed by Moo K. Chung, Kim M. Dalton and Richard J. Davidson. The weighted-SPHARM representation is a spectral method [32], where a linear combination explicit basis functions is used to represent noisy cortical surface data. The basis expansion corresponds to the solution of an isotropic heat equation on a unit sphere. The result of the weighted-SPHARM is explicitly given as a weighted linear combination of spherical harmonics. This provides a more natural setting for statistical modeling. The representation can be further used in surface registration that reduces the improper alignment of brain sulcus folding patterns between subjects and across hemispheres within a subject.

The system generates harmonics from the original distribution of coordinates. This ensures that the same neighbor nodes are connected in the same order between the original and the reconstructed mesh. The harmonics are specifically generated from the unit sphere corresponding to the original mesh. The original Cartesian coordinate system of the corresponding unit sphere mesh parameterizes a coordinate $v_i = v_i(x, y, z)$ to spherical coordinates with a polar angle between 0 and π and an azimuth angle between 0 and 2π. Each point is then represented as a spherical coordinate that can be expressed as $v_i = v_i(\theta, \varphi)$. The distance from the origin, or R value, in spherical space is always equal to 1.0 for any given point on a unit sphere. [33]. The paper by Chung et al. defines the values of θ and ϕ for purposes of calculation as:

$$\theta_{SPHARM} = \frac{\pi}{2} - \varphi, \qquad \varphi_{SPHARM} = \pi + \theta \qquad (4)$$

Equation 4

The spherical harmonic $Y_{lm}$of degree l and order m [5] [6]is defined as:

$$Y_{lm} = \begin{cases} c_{lm} P_l^{|m|}(cos\theta)\sin(|m|\varphi)\,, & -l \leq m \leq -1, \\ \frac{c_{lm}}{\sqrt{2}} P_l^{|m|}(cos\theta), & m = 0, \\ c_{lm} P_l^{|m|}(cos\theta)\cos(|m|\varphi)\,, & 1 \leq m \leq l, \end{cases} \qquad (5)$$

Equation 5

$$c_{lm} = \sqrt{\frac{2l+1}{2\pi}\frac{(l-|m|)!}{(l+|m|)!}} \qquad (6)$$

Equation 6

where $P_l^{|m|}$ is the associated Legendre polynomial of order m [33,34]. These form a form a polynomial sequence of orthogonal polynomials [33].

For the purpose of this thesis only positive degrees of harmonics were used. For each degree Y_{lm} represents the Fourier coefficients capable of reconstructing the spherical harmonic as specified in code written by Moo K. Chung. This code saves the coefficients of the spherical harmonic in a new file for each degree. These can then be reloaded to expedite future calculations. [34].

A final reconstruction is created by iteratively using the desired number of harmonics to reconstruct the original brain in a linear fashion. As each harmonic is loaded into memory, it is multiplied by a factor sigma which is equivalent to the smoothing of the harmonic. A larger sigma value indicates a higher degree of smoothing, while a smaller sigma value preserves more of the data from the current harmonic degree. These values are then linearly added to the previous coordinate value, and the new coordinate is formed. During reconstruction of the original mesh, the surface coordinates can be modeled independently according to the equation:

$$v_i(\theta, \varphi) = h_i(\theta, \varphi) + \epsilon_i(\theta, \varphi) \quad (7)$$

Equation 7

where $v_i(\theta, \varphi)$represents the new coordinate, $h_i(\theta, \varphi)$ represents the original coordinate, and $\epsilon_i(\theta, \varphi)$ is the linear modifier constructed from the combination of the smoothing sigma value and the residual Fourier values for the specified coordinate calculated for the current spherical harmonic degree. This procedure is repeated for the desired number of harmonics, and a final resulting mesh is produced and returned to the user [35].

The error between the reconstructed brain mesh and the original brain mesh is found by calculating the 3-dimensional Euclidean distance between corresponding points in the original mesh and the reconstructed mesh. Due to the strict ordering of the data storage in the harmonics, the reconstructed mesh and the original mesh are already registered to one another, and thus do not require additional registration, simplifying the calculations required. Additionally, for visualization purposes, the same connected set of faces is used for both the original and reconstructed mesh [35].

III. Results

A. Visualization

All subject data was processed identically, and results were analyzed for sigma smoothing values of 0.01, 0.001, 0.0001 and 0.00001. Figure 10 through 13 demonstrate sample mesh visualizations for Autistic and normal patients. Full tables of data may be found in Appendix II.

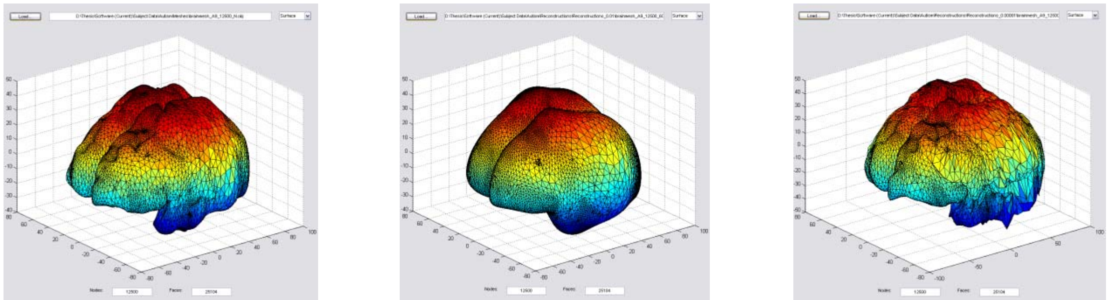

(a) (b) (c)

Figure 10 – Autistic subject A9. (a) Original mesh, (b) Reconstruction with σ=0.01, (c) Reconstruction with σ=0.00001

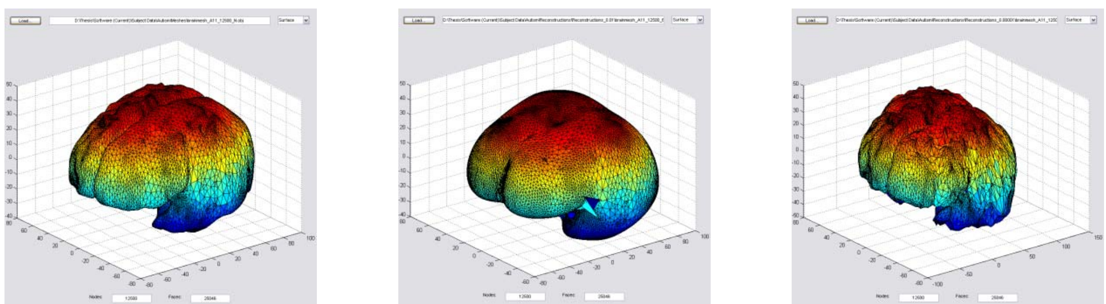

(a) (b) (c)

Figure 11 – Autistic subject A11. (a) Original mesh, (b) Reconstruction with σ=0.01, (c) Reconstruction with σ=0.00001

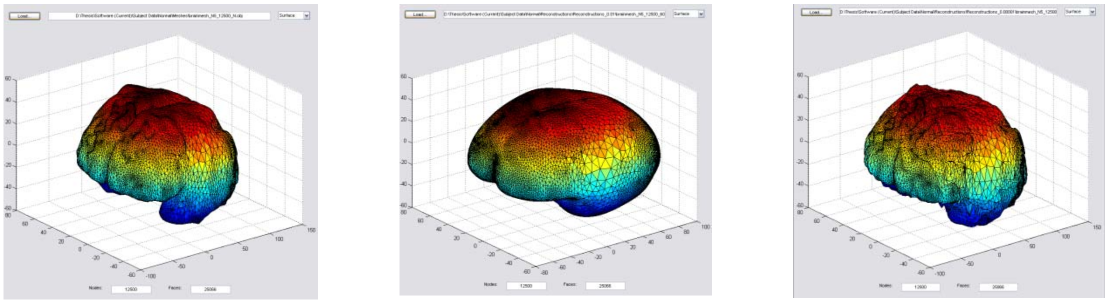

(a) (b) (c)

Figure 12 – Normal subject N5. (a) Original mesh, (b) Reconstruction with σ=0.01, (c) Reconstruction with σ=0.00001

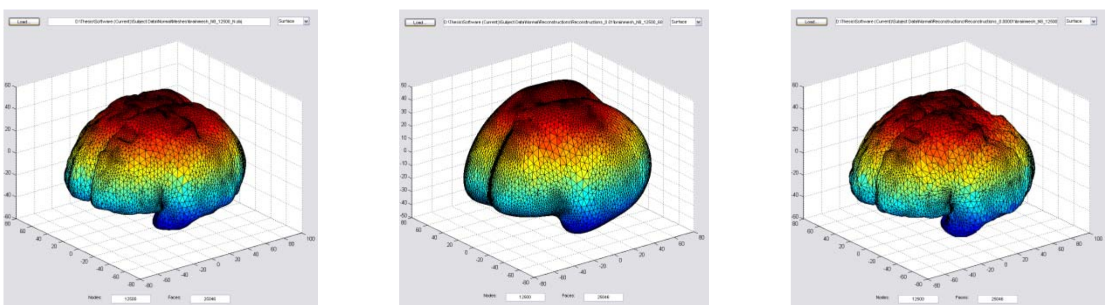

(a) (b) (c)

Figure 13 – Normal subject N8. (a) Original mesh, (b) Reconstruction with σ=0.01, (c) Reconstruction with σ=0.00001

B. Statistical Analysis

The error for each reconstruction was calculated for every set of harmonics in each of the patients. These errors were then analyzed to find the iteration at which a reconstructed brain demonstrated accuracy below a certain threshold. The thresholds of 11% and 10% were selected for accuracy. Due to the slow convergence of many of the autistic brains, an iteration value of 61 has been used to represent that the brain did not converge below the threshold within the initial 60 iterations used. Additionally, the maximum accuracy reached for each subject is included in addition to the iteration of convergence. It should be noted, that a few of the tested meshes did not return a numerical error matrix during the reconstruction. These data sets have been excluded, because they were unable to be analyzed. This is due to an error in the mesh generating singular Fourier residual matrices.

The error curves for each data set show the rate of convergence and the maximum convergence visually for a specific brain. The black lines represent autistic subjects while the blue lines represent normal patients.

C. Evaluation at σ = 0.01

With a smoothing value of σ = 0.01 the majority of the data is lost during the reconstruction. It is of notable importance that there is little distinction between the error curves of the normal and autistic brains. While final errors are ultimately reduced in many of the data sets, there is no clear way to distinguish an autistic brain from a normal brain based on data reconstructed with a smoothing σ = 0.01. (See Figure 14, Table 1). A probability density functions for the autistic and normal data groups was generated for number of iterations to reduce error below 11% and 10% in the brain mesh and for the minimum error reached. While there is a clear distinction at some levels there is significantly more overlap between the peaks found at this large sigma value than the overlap found at smaller sigma values.

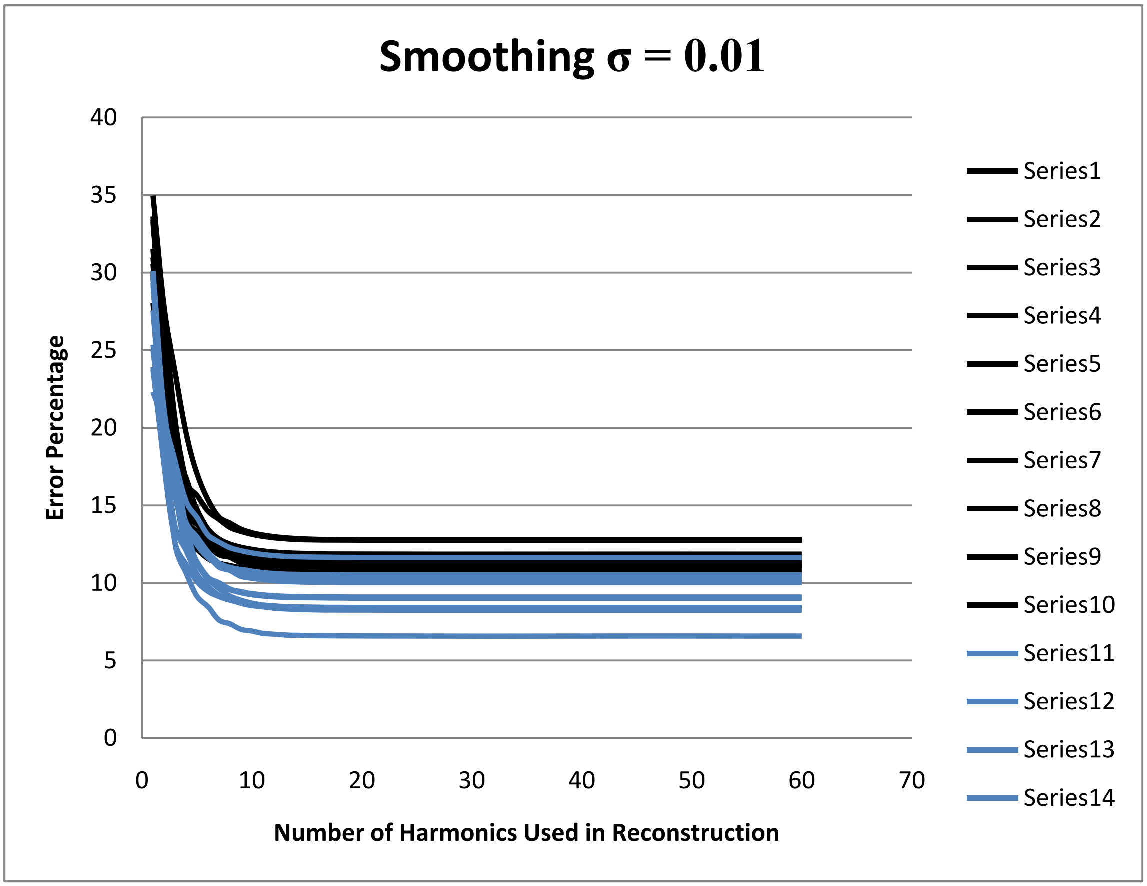

Figure 14 – Error curves for autistic (black lines) and normal (blue lines) brains during reconstruction using a smoothing σ = 0.01.

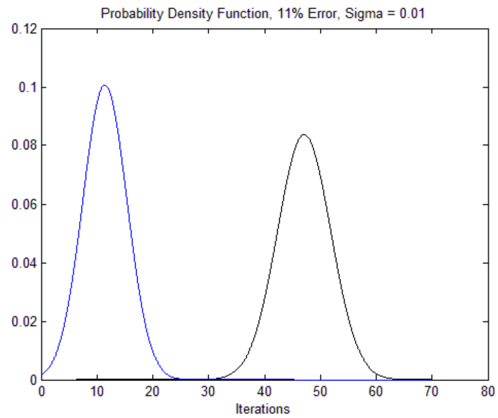

(a)

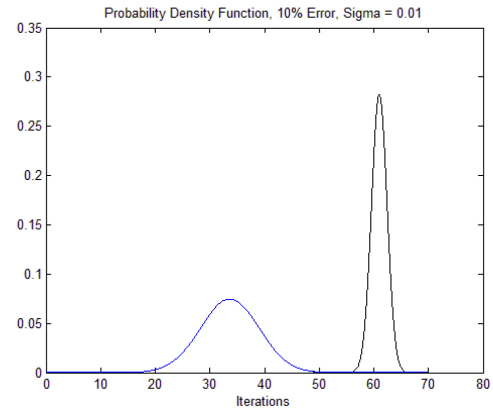

(b)

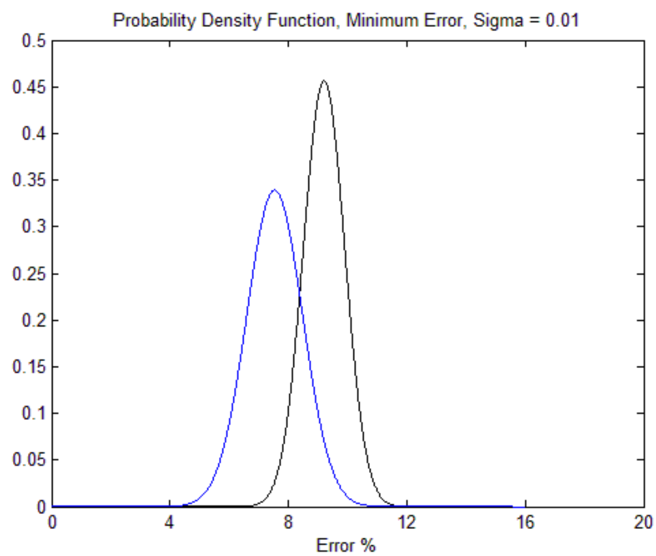

(c)

Figure 15– Probability Density Function graphs of smoothing σ = 0.001 for (a) 11% error, (b) 10% error, and (c) minimum error.

	Smoothing σ = 0.01		
	Error below < 11% (Iteration)	Error below < 10% (Iteration)	Lowest Error
A1	24	61	11
A2	9	61	10.677
A5	61	61	11.861
A6	61	61	11.548
A8	61	61	12.754
A9	11	61	10.602
A10	61	61	12.769
A11	61	61	11.342
A12	61	61	11.232
A13	61	61	11.185
N2	61	61	11.641
N3	8	61	10.461
N4	8	61	10.296
N5	5	6	8.2451
N6	8	61	10.286
N8	4	5	6.5738
N9	5	6	8.4194
N10	6	7	9.0182
N11	9	7	9.0953
N13	8	61	10.033
N16	9	61	10.526
N17	6	7	8.3444

Table 1– Convergence iteration and lowest error for a smoothing σ = 0.01.

D. Evaluation at σ = 0.001, 0.0001 and 0.00001

As the smoothing over the mesh is lowered, the amount of data used from each harmonic is increased. The harmonics begin to converge much faster in these reconstructions. It is also important to note, that visually on the graphs a noticeable differentiation can be observed between the three lower σ values and the largest σ of 0.01. (See Figures 15, 17, 19) By the time the data reaches an σ = 0.00001, the groups have nearly entirely separated from one another with only one normal brain overlapping into the autistic error curves. It is also important, that the normal error curves can be observed to converge at a faster rate than the autistic error curves. (See Tables 2,3,4 for numerical information relating to these figures).

At each smoothing sigma a corresponding probability density functions for the autistic and normal data groups was generated for number of iterations to reduce error below 11% and 10% in the brain mesh. A probability density function was also generated for the minimum error for each group. A clear distinction can be seen in the peaks in all three comparisons for each of the below smoothing factors. Additionally, the peaks become more separated as the smoothing sigma is reduced to a smaller value.

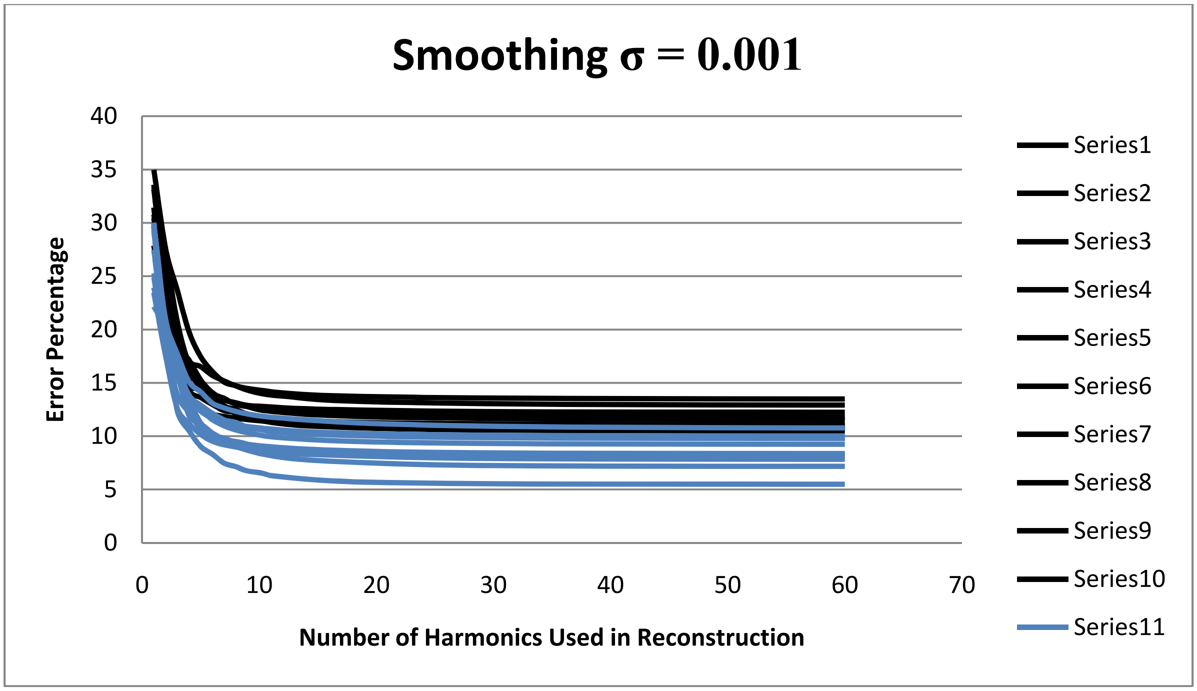

Figure 16 – Error curves for autistic (black lines) and normal (blue lines) brains during reconstruction using a smoothing σ = 0.001.

	Smoothing σ = 0.001		
	Error below < 11% (Iteration)	Error below < 10% (Iteration)	Lowest Error
A1	61	61	11.104
A2	21	61	10.849
A5	61	61	11.782
A6	61	61	12.25
A8	61	61	13.49
A9	21	61	10.72
A10	61	61	12.918
A11	61	61	11.576
A12	14	61	10.483
A13	32	61	10.943
N2	26	61	10.771
N3	9	61	10.018
N4	7	11	9.2371
N5	5	6	7.8352
N6	8	22	9.807
N8	4	5	5.5004
N9	5	6	8.0435
N10	6	7	8.3774
N11	6	7	8.3001
N13	9	29	9.9082
N16	8	21	9.7918
N17	6	7	7.1729

Table 2– Convergence iteration and lowest error for a smoothing σ = 0.001.

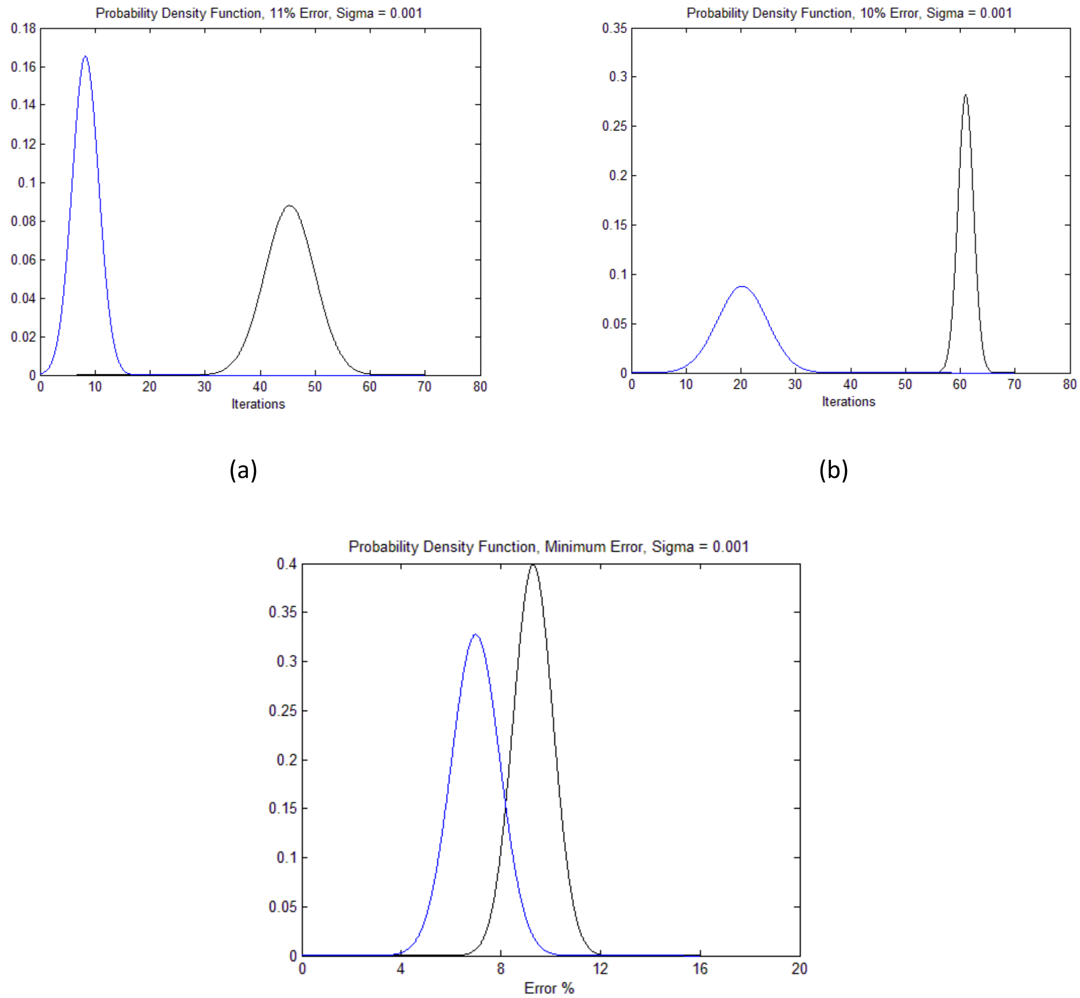

(c)

Figure 17– Probability Density Function graphs of smoothing σ = 0.001 for (a) 11% error, (b) 10% error, and (c) minimum error.

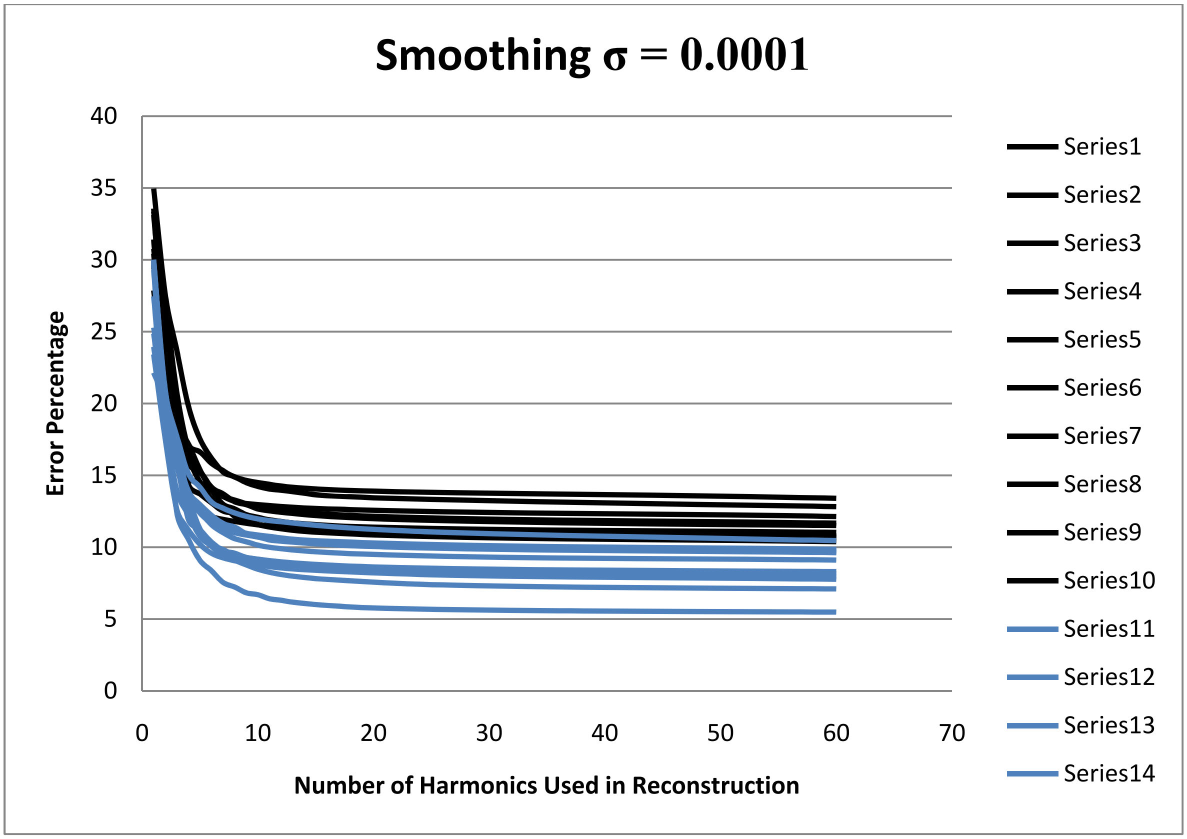

Figure 18 – Error curves for autistic (black lines) and normal (blue lines) brains during reconstruction using a smoothing σ = 0.0001.

	Smoothing σ = 0.0001		
	Error below < 11% (Iteration)	Error below < 10% (Iteration)	Lowest Error
A1	61	61	11.027
A2	25	61	10.693
A5	61	61	11.675
A6	61	61	12.134
A8	61	61	13.402
A9	27	61	10.674
A10	61	61	12.818
A11	61	61	11.507
A12	16	61	10.379
A13	34	61	10.788
N2	28	61	10.457
N3	9	42	9.8522
N4	8	11	9.1036
N5	5	7	7.7681
N6	9	27	9.6295
N8	4	5	5.4782
N9	5	6	7.9446
N10	6	7	8.3042
N11	6	7	8.1497
N13	9	37	9.7317
N16	9	22	9.6309
N17	6	7	7.0995

Table 3– Convergence iteration and lowest error for a smoothing σ = 0.0001.

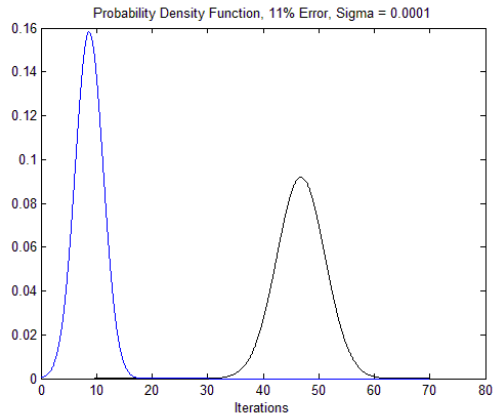

(a)

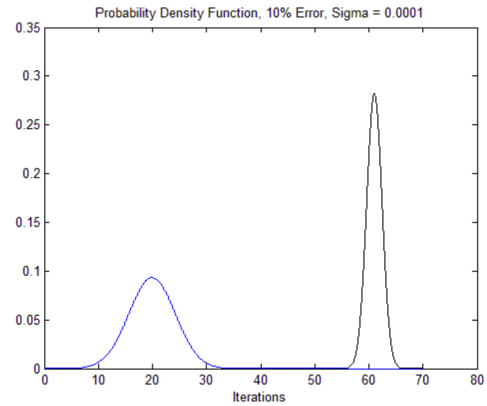

(b)

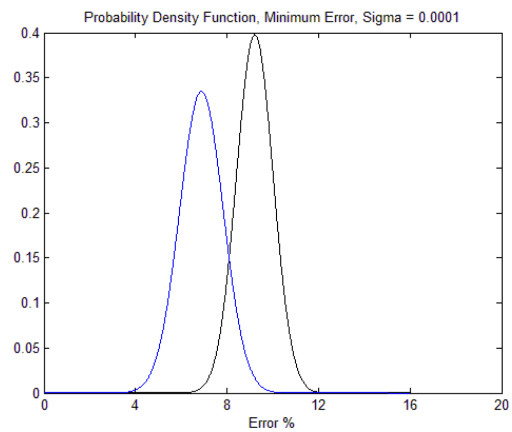

(c)

Figure 19– Probability Density Function graphs of smoothing σ = 0.0001 for (a) 11% error, (b) 10% error, and (c) minimum error.

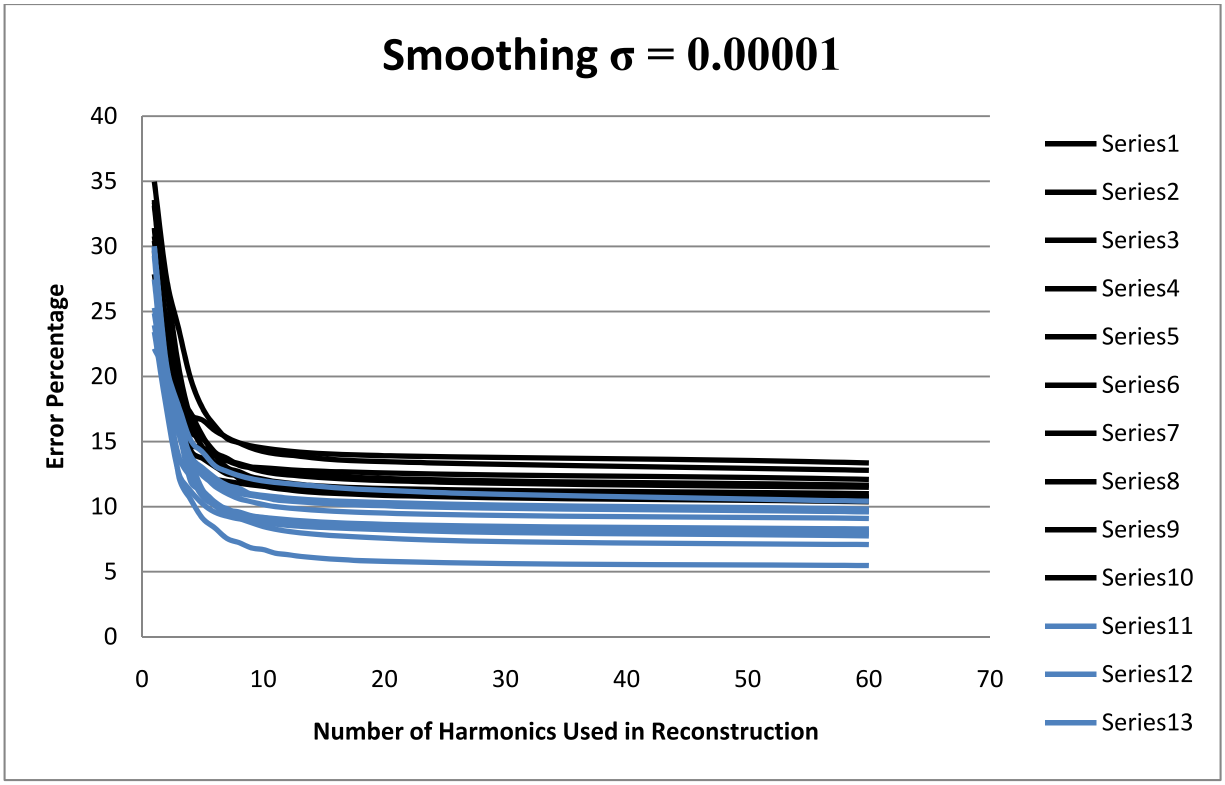

Figure 20 – Error curves for autistic (black lines) and normal (blue lines) brains during reconstruction using a smoothing σ = 0.00001.

	Smoothing σ = 0.00001		
	Error below < 11% (Iteration)	Error below < 10% (Iteration)	Lowest Error
A1	61	61	11.004
A2	26	61	10.653
A5	61	61	11.648
A6	61	61	12.091
A8	61	61	13.364
A9	28	61	10.661
A10	61	61	12.799
A11	61	61	11.493
A12	17	61	10.367
A13	34	61	10.754
N2	28	61	10.421
N3	9	42	9.8132
N4	8	11	9.0887
N5	5	7	7.7562
N6	9	28	9.5951
N8	4	5	5.4744
N9	5	6	7.9267
N10	6	7	8.2921
N11	6	7	8.1369
N13	9	37	9.6941
N16	9	23	9.6041
N17	6	7	7.0942

Table 4– Convergence iteration and lowest error for a smoothing σ = 0.00001.

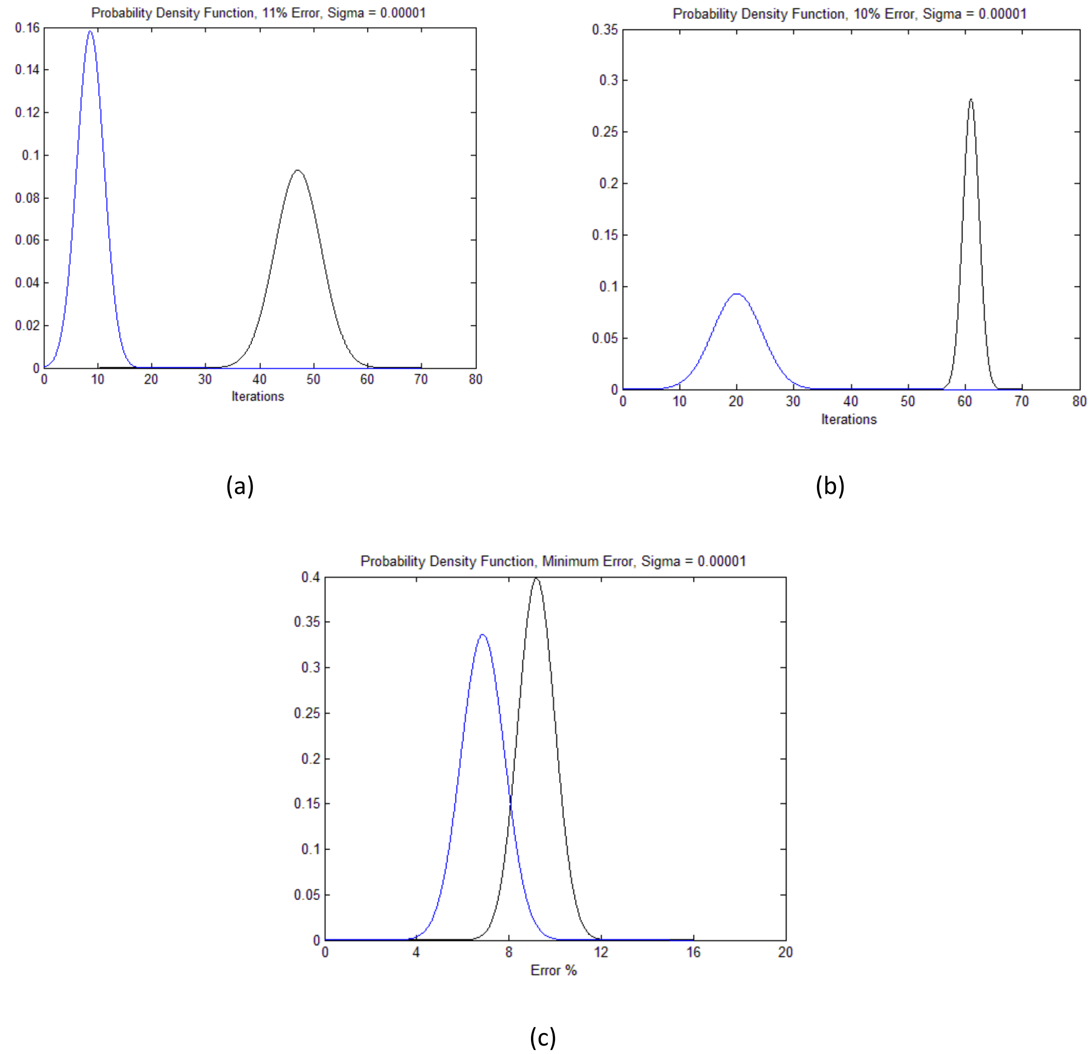

Figure 21– Probability Density Function graphs of smoothing σ = 0.0001 for (a) 11% error, (b) 10% error, and (c) minimum error.

E. Average Error and Minimum Convergence Iteration

The minimum error for each brain was then calculated along with the fastest iteration at which the brain converged below the specified error. (See Table 5) It was expected that due to the complexity of an Autistic brain these would require more iterations to converge to the same error level as a normal brain. It was also likely that within the number of iterations tested the autistic brains would record a larger final error due to this slower convergence rate. This was confirmed by the data.

The average of the minimum error for each group was calculated along with the lowest iteration at which that particular mesh dropped below a given error threshold. (See Table 5). The overall minimum error for normal brain data was significantly lower than the autistic brain data. The average error for autistic brain data was significantly higher in both convergence measurements, but was dramatically higher in the 10% category. This confirms the hypothesis that the autistic brain is significantly more difficult to reconstruct than a normal brain.

Smoothing σ = 0.01			
	Lowest Error below 11% (Iteration)	Lowest Error below 10% (Iteration)	Minimum Error
Average Minimum Error (Autistic)	47.1±22.70	61±0	11.49±0.76
Average Minimum Error (Normal)	11.41±15.70	33.66±28.55	9.41±1.38
Smoothing σ = 0.001			
	Lowest Error below 11% (Iteration)	Lowest Error below 10% (Iteration)	Minimum Error
Average Minimum Error (Autistic)	45.4±20.59	61±0	11.61±1.00
Average Minimum Error (Normal)	8.25±5.81	20.25±20.56	8.73±1.48
Smoothing σ = 0.0001			
	Lowest Error below 11% (Iteration)	Lowest Error below 10% (Iteration)	Minimum Error
Average Minimum Error (Autistic)	46.8±18.82	61±0	11.50±1.00
Average Minimum Error (Normal)	8.66±6.35	19.91±18.30	8.59±1.41
Smoothing σ = 0.00001			
	Lowest Error below 11% (Iteration)	Lowest Error below 10% (Iteration)	Minimum Error
Average Minimum Error (Autistic)	47.1±18.39	61±0	11.48±1.00
Average Minimum Error (Normal)	8.66±6.35	20.08±18.35	8.57±1.40

Table 5– Average minimum error and convergence for autistic and normal data groups

IV. Conclusions and Future Work

Considering the data from previous methods including Modified Checklist for Autism in Toddlers, eye-tracking technologies, and the prevalence of the disorder, it is essential to find alternate and scientific methods that include brain analysis as a diagnostic and evaluative method. The research of doctors at Yale has determined that brain scans can predict the development of autism, leading to early detection and early intervention.

Using this method of analyzing data can demonstrate accurate differences in normal and autistic brains. The research that has been generated in this thesis can clearly demonstrate that the normal brain data converged both faster and with a lower rate of error level than the Autistic brain data. This result proves that the autistic brain is a more complex structure, and would be more difficult to reconstruct using this Shape-Based Detection of Cortex Variability process.

The flexibility of the created package is of additional importance to the expansion of the project. The algorithms and theories introduced in this thesis can readily be applied to any object freely. The object can be converted from 2-dimensional scans into a 3-dimensional mesh, deformed and analyzed. This would allow for future analysis of many other organs including cancerous growths and individual components of the brain. Examining the difference between reconstructions can enable change in an object to be tracked over time and compared as well. This would allow for an analysis of the rate of the progression of autism in the individual. This can provide valuable information that can be used to improve treatments by providing physicians with a detailed mathematical representation of the current state of their patient. It is also potentially possible to use this technique to understand what areas of the brain begin to alter at different times in the subject and to track their impact on the overall autism. Gaining a detailed understanding of the progression of autism in patients can help lead to meaningful solutions for autistic patients.

Future plans are to improve the efficiency of the algorithms to allow accurate deformation and analysis of larger and more detailed mesh structures. Improvements in the algorithm will allow for faster and more accurate analysis of the subject. As previously mentioned, it is also planned to make the package more flexible so that it can readily be applied to a variety of structures and used as a meaningful evaluation technique for multiple disorders.

After numerous attempts to create a package for Shape-Based Detection of Cortex Variability, the primary difficulties arose in generating an accurate mesh from a variety of data and deforming the mesh into an accurate unit sphere while preserving the integrity and positioning of nodes within the mesh. Through the combination of techniques from a variety of fields including engineering, computer science and graphical art design these challenges were overcome. Using this technique it will be possible to analyze a large variety of MRI scans to compare the complexities of normal and Autistic brains.

II. References

1. Minshew, NJ, Payton, JB (1988). New perspectives in autism, Part I: The clinical spectrum of autism. Curr Probl Pediatr, 18, 10:561-610.
2. Kanner Child Psychiatry ISBN-10: 0398021996 Publisher: Charles C. Thomas, Publisher Ltd (April 1979)
3. Kanner L (1943). "Autistic disturbances of affective contact". Nerv Child 2: 217–50. Kanner, L (1968). "Reprint". Acta Paedopsychiatr 35 (4): 100–36.
4. Bauman ML, Kemper TL. The neuropathology of the autism spectrum disorders: what have we learned? Children's Neurology Service, Massachusetts General Hospital, 55 Fruit Street, Boston, MA 02114, USA.
5 Wing, L (1981). Asperger's syndrome: a clinical account. *Psychol Med*, 11, 1:115-29.
6. Schaefer, GB, Mendelsohn, NJ (2008). Clinical genetics evaluation in identifying the etiology of autism spectrum disorders. Genet. Med., 10, 4:301-5.
7. Losh, M, Adolphs, R, Poe, MD, Couture, S, Penn, D, Baranek, GT, Piven, J (2009). Neuropsychological profile of autism and the broad autism phenotype. Arch. Gen. Psychiatry, 66, 5:518-26.
8. Jacobson, JW. Is Autism on the Rise? 2000. Science in Autism Vol 2. No 1,
9. Rapin, I, Tuchman, RF (2008). What is new in autism?. Curr. Opin. Neurol., 21, 2:143-9.
10. Department of Developmental Services. (1999, March 1). Changes in the population of persons with autism and pervasive developmental disorders in California's developmental services system: 1987 through 1998. Sacramento, CA: Author.
11. Department of Education (1999). Digest of education statistics, 1998. Washington, DC: Author (GPO No. 065-000-01174-3, NCES No. NCES 1999036).
12. DiGuiseppi, C, Hepburn, S, Davis, JM, Fidler, DJ, Hartway, S, Lee, NR, Miller, L, Ruttenber, M, Robinson, C (2010). Screening for autism spectrum disorders in children with Down syndrome: population prevalence and screening test characteristics. J Dev Behav Pediatr, 31, 3:181-91.
13. Stevens, M., Fein, D., Dunn, M., Allen, D., Waterhouse, L. H., Feinstein, C., and Rapin, I., Subgroups of children with autism by cluster analysis: A longitudinal examination. J. Am. Acad. Child Adolesc. Psychiatry 39:346–352, 2000.
14. Robins, D.L., Fein, D, Barton, M, Green, J. The Modified Checklist for Autism in Toddlers: An Initial Study Investigating the Early Detection of Autism and Pervasive Developmental Disorders. Journal of Autism and Developmental Disorders, Vol. 31, No. 2, 2001

15. El-Baz, A., Elnakib A., Casanova M., Gimel'farb G., Switala, A., Jordan, D. Rainey, S. Accurate Automated Detection of Autism Related Corpus Callosum Abnormalities. J Med Syst. March 2010. DOI 10.1007/s10916-010-9510-3
16. Abell, F., Krams, M., Ashburner, J., Passingham, R., Friston, K., Frackowiak, R., Happe, F., Frith, C., and Frith, U., The neuro-anatomy of autism: A voxel-based whole brain analysis of structural scans. NeuroReport 10(8):647–1651, 1999.
17. Boddaert, N., Chabane, N., Gervais, H., Good, C. D., Bourgeois, M., Plumet, M. H., Barthelemy, C., Mouren, M. C., Artiges, E., Samson, Y., Brunelle, F., Frackowiak, R. S. J., and Zilbovicius, M., Superior temporal sulcus anatomical abnormalities in childhood autism: a voxel-based morphometry MRI study. Neuroimage 23:364–369, 2004.
18. Herbert, M. R., Ziegler, D. A., Deutsch, C. K., O'Brien, L. M., Lange, N., Bakardjiev, A., Hodgson, J., Adrien, K. T., Steele, S., Makris, N., Kennedy, D., Harris, G. J., and Caviness, V. S., Jr., Dissociations of cerebral cortex, subcortical and cerebral white matter volumes in autistic boys. Brain 126:1182–1192, 2003.
19. Egaas, B., Courchesne, E., and Saitoh, O., Reduced size of corpus 576 callosum in autism. Arch. Neurol. 52(8):794–801, 1995.
20. Schumann, CM, Barnes, CC, Lord, C, Courchesne, E (2009). Amygdala enlargement in toddlers with autism related to severity of social and communication impairments. *Biol. Psychiatry*, 66, 10:942-9.
21. Courchesne, E, Press, GA, Yeung-Courchesne, R (1993). Parietal lobe abnormalities detected with MR in patients with infantile autism. *AJR Am J Roentgenol*, 160, 2:387-93.
22. Schumann, CM, Bloss, CS, Barnes, CC, Wideman, GM, Carper, RA, Akshoomoff, N, Pierce, K, Hagler, D, Schork, N, Lord, C, Courchesne, E (2010). Longitudinal magnetic resonance imaging study of cortical development through early childhood in autism. *J. Neurosci.*, 30, 12:4419-27.
23. Kennedy, DP, Courchesne, E (2008). Functional abnormalities of the default network during self- and other-reflection in autism. *Soc Cogn Affect Neurosci*, 3, 2:177-90.
24. Hitti, M., Chang, L. Autism: New Clue to Earlier Detection. WebMD Health News. March 29, 2009.
25. Klin, A, Lin, DJ, Gorrindo, P, Ramsay, G, Jones, W (2009). Two-year-olds with autism orient to non-social contingencies rather than biological motion. Nature, 459, 7244:257-61.
26. Jones, W, Klin, A (2009). Heterogeneity and homogeneity across the autism spectrum: the role of development. J Am Acad Child Adolesc Psychiatry, 48, 5:471-3.
27. Jones, W, Carr, K, Klin, A (2008). Absence of preferential looking to the eyes of approaching adults predicts level of social disability in 2-year-old toddlers with autism spectrum disorder. Arch. Gen. Psychiatry, 65, 8:946-54.
28. Gardner, A. New Hope for Early Detection of Autism. US News: Health Day. May 19, 2010

29. Fang, Q., Boas, D.A., "Tetrahedral mesh generation from volumetric binary and gray-scale images," Proceedings of IEEE International Symposium on Biomedical Imaging 2009, pp. 1142-1145, 2009
30. Fang, Q., Carp, S.A., Selb, J., Moore, R., Kopans, D.B., Miller, E.L., Brooks, D.H., Boas, D.A., "A Multi-Modality Image Reconstruction Platform for Diffuse Optical Tomography," Biomedical Optics 2008, BIOMED Poster Session II (BMD), Mar. 2008.
31. Zhang, Hamza, (2006) Vertex-based anisotropic smoothing of 3D mesh data, IEEE CCECE
32. Fornberg, B., A practical guide to pseudospectral methods. Cambridge University Press, 1998.
33. Chung. M.K., Shen, L., Dalton, K.M., Evans, A.C., Davidson, R.J. Weighted fourier representation and its application to quantifying the amount of gray matter. IEEE Transactions on Medical Imaging, 26:566–581, 2007.
34. Courant, R. and Hilbert, D. Methods of Mathematical Physics: Volume II. Interscience, New York, English edition, 1953.
35. Chung, M.K., Dalton, K.M., Shen, L., L., Evans, A.C., Davidson, R.J. 2007. Weighted Fourier series representation and its application to quantifying the amount of gray matter. IEEE Transactions on Medical Imaging, 26:566-581.

Appendix 1: Wavefront OBJ Format

i.) Format Specification

Lines beginning with a hash character (#) are comments.

```
# this is a comment
```

An OBJ file contains several types of definition:

```
# List of Vertices, with (x,y,z) coordinates.
v 0.123 0.234 0.345
v ...
...
# Texture coordinates, in (u,v) coordinates.
vt 0.500 -1.352
vt ...
...
# Normals in (x,y,z) form; normals might not be unit.
vn 0.707 0.000 0.707
vn ...
..
```

Face Definitions

Faces are defined using lists of vertex, texture and normal indicies. Polygons such as quadrilaterals can be defined by using more than three vertex/texture/normal indices.

OBJ files also support free form curved surface objects such as NURB surfaces.

There are several way to define a face, but each face line definition starts with "f" character.

Vertex

A valid vertex index starts from 1 and match first vertex element of vertex list previously defined. Each face can contain more than three elements.

```
f v1 v2 v3 v4 ...
```

Vertex/Texture-coordinate

Each texture coordinate index must follow with no space the first slash. Texture coordinates index are optional. A valid texture coordinate index starts from 1 and match first texture coordinate element of texture coordinate list previously defined. Each face can contain more than three elements.

```
f v1/vt1 v2/vt2 v3/vt3 ...
```

Vertex/Texture-coordinate/Normal

Each normal index must follow with no space the second slash. Normals index are optional. A valid normal index starts from 1 and match first normal element of normal list previously defined. Each face can contain more than three elements.

```
f v1/vt1/vn1 v2/vt2/vn2 v3/vt3/vn3 ...
```

Vertex/Normal

As texture coordinates are optional, one can define geometry without them, but one must put normal index after second slash.

```
f v1//vn1 v2//vn2 v3//vn3 ...
```

ii.) ingOBJSave.m Matlab Code

```
function [null] = ingOBJSave(fileName,vertex,faces)
fprintf('Saving data to OBJ file...');
[vertexN] = compute_normal(vertex',faces');
vertexN = vertexN';

vertCount = size(vertex,1);
faceCount = size(faces,1);

fid = fopen(fileName,'w');
fprintf(fid,'####\r\n');
fprintf(fid,'#\r\n');
fprintf(fid,'# OBJ File Generated by ingMesh\r\n');
fprintf(fid,'#\r\n');
fprintf(fid,'####\r\n');
fprintf(fid,'# Object %s\r\n',fileName);
fprintf(fid,'#\r\n');
fprintf(fid,'# Vertices: %d\r\n',vertCount);
fprintf(fid,'# Faces: %d\r\n',faceCount);
fprintf(fid,'#\r\n');
fprintf(fid,'####\r\n');

for i=1:vertCount
    fprintf(fid,'vn %f %f %f\r\n',vertexN(i,1),vertexN(i,2),vertexN(i,3));
    fprintf(fid,'v %f %f %f\r\n',vertex(i,1),vertex(i,2),vertex(i,3));
end
fprintf(fid,'# %d vertices, %d vertices normals\r\n',vertCount,vertCount);
fprintf(fid,'\r\n');

for i=1:faceCount
fprintf(fid,'f %d//%d %d//%d
%d//%d\r\n',faces(i,1),faces(i,1),faces(i,2),faces(i,2),faces(i,3),faces(i,3));
end
fprintf(fid,'# %d faces, %d coords texture\r\n',faceCount,0);
fprintf(fid,'\r\n');
fprintf(fid,'# End of File');

fprintf('Complete.\n');
fclose(fid);
fprintf('File closed.\n');
```

iii.) ingOBJRead.m Matlab Code

```
function [nodes faces] = ingOBJRead(filename)
fprintf('Reading data from OBJ file...\n');

fid=fopen(filename);
frewind(fid);

for i=1:7
    fgetl(fid);
end
fscanf(fid,'%s',2);
n_nodes=fscanf(fid,'%i',1);
fscanf(fid,'%s',2);
n_faces=fscanf(fid,'%i',1);
for i=1:3
    fgetl(fid);
end

fprintf('Detected Nodes: %i  Faces: %i\n',n_nodes,n_faces);
nodes = zeros(n_nodes,3);
normals = zeros(n_nodes,3);
c_norm = 1;
c_node = 1;
for i = 1:(n_nodes*2)
    fscanf(fid,'%s',1);
    if (mod(i,2) == 1)
       temp =  fscanf(fid,'%f',3);
       normals(c_norm,:) = temp;
       c_norm = c_norm + 1;
    else
       temp =  fscanf(fid,'%f',3);
       nodes(c_node,:) = temp;
       c_node = c_node + 1;
    end
end

fscanf(fid,'%s',6);
faces = zeros(n_faces,3);
face_normals = zeros(n_faces,3);
for i = 1:n_faces
    fscanf(fid,'%s',1);

    faces(i,1) = fscanf(fid,'%i',1);
    fscanf(fid,'%c',2);
    face_normals(i,1) = fscanf(fid,'%i',1);
    fscanf(fid,'%c',1);
    faces(i,2) = fscanf(fid,'%i',1);
    fscanf(fid,'%c',2);
    face_normals(i,2) = fscanf(fid,'%i',1);
    fscanf(fid,'%c',1);
    faces(i,3) = fscanf(fid,'%i',1);
    fscanf(fid,'%c',2);
    face_normals(i,3) = fscanf(fid,'%i',1);
    fscanf(fid,'%c',1);
end

fclose(fid);
fprintf('File closed.\n');
```

Appendix 3: Data Tables

TABLE I

Autistic error curves for reconstruction sigma = 0.01

Iteration	A1	A2	A5	A6	A8	A9	A10	A11	A12	A13
	0.01									
1	33.625	29.77	33.259	31.547	30.976	29.521	34.967	33.401	28.034	30.574
2	23.133	19.324	24.305	21.358	23.569	27.082	27.831	27.355	21.213	22.306
3	18.587	15.799	19.549	17.446	19.119	18.486	23.631	20.559	17.678	18.318
4	14.228	12.915	15.489	14.361	16.474	16.792	19.675	16.646	15.852	14.735
5	13.264	12.17	14.645	13.782	15.641	14.631	17.057	14.745	14.413	14.11
6	12.452	11.565	13.481	12.901	14.63	13.191	15.348	13.328	13.198	12.896
7	11.819	11.268	12.844	12.359	14.103	12.133	14.246	12.748	12.733	12.397
8	11.659	11.125	12.512	12.096	13.571	11.673	13.856	12.166	12.047	11.991
9	11.408	10.945	12.309	11.819	13.322	11.271	13.462	11.94	11.787	11.716
10	11.266	10.851	12.18	11.772	13.135	11.033	13.228	11.716	11.602	11.535
11	11.169	10.805	12.054	11.675	12.997	10.905	13.075	11.578	11.448	11.397
12	11.11	10.769	12.007	11.636	12.908	10.787	12.981	11.5	11.379	11.31
13	11.072	10.733	11.945	11.6	12.845	10.739	12.91	11.438	11.309	11.264
14	11.041	10.713	11.922	11.582	12.808	10.672	12.856	11.398	11.282	11.235
15	11.027	10.7	11.897	11.57	12.785	10.647	12.82	11.37	11.262	11.215
16	11.016	10.69	11.883	11.561	12.772	10.627	12.797	11.362	11.25	11.204
17	11.009	10.685	11.875	11.557	12.765	10.619	12.787	11.353	11.242	11.195
18	11.005	10.681	11.869	11.553	12.76	10.611	12.778	11.348	11.238	11.191
19	11.003	10.68	11.866	11.551	12.758	10.608	12.775	11.345	11.235	11.188
20	11.002	10.679	11.863	11.55	12.756	10.605	12.773	11.344	11.234	11.186
21	11.001	10.678	11.862	11.549	12.756	10.604	12.771	11.343	11.233	11.186
22	11.001	10.678	11.862	11.549	12.755	10.603	12.77	11.343	11.232	11.185
23	11.001	10.678	11.861	11.548	12.755	10.603	12.77	11.342	11.232	11.185

24	11	10.677	11.861	11.548	12.754	10.602	12.769	11.342	11.232	11.185
25	11	10.677	11.861	11.548	12.754	10.602	12.769	11.342	11.232	11.185
26	11	10.677	11.861	11.548	12.754	10.602	12.769	11.342	11.232	11.185
27	11	10.677	11.861	11.548	12.754	10.602	12.769	11.342	11.232	11.185
28	11	10.677	11.861	11.548	12.754	10.602	12.769	11.342	11.232	11.185
29	11	10.677	11.861	11.548	12.754	10.602	12.769	11.342	11.232	11.185
30	11	10.677	11.861	11.548	12.754	10.602	12.769	11.342	11.232	11.185
31	11	10.677	11.861	11.548	12.754	10.602	12.769	11.342	11.232	11.185
32	11	10.677	11.861	11.548	12.754	10.602	12.769	11.342	11.232	11.185
33	11	10.677	11.861	11.548	12.754	10.602	12.769	11.342	11.232	11.185
34	11	10.677	11.861	11.548	12.754	10.602	12.769	11.342	11.232	11.185
35	11	10.677	11.861	11.548	12.754	10.602	12.769	11.342	11.232	11.185
36	11	10.677	11.861	11.548	12.754	10.602	12.769	11.342	11.232	11.185
37	11	10.677	11.861	11.548	12.754	10.602	12.769	11.342	11.232	11.185
38	11	10.677	11.861	11.548	12.754	10.602	12.769	11.342	11.232	11.185
39	11	10.677	11.861	11.548	12.754	10.602	12.769	11.342	11.232	11.185
40	11	10.677	11.861	11.548	12.754	10.602	12.769	11.342	11.232	11.185
41	11	10.677	11.861	11.548	12.754	10.602	12.769	11.342	11.232	11.185
42	11	10.677	11.861	11.548	12.754	10.602	12.769	11.342	11.232	11.185
43	11	10.677	11.861	11.548	12.754	10.602	12.769	11.342	11.232	11.185
44	11	10.677	11.861	11.548	12.754	10.602	12.769	11.342	11.232	11.185
45	11	10.677	11.861	11.548	12.754	10.602	12.769	11.342	11.232	11.185
46	11	10.677	11.861	11.548	12.754	10.602	12.769	11.342	11.232	11.185
47	11	10.677	11.861	11.548	12.754	10.602	12.769	11.342	11.232	11.185
48	11	10.677	11.861	11.548	12.754	10.602	12.769	11.342	11.232	11.185
49	11	10.677	11.861	11.548	12.754	10.602	12.769	11.342	11.232	11.185
50	11	10.677	11.861	11.548	12.754	10.602	12.769	11.342	11.232	11.185
51	11	10.677	11.861	11.548	12.754	10.602	12.769	11.342	11.232	11.185
52	11	10.677	11.861	11.548	12.754	10.602	12.769	11.342	11.232	11.185
53	11	10.677	11.861	11.548	12.754	10.602	12.769	11.342	11.232	11.185
54	11	10.677	11.861	11.548	12.754	10.602	12.769	11.342	11.232	11.185
55	11	10.677	11.861	11.548	12.754	10.602	12.769	11.342	11.232	11.185
56	11	10.677	11.861	11.548	12.754	10.602	12.769	11.342	11.232	11.185

57	11	10.677	11.861	11.548	12.754	10.602	12.769	11.342	11.232	11.185
58	11	10.677	11.861	11.548	12.754	10.602	12.769	11.342	11.232	11.185
59	11	10.677	11.861	11.548	12.754	10.602	12.769	11.342	11.232	11.185
60	11	10.677	11.861	11.548	12.754	10.602	12.769	11.342	11.232	11.185

TABLE II

Autistic error curves for reconstruction sigma = 0.001

Iteration	A1	A2	A5	A6	A8	A9	A10	A11	A12	A13
	0.001									
1	33.574	29.659	33.148	31.427	30.781	29.48	34.965	33.371	27.877	30.435
2	22.838	18.983	24.015	20.986	23.239	27.011	27.605	27.204	21.076	22.167
3	18.652	15.929	19.699	17.599	19.455	18.883	23.679	20.751	17.814	18.431
4	14.319	13.164	15.774	14.785	17.043	17.141	19.789	16.744	16.029	14.917
5	13.623	12.54	15.126	14.409	16.519	15.276	17.441	15.242	14.496	14.401
6	12.975	12.048	14.072	13.768	15.694	13.832	16.068	14.026	13.296	13.244
7	12.392	11.829	13.424	13.373	15.176	12.84	15.068	13.555	12.842	12.773
8	12.252	11.701	13.074	13.143	14.714	12.487	14.721	12.989	12.069	12.326
9	11.997	11.555	12.889	12.876	14.476	12.079	14.304	12.77	11.77	12.067
10	11.812	11.439	12.741	12.819	14.312	11.877	14.037	12.482	11.478	11.872
11	11.702	11.378	12.584	12.74	14.17	11.687	13.847	12.336	11.285	11.702
12	11.603	11.32	12.487	12.67	14.056	11.569	13.759	12.238	11.166	11.567
13	11.555	11.246	12.383	12.607	13.963	11.481	13.65	12.148	11.041	11.486
14	11.478	11.19	12.304	12.573	13.901	11.35	13.545	12.061	10.963	11.412
15	11.419	11.15	12.227	12.54	13.841	11.272	13.423	11.991	10.921	11.362
16	11.381	11.104	12.169	12.51	13.803	11.208	13.359	11.96	10.862	11.315
17	11.338	11.072	12.125	12.491	13.769	11.145	13.322	11.915	10.823	11.269
18	11.31	11.043	12.085	12.46	13.735	11.087	13.282	11.868	10.796	11.222
19	11.282	11.02	12.048	12.44	13.721	11.041	13.251	11.831	10.758	11.186
20	11.258	11.001	12.02	12.416	13.697	11.004	13.218	11.808	10.726	11.162
21	11.242	10.985	11.991	12.404	13.681	10.973	13.193	11.788	10.702	11.137
22	11.228	10.971	11.969	12.389	13.663	10.944	13.17	11.769	10.683	11.116
23	11.214	10.958	11.953	12.379	13.648	10.918	13.153	11.748	10.661	11.095
24	11.202	10.948	11.933	12.365	13.632	10.898	13.13	11.735	10.641	11.078
25	11.191	10.938	11.917	12.352	13.62	10.878	13.115	11.716	10.622	11.061

26	11.184	10.93	11.903	12.34	13.611	10.859	13.095	11.705	10.609	11.046
27	11.176	10.923	11.889	12.332	13.602	10.839	13.084	11.691	10.598	11.036
28	11.167	10.915	11.881	12.322	13.59	10.824	13.068	11.679	10.589	11.027
29	11.161	10.91	11.87	12.315	13.582	10.814	13.058	11.668	10.579	11.016
30	11.155	10.905	11.861	12.308	13.573	10.801	13.045	11.658	10.567	11.007
31	11.15	10.901	11.854	12.303	13.567	10.791	13.034	11.651	10.557	11.001
32	11.145	10.896	11.847	12.298	13.561	10.781	13.02	11.644	10.551	10.994
33	11.141	10.891	11.841	12.293	13.554	10.774	13.011	11.637	10.544	10.988
34	11.138	10.888	11.834	12.29	13.548	10.768	13	11.632	10.539	10.983
35	11.134	10.884	11.829	12.286	13.543	10.762	12.992	11.625	10.533	10.979
36	11.13	10.88	11.824	12.283	13.537	10.756	12.985	11.62	10.527	10.975
37	11.127	10.877	11.819	12.28	13.533	10.751	12.978	11.614	10.523	10.972
38	11.125	10.874	11.814	12.276	13.529	10.747	12.973	11.609	10.519	10.969
39	11.123	10.871	11.811	12.273	13.526	10.745	12.968	11.606	10.515	10.966
40	11.121	10.868	11.807	12.271	13.522	10.741	12.962	11.602	10.511	10.963
41	11.119	10.866	11.804	12.269	13.52	10.738	12.957	11.599	10.509	10.961
42	11.117	10.865	11.802	12.267	13.517	10.736	12.953	11.596	10.506	10.959
43	11.116	10.863	11.8	12.266	13.514	10.734	12.95	11.594	10.503	10.957
44	11.115	10.861	11.798	12.264	13.512	10.732	12.946	11.591	10.501	10.955
45	11.113	10.859	11.796	12.263	13.51	10.73	12.943	11.589	10.499	10.954
46	11.112	10.857	11.794	12.262	13.508	10.729	12.94	11.587	10.497	10.952
47	11.111	10.856	11.793	12.26	13.506	10.728	12.937	11.585	10.494	10.951
48	11.11	10.855	11.791	12.259	13.504	10.726	12.935	11.584	10.493	10.95
49	11.11	10.854	11.79	12.258	13.502	10.725	12.933	11.583	10.492	10.949
50	11.109	10.854	11.789	12.257	13.501	10.725	12.931	11.582	10.491	10.948
51	11.108	10.853	11.788	12.256	13.499	10.724	12.929	11.581	10.489	10.948
52	11.107	10.852	11.787	12.255	13.498	10.723	12.927	11.58	10.488	10.947
53	11.107	10.852	11.786	12.254	13.497	10.723	12.925	11.579	10.487	10.946
54	11.106	10.851	11.785	12.253	13.496	10.722	12.924	11.579	10.486	10.946
55	11.106	10.851	11.785	12.253	13.494	10.722	12.923	11.578	10.486	10.945
56	11.105	10.85	11.784	12.252	13.493	10.721	12.922	11.577	10.485	10.945
57	11.105	10.85	11.783	12.251	13.493	10.721	12.921	11.577	10.484	10.944
58	11.104	10.85	11.783	12.251	13.492	10.72	12.92	11.577	10.484	10.944

59	11.104	10.849	11.782	12.25	13.491	10.72	12.919	11.576	10.483	10.944
60	11.104	10.849	11.782	12.25	13.49	10.72	12.918	11.576	10.483	10.943

TABLE III

Autistic error curves for reconstruction sigma = 0.0001

Iteration	A1	A2	A5	A6	A8	A9	A10	A11	A12	A13
	0.0001									
1	33.573	29.651	33.14	31.419	30.765	29.48	34.968	33.372	27.866	30.425
2	22.816	18.958	23.992	20.957	23.212	27.008	27.588	27.194	21.069	22.16
3	18.674	15.958	19.732	17.629	19.504	18.945	23.694	20.786	17.843	18.458
4	14.365	13.218	15.838	14.855	17.122	17.199	19.826	16.785	16.064	14.965
5	13.7	12.607	15.211	14.503	16.631	15.381	17.528	15.347	14.533	14.459
6	13.08	12.131	14.175	13.894	15.836	13.956	16.197	14.168	13.352	13.327
7	12.509	11.926	13.538	13.519	15.327	12.991	15.222	13.713	12.905	12.868
8	12.374	11.801	13.189	13.294	14.884	12.665	14.892	13.162	12.145	12.423
9	12.127	11.661	13.015	13.034	14.656	12.269	14.488	12.954	11.855	12.178
10	11.944	11.546	12.874	12.975	14.503	12.085	14.228	12.662	11.57	11.996
11	11.837	11.484	12.714	12.904	14.365	11.898	14.044	12.528	11.4	11.83
12	11.737	11.425	12.616	12.831	14.259	11.791	13.964	12.432	11.284	11.697
13	11.697	11.349	12.516	12.767	14.165	11.701	13.86	12.348	11.165	11.613
14	11.618	11.29	12.433	12.732	14.11	11.572	13.76	12.261	11.087	11.54
15	11.556	11.249	12.355	12.698	14.05	11.492	13.641	12.191	11.051	11.49
16	11.518	11.199	12.3	12.667	14.012	11.428	13.578	12.158	10.99	11.437
17	11.47	11.163	12.256	12.65	13.975	11.36	13.545	12.108	10.953	11.39
18	11.438	11.133	12.217	12.616	13.938	11.295	13.508	12.055	10.925	11.333
19	11.407	11.106	12.18	12.594	13.928	11.247	13.472	12.011	10.884	11.29
20	11.38	11.082	12.154	12.565	13.9	11.199	13.434	11.985	10.849	11.262
21	11.361	11.062	12.12	12.55	13.883	11.163	13.41	11.958	10.823	11.233
22	11.346	11.044	12.094	12.533	13.862	11.131	13.389	11.935	10.803	11.206
23	11.327	11.025	12.075	12.521	13.846	11.1	13.369	11.909	10.777	11.178
24	11.312	11.012	12.05	12.502	13.831	11.072	13.344	11.888	10.75	11.154
25	11.297	10.998	12.031	12.483	13.818	11.05	13.325	11.862	10.727	11.127

26	11.287	10.985	12.011	12.463	13.807	11.025	13.303	11.848	10.71	11.106
27	11.276	10.975	11.994	12.452	13.798	10.995	13.286	11.829	10.696	11.091
28	11.261	10.962	11.982	12.438	13.781	10.974	13.265	11.812	10.684	11.075
29	11.251	10.954	11.967	12.426	13.77	10.957	13.248	11.796	10.67	11.057
30	11.241	10.944	11.953	12.414	13.758	10.936	13.233	11.777	10.649	11.041
31	11.232	10.936	11.942	12.405	13.749	10.92	13.219	11.764	10.635	11.03
32	11.223	10.926	11.929	12.395	13.739	10.902	13.196	11.754	10.625	11.017
33	11.214	10.915	11.919	12.386	13.729	10.891	13.179	11.742	10.615	11.005
34	11.206	10.906	11.907	12.379	13.718	10.879	13.163	11.73	10.605	10.994
35	11.196	10.896	11.897	12.37	13.707	10.866	13.148	11.717	10.595	10.985
36	11.187	10.888	11.887	12.362	13.695	10.854	13.134	11.704	10.585	10.975
37	11.179	10.876	11.877	12.353	13.685	10.841	13.119	11.692	10.578	10.967
38	11.174	10.868	11.865	12.344	13.676	10.831	13.108	11.678	10.57	10.957
39	11.167	10.86	11.857	12.335	13.667	10.823	13.097	11.669	10.559	10.947
40	11.16	10.848	11.849	12.327	13.657	10.814	13.079	11.656	10.551	10.938
41	11.153	10.839	11.842	12.32	13.649	10.804	13.06	11.646	10.546	10.931
42	11.147	10.832	11.836	12.315	13.64	10.796	13.046	11.637	10.536	10.923
43	11.141	10.822	11.828	12.308	13.63	10.787	13.037	11.631	10.528	10.914
44	11.136	10.814	11.818	12.301	13.62	10.779	13.024	11.622	10.52	10.907
45	11.13	10.803	11.808	12.295	13.61	10.773	13.013	11.612	10.514	10.9
46	11.123	10.792	11.799	12.287	13.599	10.767	12.998	11.603	10.505	10.892
47	11.118	10.785	11.793	12.278	13.588	10.759	12.983	11.596	10.495	10.884
48	11.113	10.778	11.785	12.271	13.576	10.752	12.974	11.59	10.49	10.879
49	11.106	10.771	11.775	12.262	13.563	10.746	12.96	11.582	10.483	10.873
50	11.099	10.764	11.767	12.253	13.551	10.739	12.945	11.574	10.474	10.866
51	11.094	10.756	11.76	12.241	13.538	10.733	12.932	11.567	10.465	10.86
52	11.088	10.75	11.751	12.229	13.526	10.728	12.92	11.56	10.457	10.854
53	11.08	10.745	11.74	12.22	13.513	10.723	12.91	11.553	10.448	10.845
54	11.074	10.737	11.731	12.21	13.499	10.717	12.897	11.547	10.438	10.839
55	11.067	10.731	11.722	12.198	13.482	10.71	12.883	11.541	10.43	10.832
56	11.061	10.724	11.713	12.184	13.466	10.704	12.871	11.534	10.421	10.826
57	11.051	10.717	11.702	12.173	13.452	10.697	12.859	11.528	10.411	10.818
58	11.042	10.707	11.691	12.163	13.437	10.69	12.847	11.521	10.398	10.809

59	11.033	10.698	11.684	12.149	13.42	10.683	12.833	11.514	10.39	10.798
60	11.027	10.693	11.675	12.134	13.402	10.674	12.818	11.507	10.379	10.788

TABLE IV

Autistic error curves for reconstruction sigma = 0.00001

Iteration	A1	A2	A5	A6	A8	A9	A10	A11	A12	A13
	0.00001									
1	33.573	29.651	33.14	31.418	30.764	29.48	34.968	33.372	27.865	30.424
2	22.814	18.956	23.99	20.954	23.209	27.008	27.586	27.193	21.069	22.16
3	18.676	15.961	19.735	17.632	19.509	18.951	23.695	20.79	17.846	18.461
4	14.37	13.224	15.844	14.863	17.131	17.205	19.83	16.79	16.068	14.97
5	13.708	12.614	15.22	14.513	16.643	15.392	17.537	15.358	14.537	14.465
6	13.091	12.14	14.186	13.907	15.85	13.969	16.211	14.183	13.358	13.336
7	12.521	11.936	13.55	13.534	15.342	13.007	15.238	13.729	12.912	12.878
8	12.387	11.812	13.201	13.309	14.901	12.684	14.91	13.18	12.154	12.433
9	12.141	11.672	13.029	13.05	14.675	12.29	14.508	12.974	11.865	12.19
10	11.958	11.557	12.888	12.991	14.523	12.108	14.248	12.681	11.581	12.009
11	11.851	11.495	12.728	12.921	14.386	11.92	14.065	12.548	11.413	11.844
12	11.752	11.436	12.63	12.847	14.28	11.815	13.986	12.453	11.297	11.711
13	11.712	11.36	12.53	12.783	14.187	11.725	13.882	12.369	11.179	11.627
14	11.634	11.3	12.447	12.749	14.133	11.596	13.784	12.283	11.101	11.554
15	11.571	11.26	12.369	12.715	14.073	11.516	13.665	12.213	11.066	11.504
16	11.534	11.209	12.315	12.684	14.035	11.452	13.603	12.179	11.006	11.451
17	11.485	11.173	12.271	12.666	13.997	11.383	13.57	12.129	10.969	11.403
18	11.453	11.143	12.233	12.632	13.96	11.319	13.534	12.076	10.941	11.346
19	11.421	11.115	12.196	12.611	13.951	11.27	13.497	12.031	10.9	11.303
20	11.394	11.091	12.17	12.581	13.922	11.222	13.459	12.005	10.864	11.274
21	11.375	11.071	12.136	12.565	13.906	11.185	13.435	11.977	10.839	11.244
22	11.36	11.052	12.109	12.549	13.884	11.153	13.414	11.954	10.819	11.218
23	11.341	11.033	12.091	12.536	13.869	11.122	13.395	11.928	10.793	11.189
24	11.325	11.019	12.066	12.517	13.853	11.093	13.369	11.906	10.765	11.164
25	11.31	11.005	12.046	12.497	13.841	11.071	13.351	11.879	10.742	11.136

26	11.299	10.991	12.026	12.477	13.83	11.046	13.328	11.865	10.725	11.115
27	11.288	10.981	12.008	12.466	13.821	11.015	13.312	11.846	10.711	11.099
28	11.273	10.968	11.996	12.451	13.804	10.993	13.29	11.829	10.699	11.082
29	11.263	10.959	11.981	12.439	13.793	10.975	13.272	11.812	10.685	11.064
30	11.252	10.949	11.966	12.426	13.781	10.954	13.258	11.792	10.663	11.047
31	11.243	10.941	11.955	12.416	13.772	10.938	13.244	11.779	10.649	11.035
32	11.233	10.93	11.942	12.407	13.762	10.919	13.219	11.768	10.639	11.022
33	11.223	10.917	11.931	12.396	13.752	10.908	13.203	11.755	10.628	11.01
34	11.215	10.908	11.919	12.389	13.74	10.895	13.185	11.743	10.619	10.997
35	11.204	10.898	11.908	12.379	13.728	10.881	13.17	11.73	10.609	10.988
36	11.195	10.888	11.898	12.371	13.715	10.869	13.155	11.716	10.599	10.977
37	11.186	10.875	11.887	12.362	13.705	10.855	13.141	11.703	10.592	10.968
38	11.181	10.867	11.875	12.352	13.695	10.844	13.128	11.689	10.583	10.958
39	11.173	10.857	11.866	12.342	13.686	10.836	13.117	11.678	10.573	10.947
40	11.166	10.844	11.857	12.333	13.676	10.826	13.098	11.664	10.565	10.936
41	11.158	10.834	11.85	12.326	13.666	10.815	13.077	11.653	10.56	10.929
42	11.151	10.826	11.843	12.32	13.657	10.806	13.061	11.644	10.549	10.92
43	11.145	10.814	11.834	12.312	13.645	10.797	13.051	11.637	10.541	10.91
44	11.139	10.806	11.823	12.305	13.635	10.787	13.037	11.627	10.532	10.902
45	11.132	10.792	11.812	12.298	13.624	10.781	13.025	11.617	10.527	10.894
46	11.124	10.779	11.802	12.288	13.611	10.774	13.008	11.607	10.517	10.884
47	11.119	10.771	11.795	12.277	13.599	10.765	12.991	11.599	10.506	10.875
48	11.112	10.761	11.785	12.27	13.585	10.757	12.98	11.593	10.5	10.869
49	11.104	10.753	11.774	12.258	13.569	10.749	12.965	11.583	10.493	10.863
50	11.096	10.744	11.764	12.248	13.555	10.742	12.948	11.574	10.483	10.855
51	11.09	10.735	11.755	12.233	13.54	10.735	12.933	11.566	10.472	10.848
52	11.083	10.728	11.743	12.218	13.525	10.729	12.92	11.558	10.464	10.84
53	11.073	10.721	11.729	12.207	13.509	10.723	12.908	11.55	10.453	10.83
54	11.065	10.711	11.718	12.194	13.492	10.716	12.894	11.544	10.442	10.821
55	11.057	10.704	11.707	12.178	13.47	10.707	12.877	11.537	10.431	10.814
56	11.05	10.693	11.696	12.159	13.449	10.699	12.864	11.528	10.42	10.807
57	11.036	10.684	11.681	12.145	13.431	10.691	12.849	11.52	10.407	10.795
58	11.025	10.671	11.668	12.131	13.412	10.683	12.834	11.512	10.392	10.784

59	11.012	10.66	11.659	12.112	13.387	10.672	12.816	11.502	10.381	10.769
60	11.004	10.653	11.648	12.091	13.364	10.661	12.799	11.493	10.367	10.754

TABLE V

Normal error curves for reconstruction sigma = 0.01

Iteration	N2	N3	N4	N5	N6	N8	N9	N10	N11	N13	N16	N17
	0.01											
1	30.107	29.921	29.843	23.919	29.346	22.31	23.742	29.99	25.051	27.573	30.036	25.352
2	20.777	21.202	21.009	18.735	19.062	19.93	17.667	20.49	18.748	19.098	19.499	20.719
3	17.867	17.245	17.824	13.662	16.392	12.519	12.597	15.93	15.668	16.47	16.381	16.196
4	15.279	13.616	13.736	12.097	13.781	10.652	11.212	12.156	12.79	13.701	13.906	13.473
5	14.221	12.67	12.719	10.571	12.458	9.1408	10.092	11.233	11.369	12.582	12.97	11.307
6	13.087	11.767	11.77	9.7784	11.633	8.4695	9.4532	10.221	10.367	11.785	12.002	10.283
7	12.643	11.265	11.223	9.2005	11.192	7.605	9.1178	9.7655	10.021	11.024	11.277	9.6368
8	12.268	10.99	10.872	8.9251	10.849	7.363	8.881	9.5584	9.608	10.805	11.001	9.1599
9	12.079	10.827	10.671	8.6898	10.684	7.0062	8.7347	9.3557	9.4457	10.427	10.871	8.8911
10	11.933	10.715	10.514	8.5291	10.516	6.9002	8.6416	9.2341	9.3036	10.311	10.772	8.7028
11	11.825	10.641	10.431	8.4644	10.437	6.7431	8.5725	9.1607	9.2375	10.211	10.65	8.5766
12	11.768	10.571	10.39	8.3725	10.379	6.6949	8.5187	9.1152	9.1812	10.145	10.616	8.4786
13	11.721	10.527	10.351	8.328	10.344	6.6418	8.479	9.0739	9.1466	10.103	10.586	8.4273
14	11.695	10.503	10.334	8.2892	10.326	6.6223	8.4559	9.0555	9.1267	10.074	10.564	8.3919
15	11.674	10.486	10.319	8.2739	10.313	6.6012	8.4404	9.0422	9.1143	10.058	10.549	8.3733
16	11.662	10.477	10.31	8.2646	10.301	6.5906	8.4327	9.0349	9.1061	10.047	10.54	8.3632
17	11.653	10.471	10.305	8.2565	10.296	6.5827	8.4273	9.0284	9.1021	10.041	10.534	8.356
18	11.649	10.468	10.301	8.2518	10.292	6.5789	8.4238	9.0245	9.0991	10.037	10.531	8.3516
19	11.646	10.465	10.299	8.2492	10.289	6.5762	8.4222	9.022	9.0975	10.035	10.529	8.3482
20	11.643	10.464	10.298	8.2475	10.288	6.5754	8.421	9.0204	9.0966	10.034	10.527	8.3467
21	11.642	10.462	10.297	8.2464	10.288	6.5745	8.4204	9.0194	9.0961	10.034	10.527	8.3458
22	11.642	10.462	10.296	8.2459	10.287	6.5742	8.4199	9.0188	9.0958	10.033	10.526	8.3452
23	11.641	10.462	10.296	8.2455	10.287	6.574	8.4196	9.0185	9.0956	10.033	10.526	8.3448
24	11.641	10.462	10.296	8.2453	10.287	6.5739	8.4195	9.0184	9.0955	10.033	10.526	8.3446
25	11.641	10.461	10.296	8.2452	10.287	6.5738	8.4195	9.0183	9.0954	10.033	10.526	8.3445

26	11.641	10.461	10.296	8.2451	10.287	6.5738	8.4194	9.0182	9.0954	10.033	10.526	8.3445
27	11.641	10.461	10.296	8.2451	10.286	6.5738	8.4194	9.0182	9.0953	10.033	10.526	8.3444
28	11.641	10.461	10.296	8.2451	10.286	6.5738	8.4194	9.0182	9.0953	10.033	10.526	8.3444
29	11.641	10.461	10.296	8.2451	10.286	6.5738	8.4194	9.0182	9.0953	10.033	10.526	8.3444
30	11.641	10.461	10.296	8.2451	10.286	6.5738	8.4194	9.0182	9.0953	10.033	10.526	8.3444
31	11.641	10.461	10.296	8.2451	10.286	6.5738	8.4194	9.0182	9.0953	10.033	10.526	8.3444
32	11.641	10.461	10.296	8.2451	10.286	6.5738	8.4194	9.0182	9.0953	10.033	10.526	8.3444
33	11.641	10.461	10.296	8.2451	10.286	6.5738	8.4194	9.0182	9.0953	10.033	10.526	8.3444
34	11.641	10.461	10.296	8.2451	10.286	6.5738	8.4194	9.0182	9.0953	10.033	10.526	8.3444
35	11.641	10.461	10.296	8.2451	10.286	6.5738	8.4194	9.0182	9.0953	10.033	10.526	8.3444
36	11.641	10.461	10.296	8.2451	10.286	6.5738	8.4194	9.0182	9.0953	10.033	10.526	8.3444
37	11.641	10.461	10.296	8.2451	10.286	6.5738	8.4194	9.0182	9.0953	10.033	10.526	8.3444
38	11.641	10.461	10.296	8.2451	10.286	6.5738	8.4194	9.0182	9.0953	10.033	10.526	8.3444
39	11.641	10.461	10.296	8.2451	10.286	6.5738	8.4194	9.0182	9.0953	10.033	10.526	8.3444
40	11.641	10.461	10.296	8.2451	10.286	6.5738	8.4194	9.0182	9.0953	10.033	10.526	8.3444
41	11.641	10.461	10.296	8.2451	10.286	6.5738	8.4194	9.0182	9.0953	10.033	10.526	8.3444
42	11.641	10.461	10.296	8.2451	10.286	6.5738	8.4194	9.0182	9.0953	10.033	10.526	8.3444
43	11.641	10.461	10.296	8.2451	10.286	6.5738	8.4194	9.0182	9.0953	10.033	10.526	8.3444
44	11.641	10.461	10.296	8.2451	10.286	6.5738	8.4194	9.0182	9.0953	10.033	10.526	8.3444
45	11.641	10.461	10.296	8.2451	10.286	6.5738	8.4194	9.0182	9.0953	10.033	10.526	8.3444
46	11.641	10.461	10.296	8.2451	10.286	6.5738	8.4194	9.0182	9.0953	10.033	10.526	8.3444
47	11.641	10.461	10.296	8.2451	10.286	6.5738	8.4194	9.0182	9.0953	10.033	10.526	8.3444
48	11.641	10.461	10.296	8.2451	10.286	6.5738	8.4194	9.0182	9.0953	10.033	10.526	8.3444
49	11.641	10.461	10.296	8.2451	10.286	6.5738	8.4194	9.0182	9.0953	10.033	10.526	8.3444
50	11.641	10.461	10.296	8.2451	10.286	6.5738	8.4194	9.0182	9.0953	10.033	10.526	8.3444
51	11.641	10.461	10.296	8.2451	10.286	6.5738	8.4194	9.0182	9.0953	10.033	10.526	8.3444
52	11.641	10.461	10.296	8.2451	10.286	6.5738	8.4194	9.0182	9.0953	10.033	10.526	8.3444
53	11.641	10.461	10.296	8.2451	10.286	6.5738	8.4194	9.0182	9.0953	10.033	10.526	8.3444
54	11.641	10.461	10.296	8.2451	10.286	6.5738	8.4194	9.0182	9.0953	10.033	10.526	8.3444
55	11.641	10.461	10.296	8.2451	10.286	6.5738	8.4194	9.0182	9.0953	10.033	10.526	8.3444
56	11.641	10.461	10.296	8.2451	10.286	6.5738	8.4194	9.0182	9.0953	10.033	10.526	8.3444
57	11.641	10.461	10.296	8.2451	10.286	6.5738	8.4194	9.0182	9.0953	10.033	10.526	8.3444
58	11.641	10.461	10.296	8.2451	10.286	6.5738	8.4194	9.0182	9.0953	10.033	10.526	8.3444

59	11.641	10.461	10.296	8.2451	10.286	6.5738	8.4194	9.0182	9.0953	10.033	10.526	8.3444
60	11.641	10.461	10.296	8.2451	10.286	6.5738	8.4194	9.0182	9.0953	10.033	10.526	8.3444

TABLE VI

Normal error curves for reconstruction sigma = 0.001

Iteration	N2	N3	N4	N5	N6	N8	N9	N10	N11	N13	N16	N17
	0.001											
1	30.022	29.777	29.717	23.939	29.291	22.157	23.45	29.937	24.882	27.47	29.912	25.288
2	20.414	20.969	20.856	18.6	18.748	19.837	17.527	20.336	18.657	18.749	19.29	20.757
3	17.712	17.241	17.656	13.879	16.181	12.393	12.594	16.007	15.642	16.499	16.253	16.239
4	15.099	13.51	13.379	12.223	13.703	10.526	11.188	11.918	12.545	13.859	13.769	13.448
5	14.146	12.66	12.464	10.707	12.342	9.0403	10.153	11.173	11.071	12.894	12.922	11.237
6	13.09	11.882	11.534	9.9931	11.69	8.3105	9.5223	10.296	10.148	12.156	12.016	10.18
7	12.651	11.365	10.973	9.3674	11.358	7.4729	9.2026	9.715	9.8082	11.532	11.257	9.4557
8	12.312	11.078	10.558	9.1024	10.999	7.1495	8.9916	9.5165	9.4054	11.29	10.941	9.0234
9	12.08	10.907	10.334	8.8508	10.819	6.7328	8.864	9.2366	9.233	10.831	10.784	8.6849
10	11.896	10.76	10.092	8.6646	10.628	6.5945	8.7402	9.1107	9.0836	10.683	10.644	8.3831
11	11.774	10.678	9.9397	8.5574	10.506	6.3095	8.6378	9.015	8.9678	10.553	10.439	8.1814
12	11.694	10.554	9.8605	8.4332	10.416	6.2051	8.5418	8.9238	8.8693	10.453	10.365	8.001
13	11.602	10.468	9.7493	8.3674	10.351	6.0653	8.4723	8.8453	8.7822	10.391	10.289	7.8824
14	11.535	10.428	9.6953	8.3059	10.295	5.9795	8.4121	8.7895	8.7155	10.339	10.229	7.7925
15	11.449	10.376	9.6346	8.2692	10.245	5.8975	8.3634	8.7402	8.6651	10.281	10.171	7.7094
16	11.382	10.332	9.5855	8.234	10.175	5.8365	8.337	8.7041	8.6213	10.23	10.13	7.6545
17	11.315	10.304	9.5452	8.1939	10.136	5.7814	8.2964	8.665	8.5893	10.187	10.091	7.6071
18	11.265	10.274	9.5093	8.1539	10.109	5.7272	8.2687	8.6242	8.5638	10.164	10.059	7.5593
19	11.22	10.243	9.4808	8.1172	10.067	5.6895	8.2477	8.5963	8.5396	10.14	10.031	7.5085
20	11.177	10.221	9.4542	8.0939	10.042	5.664	8.2282	8.5673	8.5176	10.122	10.011	7.468
21	11.144	10.199	9.4286	8.0625	10.017	5.64	8.2098	8.5425	8.5001	10.096	9.9789	7.4323
22	11.116	10.183	9.4039	8.0413	9.9958	5.6228	8.1883	8.5253	8.4806	10.075	9.9595	7.3992
23	11.079	10.168	9.3856	8.0161	9.9763	5.6087	8.1666	8.5054	8.4662	10.059	9.9427	7.3608
24	11.044	10.144	9.3758	7.9913	9.9536	5.5973	8.1497	8.4921	8.4486	10.047	9.9291	7.3381
25	11.022	10.132	9.3616	7.9732	9.9427	5.5848	8.1351	8.479	8.433	10.038	9.9129	7.3138

26	10.994	10.121	9.3478	7.9527	9.9267	5.5723	8.1245	8.4636	8.4213	10.023	9.8981	7.2956
27	10.975	10.108	9.3355	7.9386	9.9165	5.5638	8.1143	8.4553	8.4087	10.015	9.8846	7.279
28	10.958	10.097	9.3234	7.926	9.9058	5.5562	8.1069	8.4444	8.3966	10.003	9.875	7.2651
29	10.94	10.089	9.314	7.9146	9.8972	5.5504	8.1007	8.4363	8.3896	9.9946	9.8657	7.2527
30	10.924	10.082	9.3041	7.9058	9.8869	5.545	8.0956	8.43	8.3802	9.9864	9.8573	7.2439
31	10.91	10.074	9.2971	7.8982	9.8787	5.5394	8.0882	8.4226	8.37	9.9794	9.85	7.2373
32	10.898	10.067	9.2903	7.8907	9.8711	5.5346	8.0844	8.4157	8.3631	9.9741	9.844	7.2287
33	10.886	10.063	9.2837	7.8832	9.8661	5.53	8.0801	8.4121	8.3572	9.9682	9.8395	7.221
34	10.876	10.058	9.279	7.8788	9.8602	5.5265	8.0769	8.4069	8.3518	9.9639	9.8343	7.2147
35	10.867	10.054	9.2741	7.8741	9.8539	5.5232	8.0724	8.4033	8.3462	9.9581	9.8299	7.2092
36	10.857	10.05	9.2704	7.8706	9.8498	5.5207	8.0685	8.4002	8.3412	9.9541	9.8263	7.2044
37	10.849	10.047	9.267	7.8674	9.8461	5.5185	8.0653	8.3973	8.3362	9.9499	9.823	7.1999
38	10.839	10.044	9.2639	7.8638	9.8418	5.5159	8.0624	8.3955	8.3326	9.9463	9.8198	7.1961
39	10.833	10.042	9.2612	7.8615	9.8381	5.5139	8.0599	8.3938	8.3289	9.9423	9.8169	7.1926
40	10.827	10.039	9.2583	7.8596	9.835	5.5123	8.0581	8.3917	8.3258	9.9388	9.8144	7.1899
41	10.819	10.037	9.2559	7.8575	9.8325	5.5107	8.0564	8.3898	8.3226	9.9346	9.8122	7.1874
42	10.814	10.035	9.2542	7.8557	9.8301	5.5093	8.0549	8.3886	8.32	9.9319	9.81	7.1854
43	10.809	10.033	9.2522	7.8537	9.8276	5.508	8.0533	8.3875	8.3178	9.9286	9.8083	7.1834
44	10.806	10.031	9.2507	7.852	9.8256	5.5069	8.052	8.386	8.3159	9.9264	9.8064	7.1822
45	10.802	10.03	9.2492	7.8501	9.8233	5.5061	8.0509	8.385	8.3137	9.924	9.8046	7.1809
46	10.799	10.028	9.248	7.8481	9.8215	5.5052	8.05	8.3841	8.312	9.9222	9.8031	7.1796
47	10.796	10.027	9.2469	7.8462	9.82	5.5046	8.0491	8.3833	8.3105	9.9204	9.8015	7.1788
48	10.793	10.026	9.2456	7.8446	9.8186	5.5038	8.0483	8.3824	8.3091	9.9183	9.8002	7.178
49	10.79	10.025	9.2446	7.843	9.8169	5.5032	8.0476	8.3818	8.3077	9.917	9.799	7.1772
50	10.787	10.024	9.2435	7.8417	9.8156	5.5027	8.0468	8.3809	8.3066	9.916	9.7981	7.1765
51	10.785	10.023	9.2427	7.8406	9.8146	5.5024	8.0462	8.3804	8.3056	9.9148	9.7971	7.1758
52	10.783	10.023	9.2418	7.8397	9.8134	5.5021	8.0457	8.38	8.3046	9.9137	9.7962	7.1753
53	10.781	10.022	9.2411	7.8389	9.8125	5.5018	8.0453	8.3796	8.3038	9.9127	9.7954	7.1748
54	10.779	10.021	9.2403	7.8383	9.8115	5.5015	8.045	8.3792	8.3031	9.9118	9.7947	7.1744
55	10.777	10.021	9.2398	7.8376	9.8105	5.5013	8.0446	8.3787	8.3024	9.9111	9.7941	7.1741
56	10.776	10.02	9.2392	7.8371	9.8096	5.501	8.0444	8.3784	8.3019	9.9104	9.7936	7.1738
57	10.774	10.02	9.2387	7.8365	9.8089	5.5009	8.0441	8.3781	8.3013	9.9097	9.7931	7.1735
58	10.773	10.019	9.2381	7.8361	9.8082	5.5007	8.0439	8.3778	8.3008	9.9091	9.7926	7.1733

59	10.772	10.019	9.2376	7.8356	9.8076	5.5005	8.0437	8.3776	8.3004	9.9087	9.7922	7.1731
60	10.771	10.018	9.2371	7.8352	9.807	5.5004	8.0435	8.3774	8.3001	9.9082	9.7918	7.1729

TABLE VII

Normal error curves for reconstruction sigma = 0.0001

Iteration	N2	N3	N4	N5	N6	N8	N9	N10	N11	N13	N16	N17
	0.0001											
1	30.017	29.767	29.708	23.947	29.289	22.148	23.426	29.936	24.871	27.463	29.903	25.286
2	20.387	20.955	20.848	18.593	18.728	19.833	17.521	20.328	18.656	18.723	19.278	20.767
3	17.711	17.257	17.653	13.923	16.175	12.402	12.617	16.03	15.656	16.512	16.256	16.26
4	15.106	13.532	13.377	12.259	13.722	10.551	11.213	11.929	12.548	13.897	13.785	13.471
5	14.172	12.699	12.48	10.755	12.366	9.0804	10.197	11.207	11.078	12.954	12.954	11.274
6	13.136	11.942	11.562	10.061	11.745	8.3545	9.5725	10.357	10.178	12.228	12.067	10.228
7	12.706	11.431	11.01	9.4405	11.426	7.5442	9.2601	9.772	9.8482	11.634	11.318	9.5099
8	12.378	11.149	10.595	9.1848	11.072	7.2218	9.0591	9.5814	9.4584	11.395	11.005	9.0996
9	12.148	10.983	10.381	8.9437	10.899	6.8223	8.9397	9.2941	9.2933	10.939	10.85	8.7688
10	11.964	10.839	10.142	8.7697	10.715	6.6874	8.8202	9.1732	9.1509	10.795	10.711	8.4657
11	11.848	10.761	9.991	8.662	10.591	6.4074	8.7186	9.0776	9.0349	10.673	10.508	8.2672
12	11.773	10.635	9.9094	8.5508	10.509	6.2999	8.6199	8.9846	8.9388	10.579	10.432	8.0963
13	11.681	10.55	9.7972	8.4893	10.449	6.1689	8.5545	8.9082	8.8486	10.525	10.356	7.9852
14	11.612	10.513	9.742	8.4314	10.394	6.083	8.4937	8.853	8.781	10.475	10.294	7.9013
15	11.523	10.463	9.6831	8.3957	10.345	6.003	8.4456	8.8015	8.7298	10.416	10.234	7.816
16	11.452	10.415	9.6352	8.3605	10.274	5.941	8.4219	8.7642	8.6847	10.36	10.192	7.7569
17	11.379	10.387	9.5914	8.3189	10.233	5.8863	8.3774	8.7269	8.6507	10.316	10.15	7.7117
18	11.327	10.352	9.552	8.2775	10.209	5.8319	8.3497	8.685	8.6284	10.294	10.112	7.6625
19	11.281	10.319	9.5235	8.2405	10.167	5.7917	8.3255	8.6602	8.6027	10.265	10.08	7.6098
20	11.242	10.293	9.496	8.2212	10.14	5.7634	8.3054	8.6316	8.5794	10.247	10.059	7.5664
21	11.206	10.272	9.4663	8.1855	10.113	5.7378	8.2823	8.6094	8.562	10.213	10.021	7.5269
22	11.173	10.253	9.4341	8.1629	10.093	5.7184	8.2561	8.5935	8.538	10.189	9.9977	7.491
23	11.129	10.235	9.4148	8.132	10.07	5.7029	8.2294	8.5731	8.5232	10.172	9.977	7.4469
24	11.088	10.202	9.4063	8.1033	10.042	5.6888	8.209	8.5582	8.503	10.158	9.961	7.4222
25	11.061	10.184	9.3906	8.0824	10.03	5.6722	8.1883	8.5402	8.481	10.147	9.9426	7.3945

26	11.026	10.17	9.3731	8.0577	10.008	5.6538	8.1721	8.5202	8.4668	10.126	9.9218	7.3736
27	11.002	10.151	9.3554	8.0408	9.993	5.6414	8.1579	8.5117	8.4517	10.114	9.9031	7.3529
28	10.984	10.134	9.3371	8.0245	9.9802	5.6305	8.1456	8.497	8.4333	10.096	9.8876	7.3354
29	10.961	10.119	9.3253	8.0106	9.9688	5.6228	8.1362	8.4861	8.425	10.082	9.8735	7.317
30	10.94	10.107	9.3086	7.9979	9.9497	5.6146	8.1277	8.4756	8.4122	10.068	9.8602	7.3036
31	10.919	10.092	9.2969	7.9866	9.9366	5.6049	8.1138	8.4638	8.3958	10.056	9.847	7.2942
32	10.9	10.078	9.2863	7.9739	9.9228	5.5969	8.1069	8.4525	8.3836	10.044	9.8358	7.279
33	10.879	10.069	9.2744	7.9615	9.914	5.5884	8.0977	8.4438	8.3754	10.034	9.8279	7.2678
34	10.859	10.06	9.265	7.9527	9.9021	5.5818	8.0913	8.4348	8.3662	10.026	9.8187	7.2572
35	10.841	10.051	9.2559	7.9435	9.889	5.5753	8.082	8.4267	8.3547	10.014	9.8098	7.2481
36	10.821	10.042	9.2488	7.9372	9.8778	5.5704	8.0719	8.4208	8.3427	10.004	9.8012	7.2376
37	10.804	10.033	9.2421	7.9298	9.8693	5.5647	8.064	8.4145	8.3306	9.9908	9.7931	7.2276
38	10.782	10.026	9.2358	7.9209	9.8582	5.558	8.0556	8.4099	8.3214	9.9803	9.7856	7.219
39	10.772	10.019	9.2309	7.9138	9.8495	5.5529	8.0481	8.4055	8.3144	9.9665	9.7779	7.2098
40	10.76	10.011	9.2231	7.9095	9.8392	5.5484	8.042	8.3986	8.3049	9.9551	9.7708	7.2011
41	10.739	10.003	9.2166	7.9045	9.8303	5.5436	8.0368	8.3927	8.2957	9.9377	9.7635	7.1939
42	10.721	9.9968	9.2123	7.8999	9.8223	5.5387	8.0312	8.3873	8.2873	9.9288	9.7556	7.1867
43	10.71	9.9898	9.2063	7.894	9.8163	5.5339	8.0236	8.3829	8.2801	9.9132	9.7501	7.181
44	10.698	9.9823	9.2003	7.888	9.8064	5.53	8.018	8.377	8.2727	9.9016	9.7424	7.1753
45	10.684	9.9758	9.1949	7.8803	9.7957	5.5257	8.0123	8.3717	8.2663	9.8877	9.7347	7.1699
46	10.671	9.9661	9.1919	7.873	9.7847	5.5218	8.0081	8.368	8.2592	9.8769	9.7283	7.1634
47	10.657	9.9592	9.1872	7.8649	9.7784	5.5178	8.0033	8.3635	8.2532	9.8652	9.7194	7.1589
48	10.643	9.9525	9.1819	7.8573	9.7699	5.513	7.9971	8.3596	8.2454	9.8506	9.7116	7.1546
49	10.627	9.9444	9.1768	7.8492	9.757	5.5096	7.992	8.3555	8.2375	9.8401	9.7058	7.1493
50	10.604	9.9375	9.1699	7.8415	9.7464	5.5063	7.9871	8.3493	8.2287	9.8336	9.6996	7.144
51	10.581	9.932	9.1639	7.8345	9.7409	5.5036	7.9823	8.3456	8.2219	9.8219	9.6914	7.1388
52	10.565	9.9234	9.1573	7.829	9.7282	5.5009	7.9777	8.3417	8.2126	9.8123	9.6851	7.1343
53	10.55	9.9179	9.1527	7.8224	9.7177	5.4985	7.9736	8.3368	8.2052	9.8011	9.6773	7.1293
54	10.534	9.9099	9.1457	7.8165	9.7044	5.4951	7.9687	8.333	8.1971	9.7905	9.6706	7.1252
55	10.523	9.903	9.1413	7.8087	9.6927	5.4923	7.9642	8.3273	8.1891	9.7812	9.666	7.1212
56	10.505	9.8964	9.1346	7.8021	9.6801	5.4894	7.9608	8.323	8.1813	9.7719	9.6603	7.1177
57	10.494	9.886	9.1285	7.7947	9.6669	5.4867	7.9576	8.3179	8.1735	9.7613	9.6531	7.1126
58	10.485	9.8749	9.1207	7.7875	9.6554	5.4834	7.9539	8.3131	8.1651	9.7495	9.6463	7.1096

59	10.471	9.8643	9.1116	7.7774	9.6412	5.4803	7.9496	8.3083	8.1558	9.7401	9.6394	7.1047
60	10.457	9.8522	9.1036	7.7681	9.6295	5.4782	7.9446	8.3042	8.1497	9.7317	9.6309	7.0995

TABLE VIII

Normal error curves for reconstruction sigma = 0.00001

Iteration	N2	N3	N4	N5	N6	N8	N9	N10	N11	N13	N16	N17
	0.00001											
1	30.017	29.766	29.707	23.948	29.289	22.147	23.423	29.936	24.87	27.463	29.902	25.286
2	20.384	20.954	20.847	18.592	18.726	19.833	17.521	20.327	18.656	18.721	19.277	20.768
3	17.711	17.258	17.653	13.927	16.175	12.403	12.619	16.033	15.658	16.513	16.257	16.262
4	15.107	13.534	13.378	12.263	13.724	10.554	11.216	11.931	12.548	13.901	13.787	13.474
5	14.175	12.703	12.482	10.76	12.369	9.0849	10.202	11.211	11.08	12.96	12.957	11.278
6	13.141	11.949	11.566	10.069	11.751	8.3596	9.578	10.363	10.182	12.236	12.073	10.234
7	12.712	11.438	11.014	9.4485	11.434	7.5522	9.2664	9.7784	9.8529	11.645	11.325	9.5162
8	12.386	11.156	10.6	9.1938	11.08	7.23	9.0664	9.5887	9.4645	11.406	11.012	9.1082
9	12.155	10.992	10.387	8.9539	10.907	6.8325	8.9479	9.3007	9.3003	10.95	10.857	8.7785
10	11.972	10.848	10.148	8.7813	10.725	6.698	8.829	9.1803	9.1586	10.807	10.718	8.4754
11	11.856	10.77	9.9976	8.6736	10.6	6.4189	8.7275	9.0848	9.0426	10.687	10.517	8.2775
12	11.782	10.645	9.9158	8.564	10.52	6.3111	8.6286	8.9916	8.947	10.593	10.441	8.1079
13	11.69	10.56	9.8037	8.5028	10.46	6.1816	8.5638	8.9156	8.8566	10.54	10.364	7.9979
14	11.621	10.523	9.7486	8.4454	10.405	6.0959	8.503	8.8607	8.7891	10.49	10.302	7.9148
15	11.532	10.473	9.6901	8.4099	10.356	6.0164	8.4551	8.8091	8.738	10.431	10.242	7.8295
16	11.461	10.425	9.6426	8.3749	10.286	5.9543	8.4318	8.7718	8.6929	10.376	10.2	7.7701
17	11.387	10.397	9.5987	8.3332	10.245	5.9	8.3872	8.735	8.6589	10.332	10.158	7.7255
18	11.335	10.362	9.559	8.2919	10.222	5.846	8.3597	8.6934	8.6372	10.309	10.119	7.6766
19	11.29	10.328	9.5307	8.2552	10.18	5.8058	8.3351	8.6691	8.6115	10.28	10.087	7.624
20	11.251	10.302	9.5033	8.2366	10.153	5.7773	8.3151	8.6407	8.5884	10.262	10.066	7.5806
21	11.215	10.282	9.4733	8.2007	10.126	5.7516	8.2915	8.6189	8.5712	10.228	10.027	7.5411
22	11.182	10.262	9.4406	8.1782	10.107	5.7321	8.265	8.6033	8.5468	10.204	10.004	7.5054
23	11.137	10.244	9.4214	8.1468	10.084	5.7167	8.238	8.5831	8.5323	10.187	9.9831	7.4614
24	11.096	10.211	9.4135	8.1182	10.056	5.7024	8.2175	8.5682	8.5123	10.173	9.967	7.4369
25	11.069	10.192	9.3979	8.0974	10.044	5.6852	8.1964	8.5497	8.4898	10.161	9.9488	7.4095
26	11.034	10.178	9.3802	8.0724	10.021	5.6663	8.1794	8.5295	8.4758	10.14	9.9275	7.3889

27	11.011	10.157	9.3621	8.0556	10.005	5.6534	8.1649	8.521	8.4609	10.128	9.9082	7.3682
28	10.992	10.14	9.3432	8.0393	9.9929	5.6423	8.152	8.5062	8.4419	10.109	9.8921	7.3505
29	10.97	10.124	9.3315	8.0254	9.9816	5.6345	8.1423	8.495	8.4338	10.096	9.8776	7.3318
30	10.948	10.112	9.3143	8.0124	9.9614	5.6262	8.1335	8.484	8.4212	10.081	9.8638	7.3181
31	10.926	10.096	9.3021	8.0008	9.9483	5.6161	8.119	8.472	8.4043	10.068	9.85	7.3086
32	10.907	10.081	9.2914	7.9876	9.9338	5.6077	8.1118	8.4604	8.3919	10.056	9.8382	7.293
33	10.885	10.072	9.2791	7.975	9.9246	5.5988	8.102	8.451	8.3839	10.046	9.83	7.2819
34	10.865	10.061	9.2691	7.9657	9.912	5.592	8.0952	8.4416	8.3747	10.038	9.8206	7.2712
35	10.846	10.052	9.2598	7.9562	9.8988	5.5853	8.0854	8.4329	8.3629	10.026	9.8115	7.2621
36	10.826	10.043	9.2524	7.9498	9.8863	5.5802	8.0745	8.4267	8.3503	10.015	9.8023	7.251
37	10.808	10.033	9.2456	7.942	9.8774	5.5741	8.066	8.4202	8.3375	10	9.7936	7.2405
38	10.785	10.025	9.2391	7.9326	9.8657	5.5668	8.057	8.4152	8.3277	9.9885	9.7858	7.2314
39	10.775	10.018	9.2343	7.9249	9.8567	5.5615	8.0487	8.4106	8.3208	9.9728	9.7774	7.2218
40	10.763	10.009	9.2258	7.9204	9.8455	5.5566	8.0418	8.4028	8.3106	9.9607	9.7698	7.2123
41	10.74	10.001	9.2187	7.9152	9.8359	5.5513	8.0362	8.3965	8.3012	9.9411	9.7618	7.2046
42	10.721	9.9936	9.2141	7.9105	9.8273	5.546	8.0299	8.3903	8.2922	9.9319	9.7531	7.1967
43	10.709	9.9859	9.2076	7.9043	9.8217	5.5407	8.0213	8.3855	8.2851	9.9137	9.7472	7.1907
44	10.697	9.9775	9.2007	7.8978	9.8105	5.5365	8.0149	8.3787	8.2772	9.9005	9.7388	7.1843
45	10.682	9.9701	9.195	7.8891	9.7986	5.5316	8.0084	8.3728	8.2711	9.8842	9.73	7.1783
46	10.667	9.9587	9.192	7.8814	9.7855	5.5272	8.0036	8.3688	8.2637	9.8715	9.7229	7.1711
47	10.653	9.9505	9.1868	7.8726	9.7792	5.5226	7.9981	8.3635	8.2575	9.8579	9.713	7.1663
48	10.638	9.9426	9.1809	7.8641	9.7695	5.517	7.991	8.3594	8.249	9.8402	9.7032	7.1614
49	10.621	9.9329	9.1753	7.855	9.7539	5.5131	7.9851	8.3546	8.2405	9.8272	9.6968	7.1552
50	10.594	9.9248	9.1673	7.8464	9.7416	5.5094	7.9794	8.3474	8.2305	9.8198	9.6894	7.149
51	10.567	9.9181	9.1604	7.8378	9.7358	5.5061	7.9737	8.3432	8.223	9.8055	9.6793	7.1426
52	10.547	9.9075	9.1526	7.8316	9.7199	5.5028	7.9684	8.3387	8.2123	9.7943	9.6719	7.1374
53	10.531	9.9006	9.1478	7.8236	9.7072	5.4999	7.9634	8.3329	8.2039	9.7807	9.6623	7.1315
54	10.51	9.8907	9.1397	7.8161	9.6903	5.4958	7.9571	8.3286	8.1945	9.7676	9.6542	7.1266
55	10.499	9.8814	9.1349	7.8067	9.6764	5.4924	7.9515	8.3212	8.185	9.7558	9.6487	7.1219
56	10.478	9.8733	9.1266	7.7988	9.6602	5.4888	7.9471	8.3162	8.1755	9.7445	9.6422	7.1176
57	10.463	9.8594	9.1198	7.7899	9.6435	5.4854	7.9435	8.3102	8.1663	9.7323	9.633	7.1109
58	10.453	9.8448	9.1101	7.7812	9.6292	5.4813	7.9389	8.3035	8.1556	9.7168	9.6244	7.1073
59	10.437	9.8299	9.0986	7.7686	9.6094	5.4771	7.9332	8.2975	8.1442	9.7043	9.6155	7.1008
60	10.421	9.8132	9.0887	7.7562	9.5951	5.4744	7.9267	8.2921	8.1369	9.6941	9.6041	7.0942

Appendix 3: Complete Reconstruction Mesh Representation

i.) Normal Brain (N8) Iterations 1-60 Mesh Representation

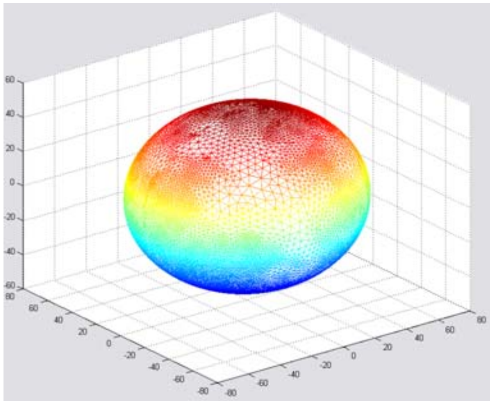

1

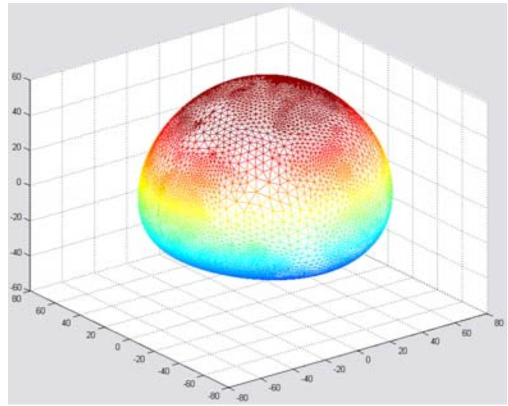

2

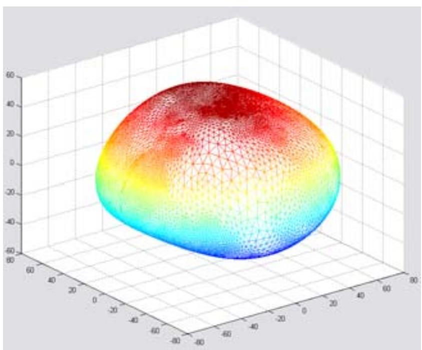

3

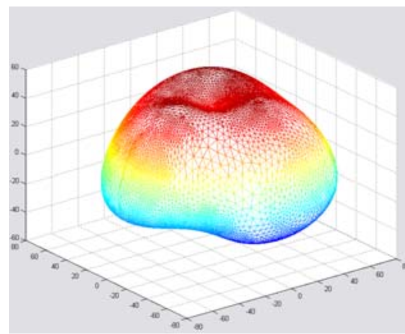

4

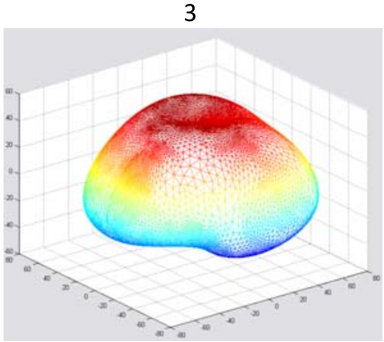

5

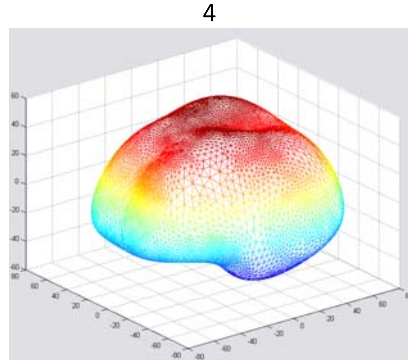

6

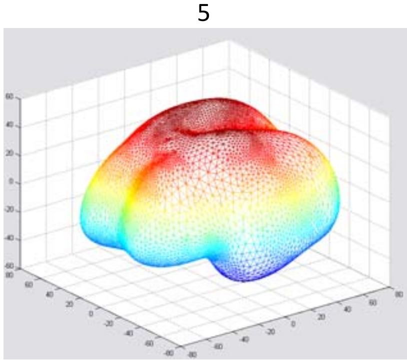

7 (error < 10%)

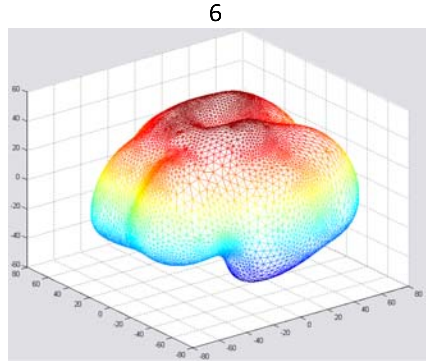

8

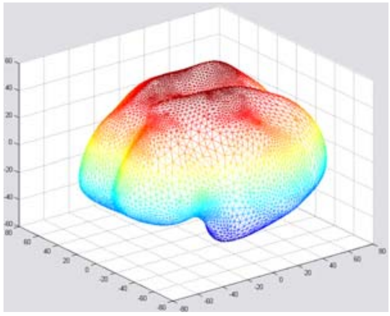

9 (error < 7%)

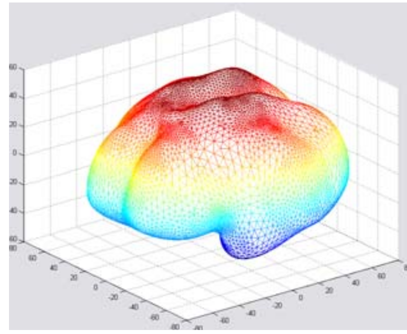

10

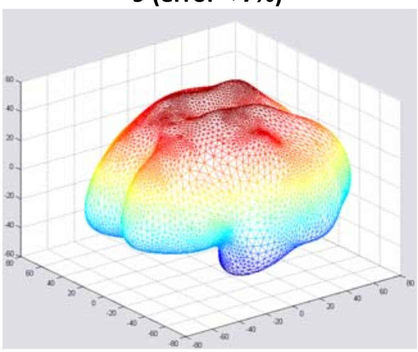

11

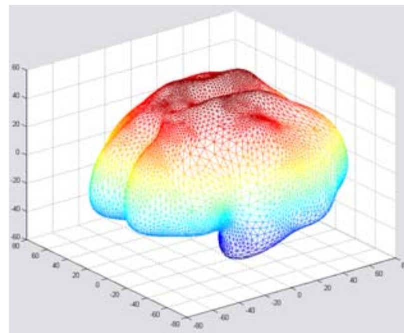

12

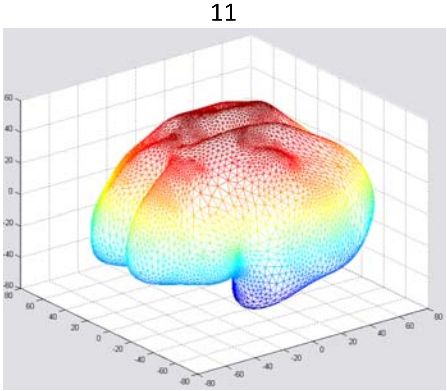

13

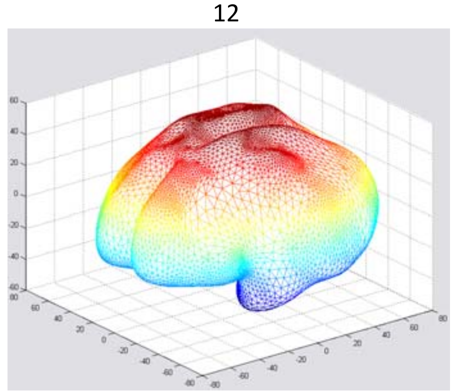

14

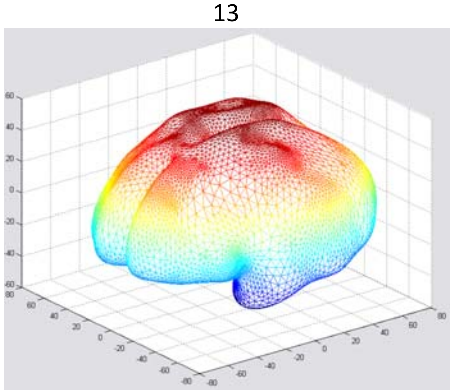

15

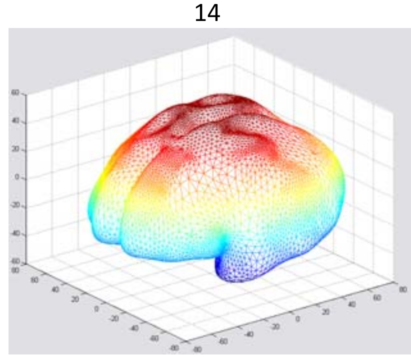

16 (error < 6%)

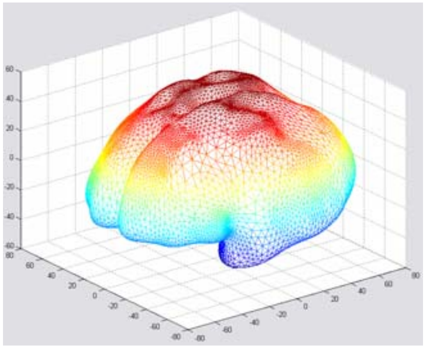
17

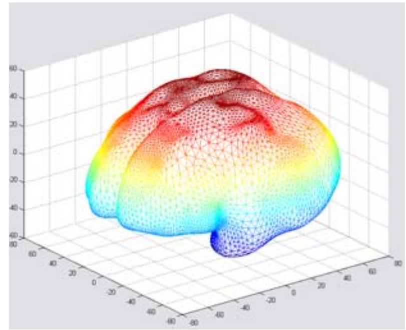
18

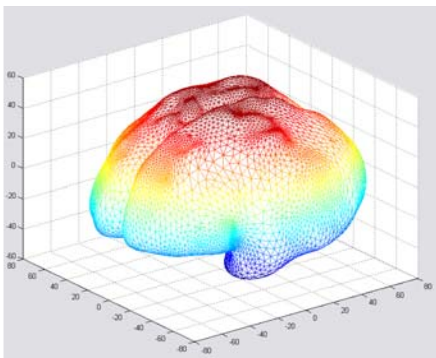
19

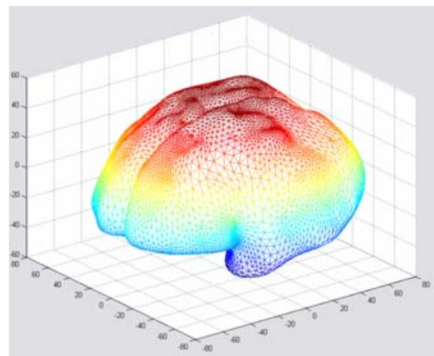
20

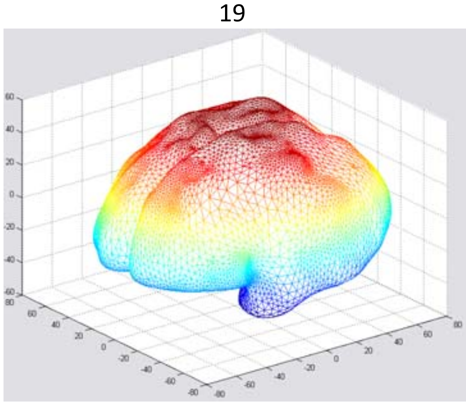
21

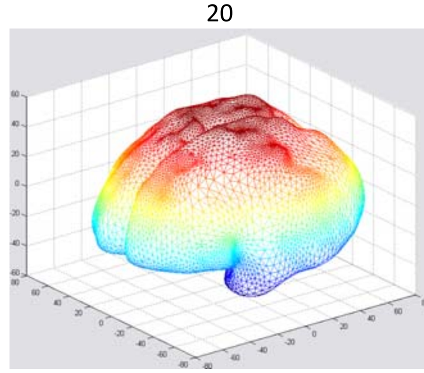
22

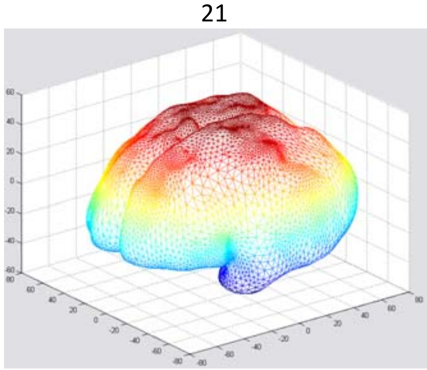
23

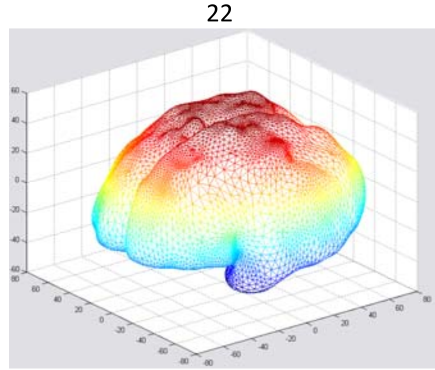
24

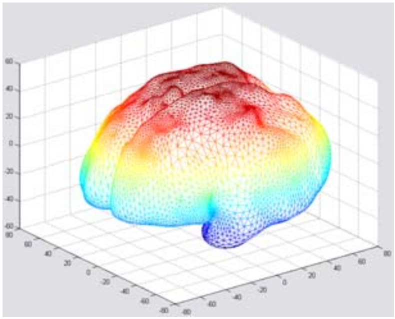

25

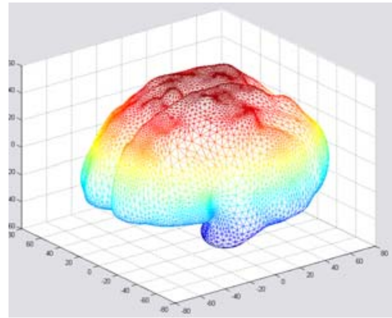

26

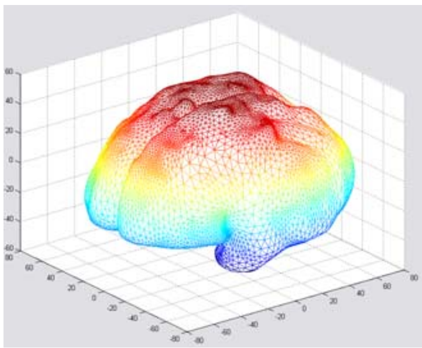

27

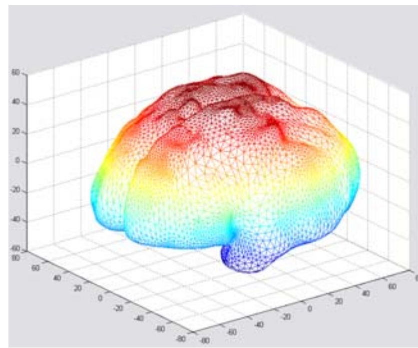

28

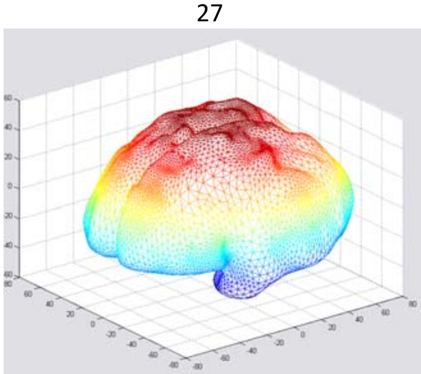

29

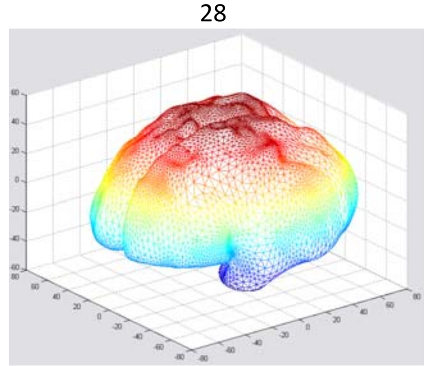

30

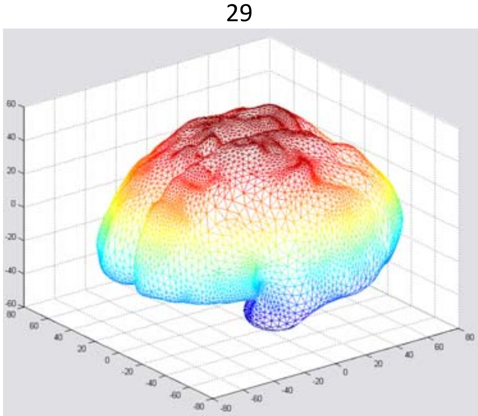

31

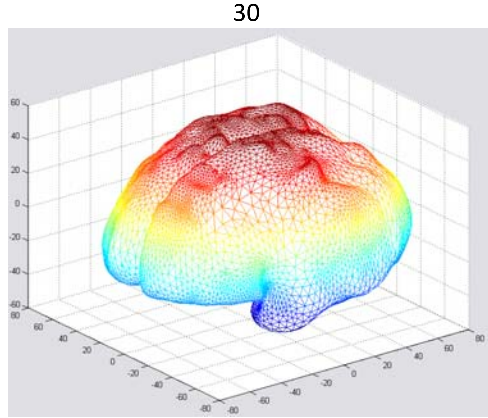

32

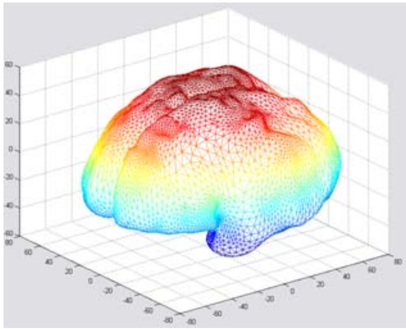
33

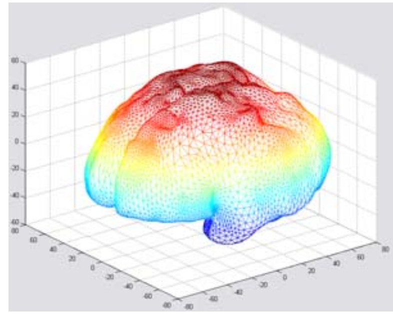
34

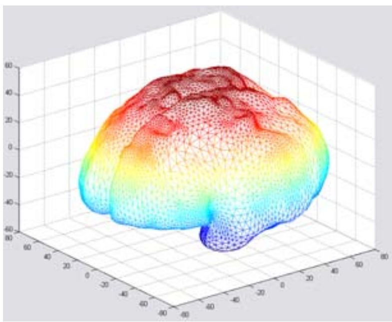
35

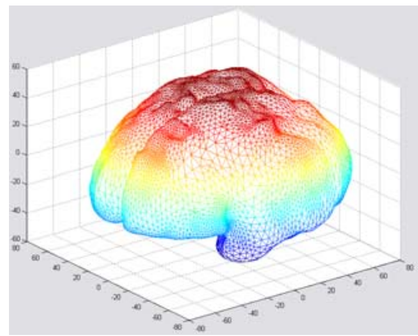
36

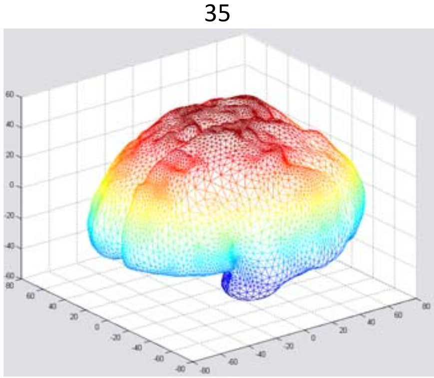
37

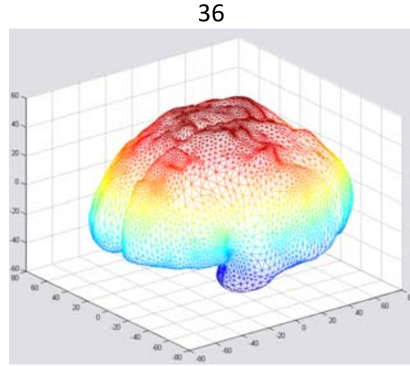
38

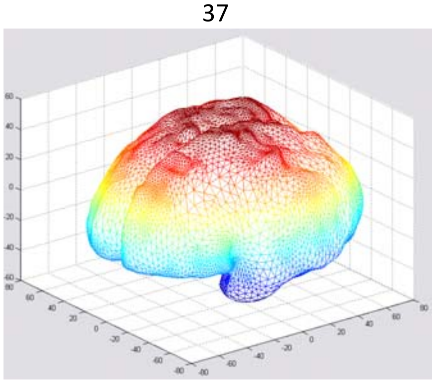
39

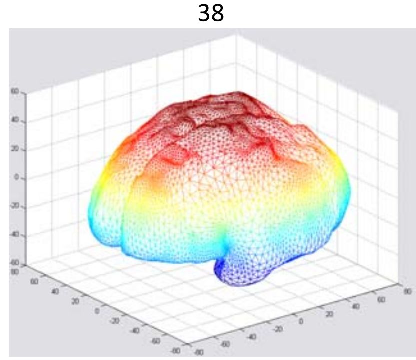
40

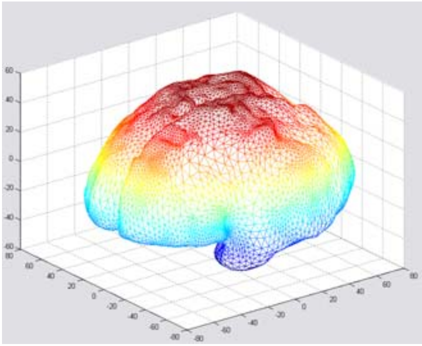
41

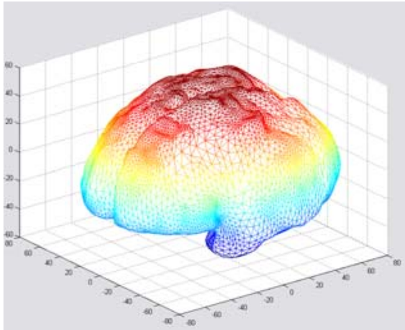
42

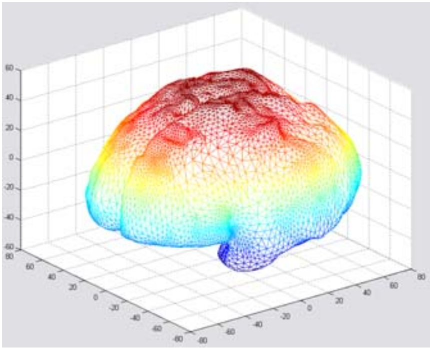
43

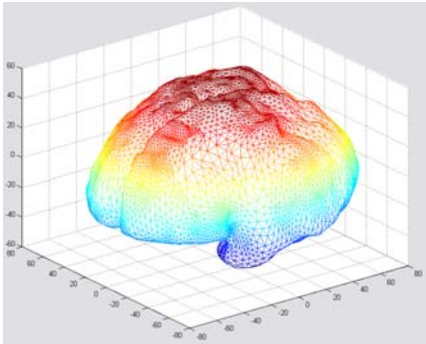
44

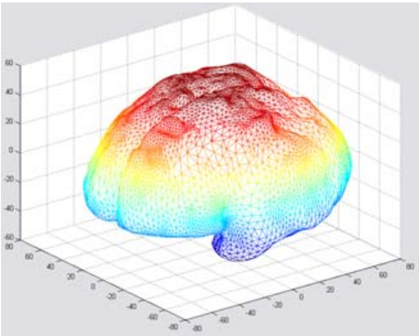
45

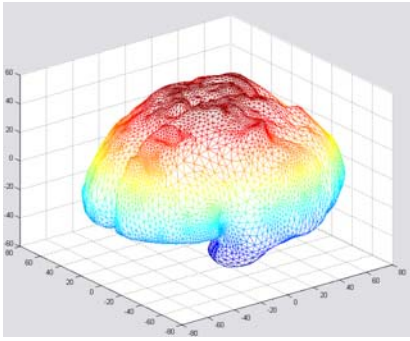
46

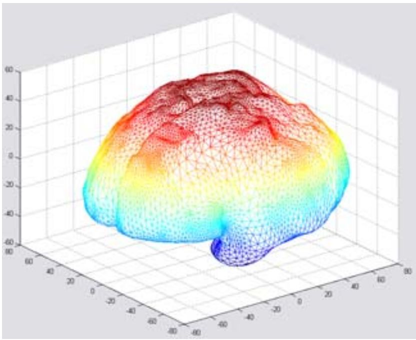
47

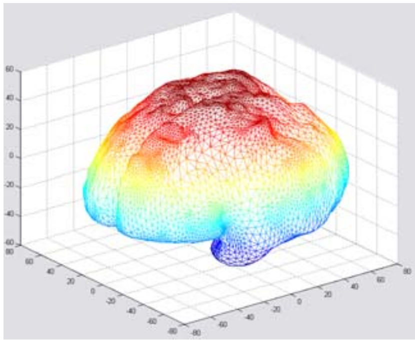
48

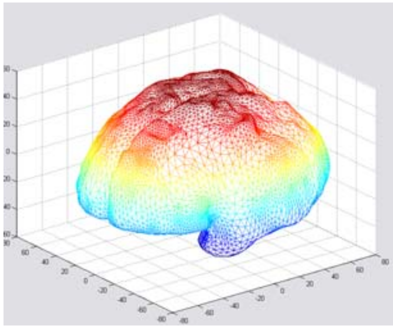
49

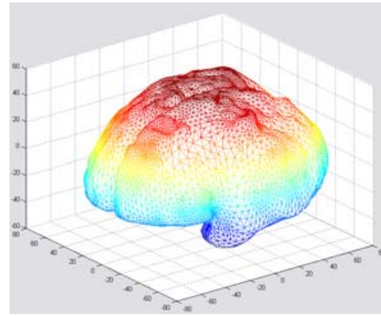
50

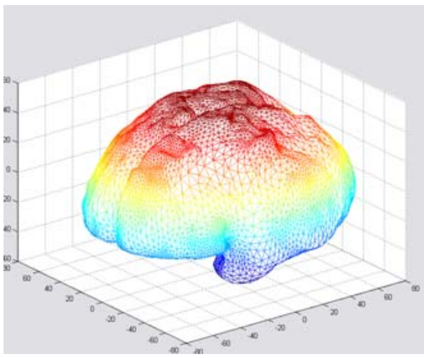
51

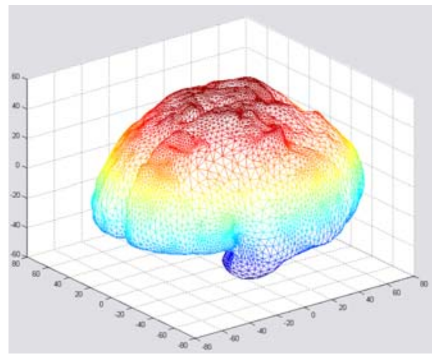
52

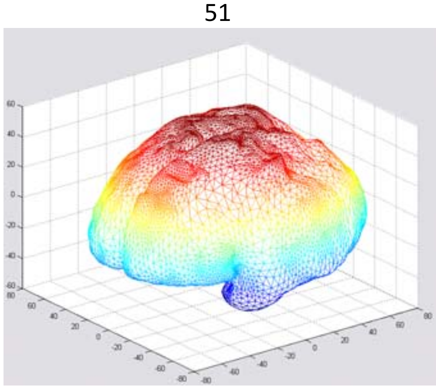
53

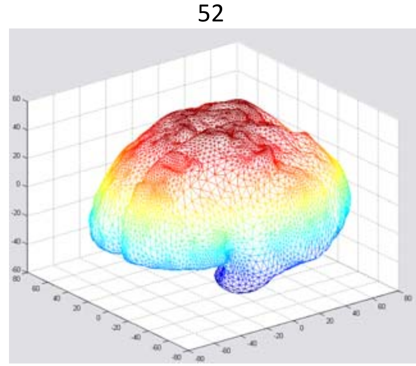
54

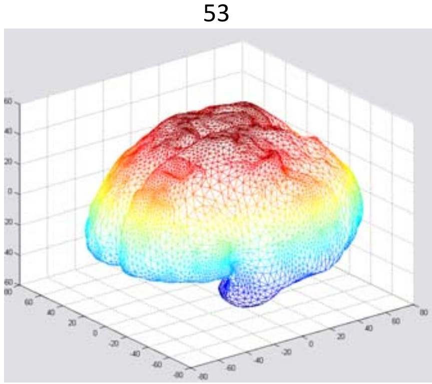
55

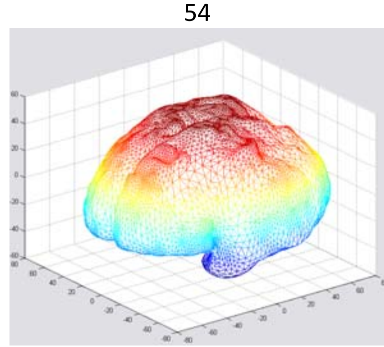
56

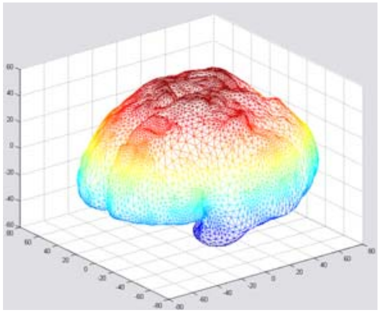

57

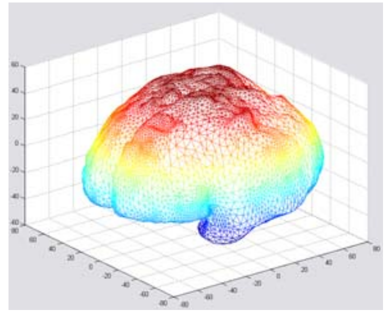

58

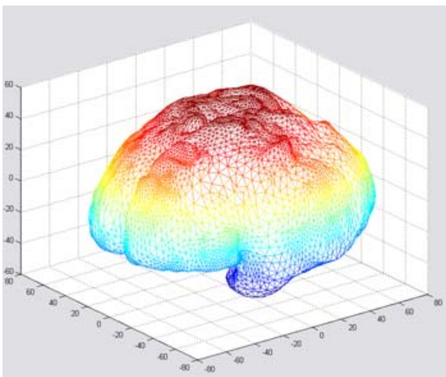

59

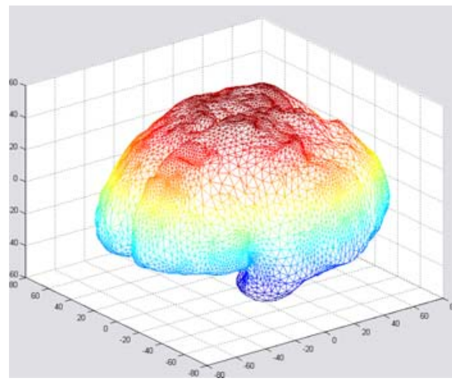

60 (error = 5.4744%)

ii.) Autistic Brain (A13) Iterations 1-60 Mesh Representation

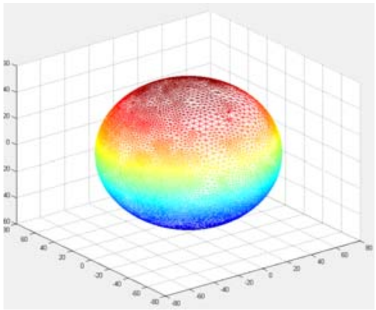
1

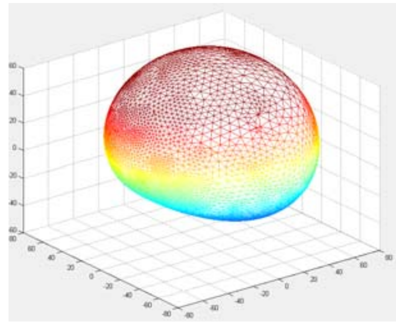
2

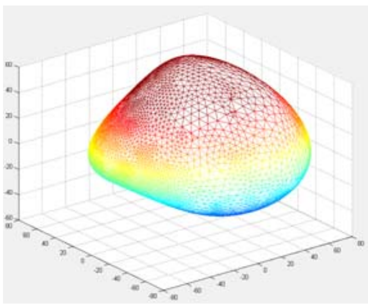
3

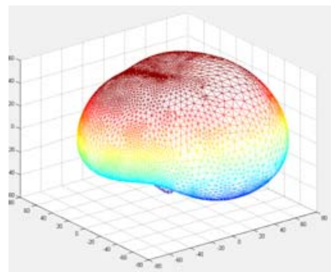
4

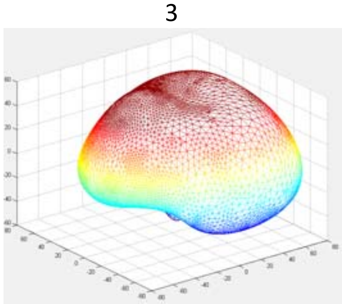
5

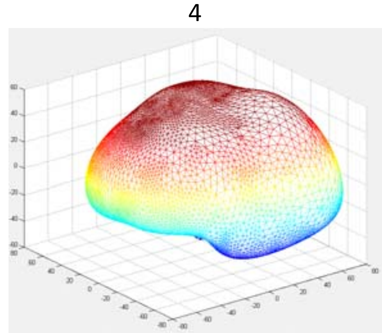
6

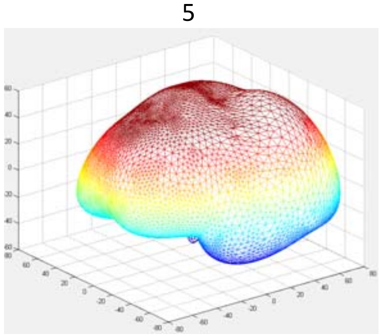
7

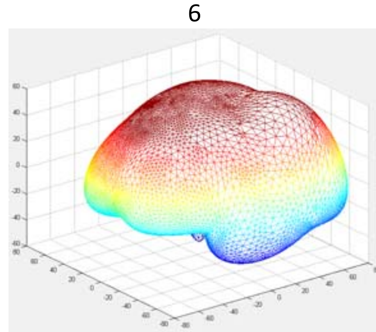
8

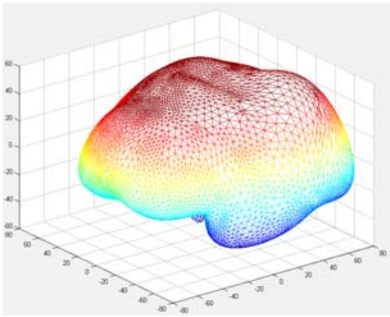
9

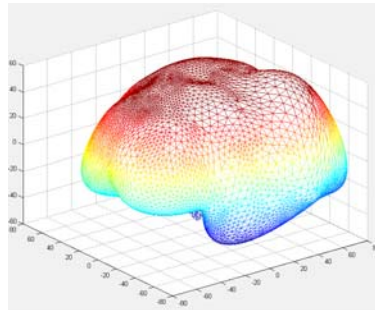
10

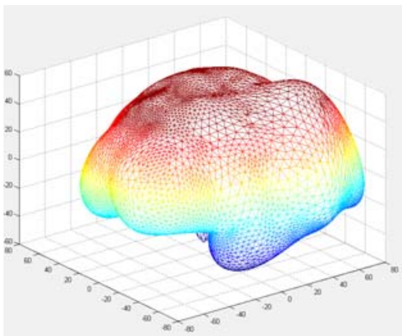
11

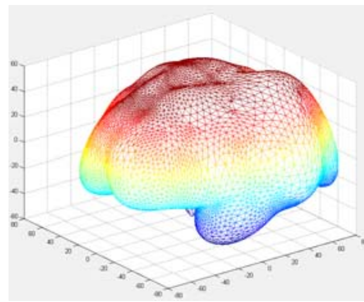
12

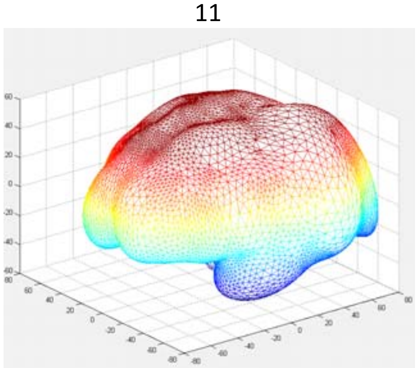
13

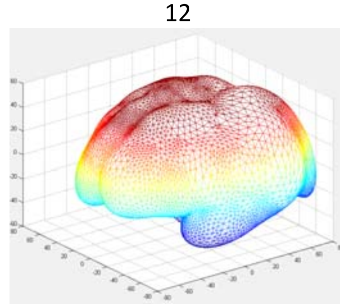
14

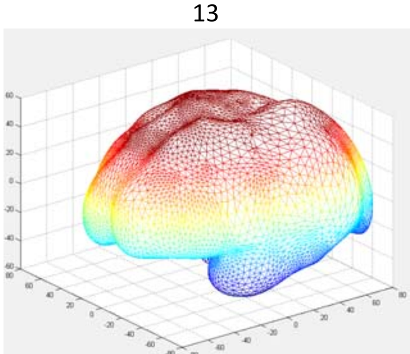
15

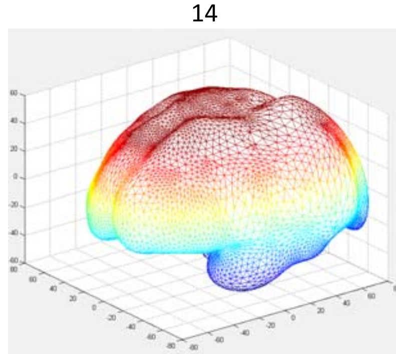
16

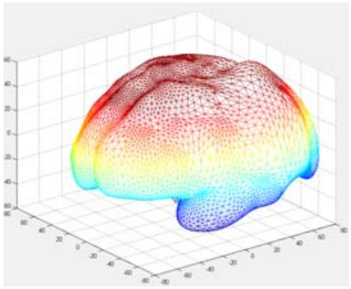
17

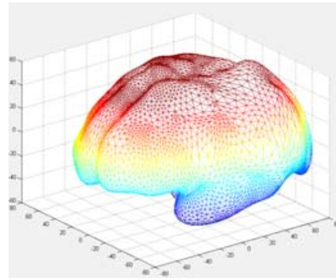
18

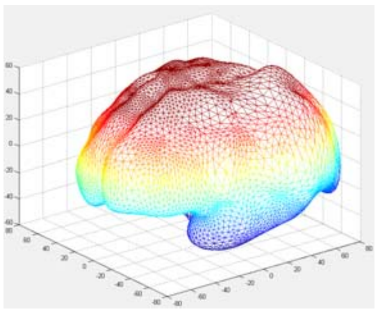
19

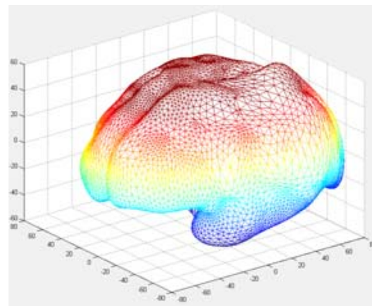
20

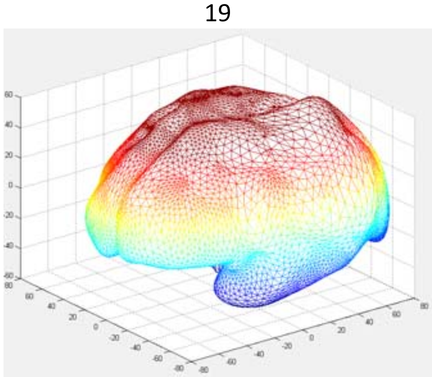
21

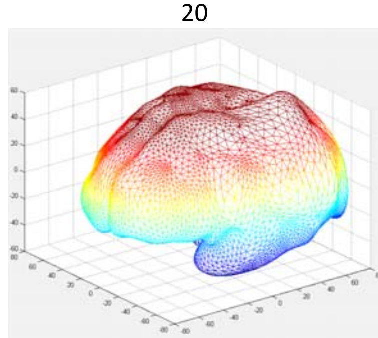
22

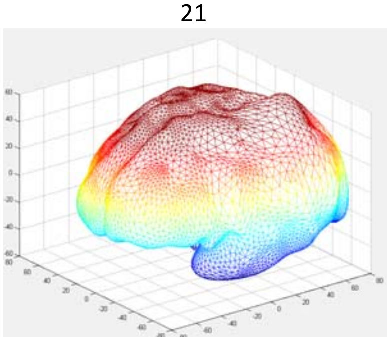
23

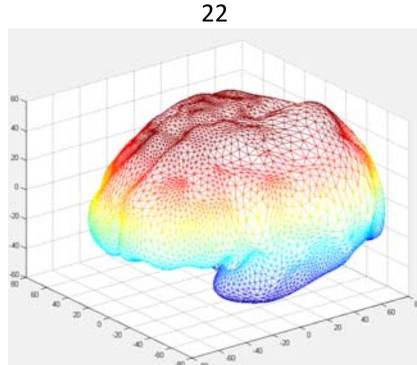
24

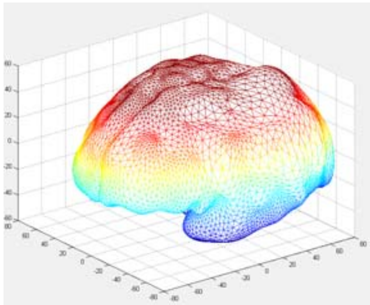
25

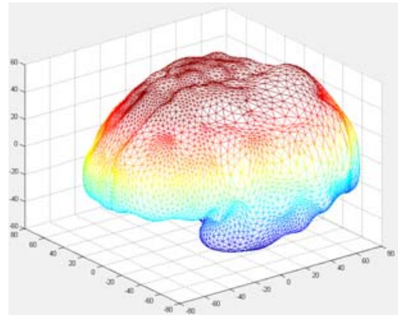
26

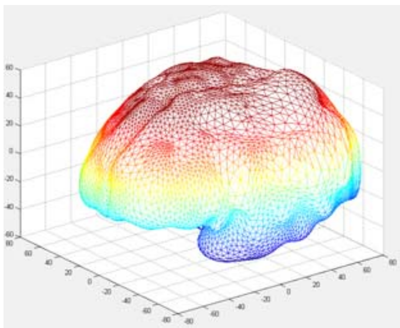
27

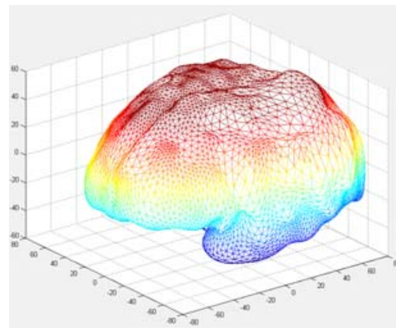
28

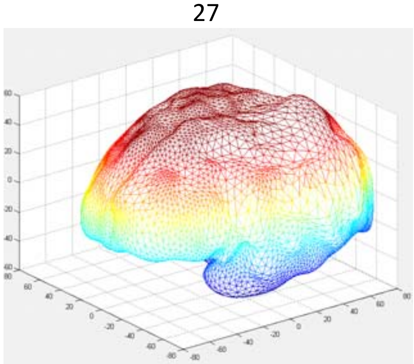
29

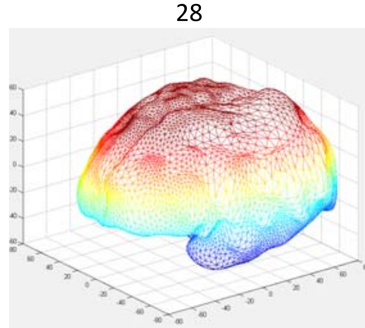
30

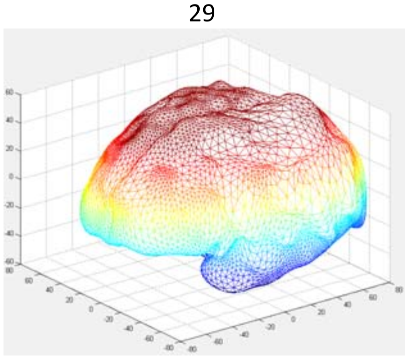
31

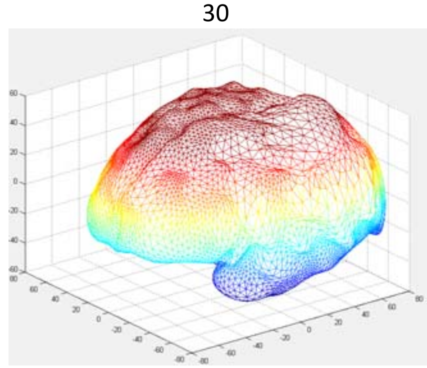
32

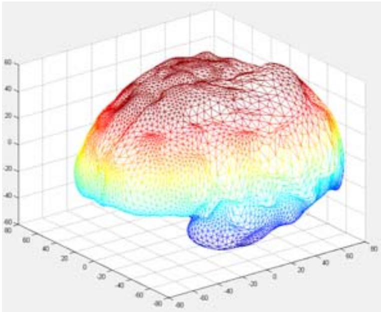
33

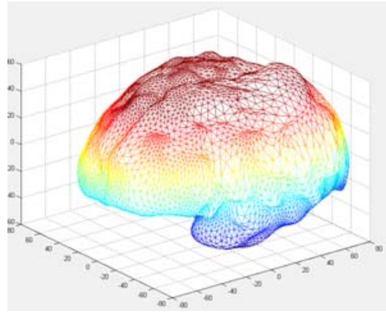
34

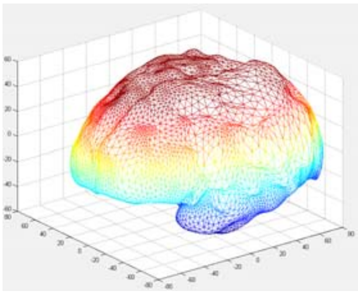
35

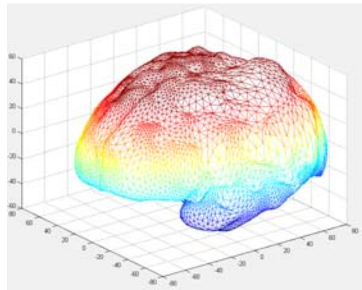
36

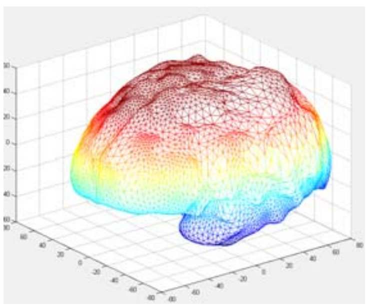
37 (error < 10%)

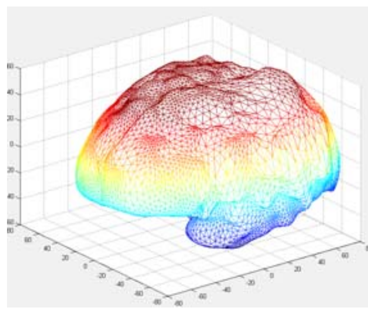
38

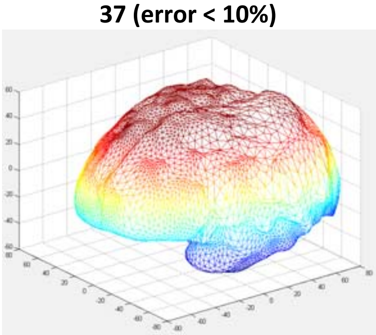
39

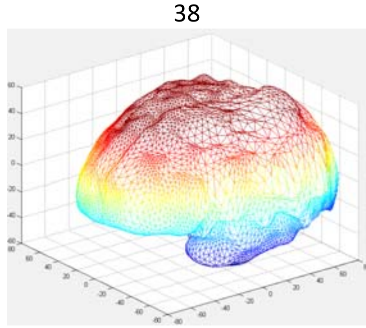
40

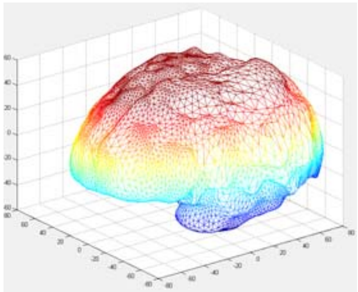

41

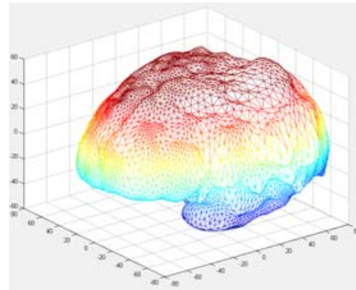

42

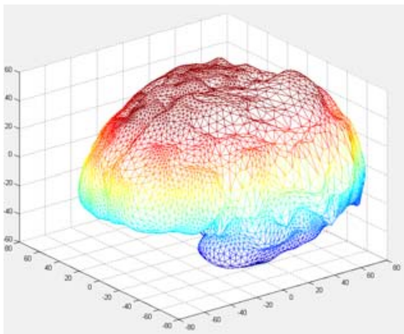

43

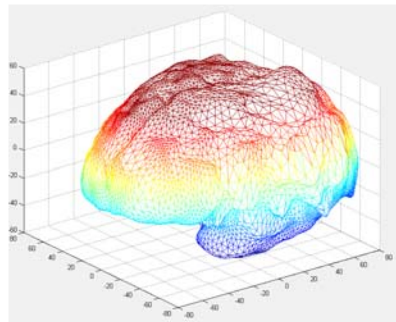

44

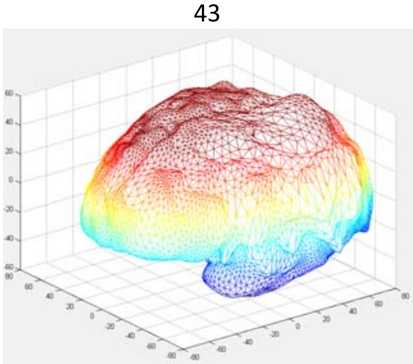

45

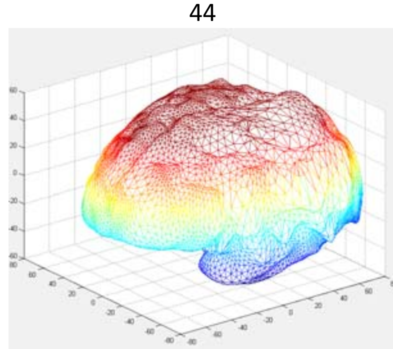

46

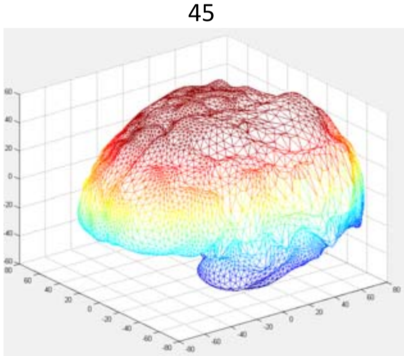

47

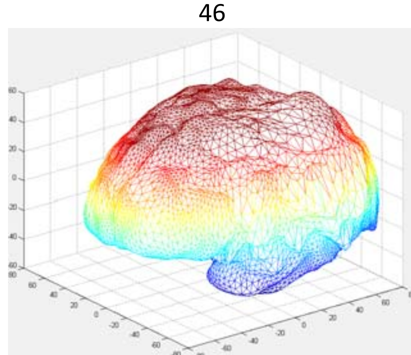

48

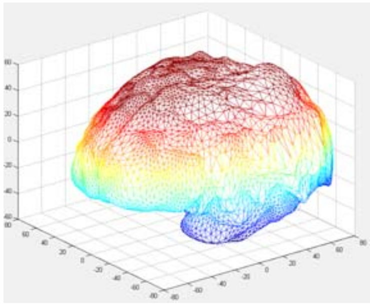

49

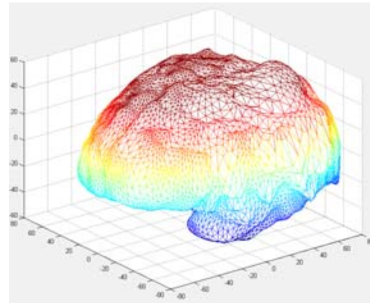

50

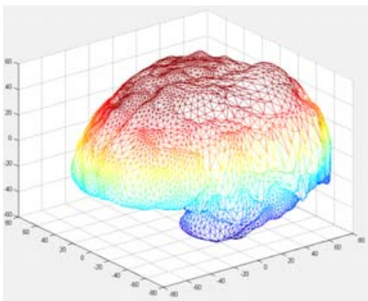

51

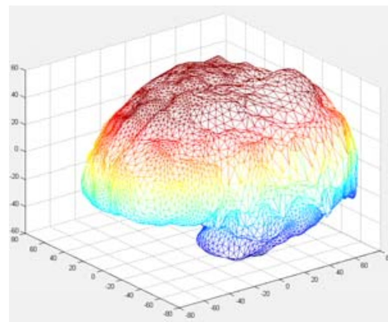

52

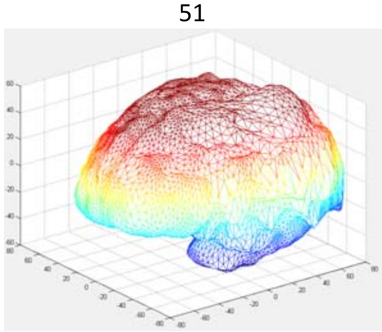

53

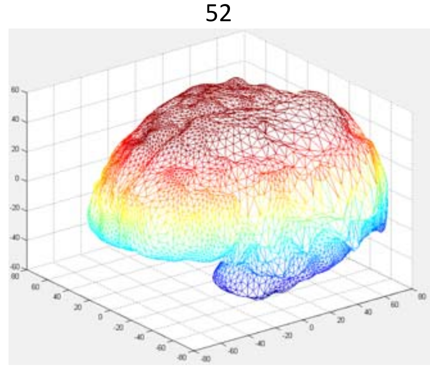

54

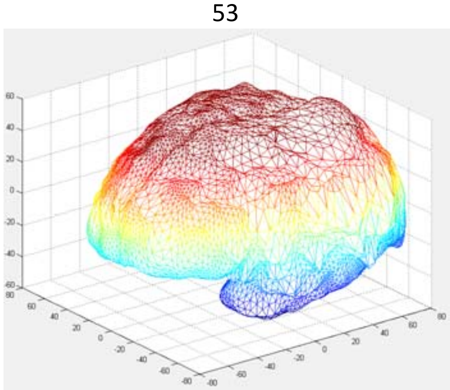

55

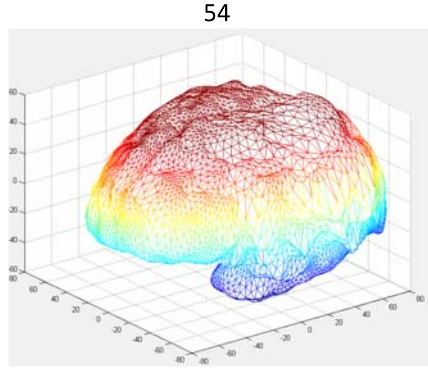

56

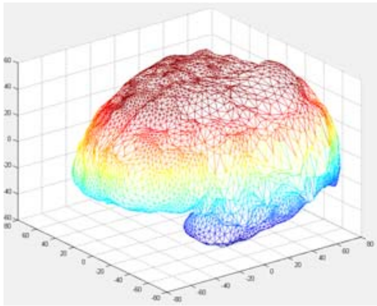

57

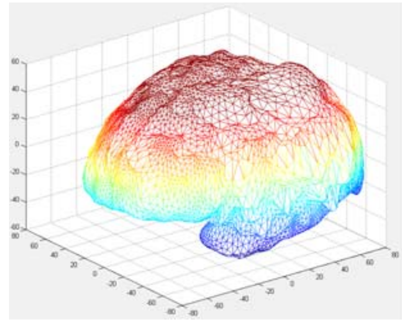

58

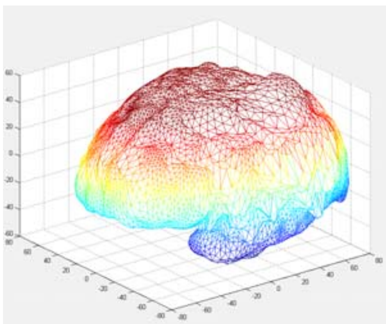

59

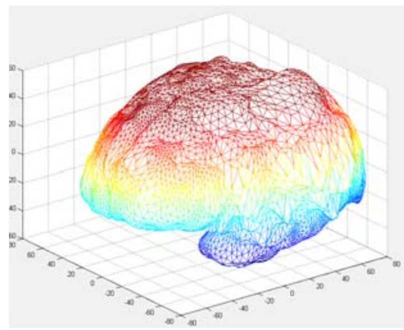

60 (error = 9.6941%)